EXPERIMENTAL INVESTIGATION OF AEROSOL PROPERTIES AND MODELLING OF ITS IMPACT ON RADIATION BUDGET

HARISH GADHAVI

Ph.D. Thesis

2005

PHYSICAL RESEARCH LABORATORY

AHMEDABAD – 380 009, INDIA

EXPERIMENTAL INVESTIGATION OF AEROSOL PROPERTIES AND MODELLING OF ITS IMPACT ON RADIATION BUDGET

A thesis submitted to

Gujarat University

Ahmedabad-India

for the degree of

Doctor of Philosophy in Physics

By

Harish Gadhavi

June 2005

Physical Research Laboratory
Ahmedabad 380 009 India

CERTIFICATE

I hereby declare that the work presented in this thesis is original and has not formed the basis for the award of any degree or diploma by any university or institution

Harish Gadhavi
(Author)

Prof. S. Krishnaswami
(Thesis Supervisor)
Physical Research Laboratory
Ahmedabad 380 009 India

Dedicated to

Mummy and Papa

ABSTRACT

Motivated from the rising concern for global climate change as a consequences of changes in atmospheric composition, this work was undertaken to investigate properties of one of the very important atmospheric components, aerosol. A detailed study of aerosol vertical profile and other aerosol properties is carried out over Ahmedabad from February 2002 to November 2004. In addition, specific field measurements at variety of places such as Antarctica, Western Gujarat, and Central India are carried out to study the spatial inhomogeneities. The observed aerosol physical and optical properties are further used to study their influence on radiation budget by employing radiative transfer models and by calculating radiative forcing.

Aerosol extinction values are characterised by a large day-to-day variation typical of urban location, while inter-annual and seasonal variations are higher that they are above the standard deviation of the daily mean value. Extinction values for year 2003 are highest during the study period, significantly higher than 2002 while marginally higher than 2004 values. Well known seasonal variation expected over India i.e. summer time increase in AOD is also observed over Ahmedabad. AOD is found to be around 0.2 during winter and around 0.8 during summer. Interestingly the observed variation is found to be different at different altitude levels. It is found that variation in aerosol extinction above 1 km is mainly responsible for the observed seasonal variation. Measurements of aerosol properties such as scattering and absorption coefficients show different seasonal variation than that of AOD with summer time low and winter time high values. Absorption coefficient over Ahmedabad is found to be in the range of 0.2 to 4 x 10^{-5} m^{-1} with a mean value of 2.1 x 10^{-5} m^{-1} and scattering coefficient is in the range 0.7 to 2.6 x 10^{-4} m^{-1}. Single scattering albedo calculated from absorption and scattering coefficients is 0.87 ± 0.09.

Contrary to observations made over Ahmedabad, which is an urban site, very different aerosol properties are observed during field studies at different locations. For example over Maitri-Antarctica, AOD is found to be very low (0.036±0.018 at 400 nm) during Jan-Feb 2001 with a flat spectral dependence, which is typical of a pristine region. The average mass concentration of PM_{10} particles at Maitri for the campaign period is 9.1±6.0 $\mu g/m^3$, of which 63 % of mass is contributed by coarse mode particles. Also, interesting day and night differences are observed in the measurements of vertical profile carried out over Western Gujarat during Dec – Jan 2003 and in central India during Feb 2004. At locations nighttime AOD is found to be 12 to 80 % lower than the nearest neighbour daytime AOD. Difference in boundary layer height is also observed during the field campaigns that can be attributed to differential heating between ocean and land over the peninsular India.

Measurements of aerosol extinction profile are carried out by airborne lidar for the first time in India. Measurements have been carried out on experimental basis and the usefulness of airborne observation is demonstrated in studying the boundary layer and free tropospheric aerosols.

Radiative forcing computation is made using observed aerosol properties in radiative transfer model. Large absorption in the atmosphere over Ahmedabad is found which ranges from 20 to 80 W/m^2 depending on season. Study on vertical profile of aerosol radiative forcing and their seasonal variation reveals that in the boundary layer aerosol radiative forcing is a factor of 2.5 higher during May than February and produces additional heating rate of ~1 K/day. Top of the atmosphere (TOA) aerosol radiative forcing (ARF) over Maitri-Antarctica is found to be positive 0.45 W/m^2 mainly because of highly reflective snow surface underneath. However, ARF over Antarctica is sensitive to the sun-earth geometry. For the same amount of aerosol, ARF over Maitri varies from +0.7 W/m^2 in December to -0.15 W/m^2 in April and August, and it becomes zero during no sunshine days in June and July. Importance of surface reflectance for ARF is

shown by carrying out calculations over ocean (Bay of Bengal) and continental locations (Ahmedabad, Hyderabad, etc.). Large difference in TOA ARF is observed between ocean and land though the difference in AOD is not of the same magnitude as the TOA forcing is very sensitive to surface reflection.

TABLE OF CONTENTS

ACKNOWLEDGMENTS

I take this opportunity to express my thanks and gratitude to all those who have helped and encouraged me for research work.

I would like to express my sincere gratitude to Prof. A. Jayaraman for his invaluable guidance and support throughout the period of this thesis work. I am greatly benefited by his vast knowledge and cheerful leadership. Journey of research wouldn't have been so rewarding and wonderful for me without his guidance. I would like to thank Prof. S. Krishnaswami for his suggestions and comments which helped me a lot to improve my scientific outcomes. He has always been my role model and I feel honoured to have him as my thesis supervisor.

I am indebted to Shri Vinchhibhai, Rajesh and Shri Acharyaji for help and support I received from them throughout the period of this thesis work for instruments and field campaigns. I am also indebted to Dr. Angom for teaching me the techniques of parallel programming.

I acknowledge National Centre for Antarctic and Ocean Research, Goa, India for providing me logistic support during 20th Indian Antarctic Expedition, NOAA Air Resources Laboratory, USA for the provision of the HySPLIT model, NOAA–CIRES Climate Diagnostic Center, USA for providing NCEP reanalysis data and Ozone Processing Team of NASA/Goddard Space Flight Center, USA for TOMS ozone data used in this study. I also acknowledge NASA's Goddard Earth Sciences (GES) Data and Information Services Center (DISC), USA for satellite AOD images and Land Processes (LP), DAAC, EOS, NASA, USA for surface reflectance data.

I would like to thank Prof. Shyam Lal, Prof. S. Bhattacharya, Prof V. B. Sheorey and members of academic committee for critically reviewing my work at various stages.

I would like to thank Dilip, Pawan (Gupta), Som Kumar and Ramachandran with whom scientific discussions were very interesting and rewarding for me. My thanks are due to all

members of SPA-AP division and in particular to Amit, Sanat, Lokesh, Shilpy, Vandana, Uma, Venkataramani, Sunil, Modhbhai, Smt. Suchita madam, Shri S. K. Shah, Dr Varun Sheel, Dipu, Dr. Subramanian, Dr. Bapat and Dr. Harish Chandra for their keen interest in my research work and moral support. My thanks are also due to people of the Chemistry Lab who are the first to introduce me the wonderland of research. In particular, I thank Prof. M. M. Sarin, Sunil Kumar Singh, Rengarajan and Ravi with whom I worked as summer trainee.

I thank staff members of Computer Centre, Library, Workshop, Maintenance and Administration for their timely help. My sincere gratitude to Shri Dholakiaji who have always taken deep interest in my work and encouraged me to use the latest of all machines. My sincere gratitude to Mr Ubale and his team for their state of art workmanship, which gave me edge in quality of data for research.

I cherish the wonderful moments shared with my friends at PRL. I am thankful to my batch-mates; Neeraj, Manoj, Anirban, Prasanta, Santosh, Sajan, Vachaspati, Sanjeev, Manish and Arpit for all the time I have spent with them. I owe a lot to my seniors, to name a few; Rishi, Sajesh, Sudheer Vempati, Sankaranarayanan, Jitti, Anil (Pattu), Soumenda, Kunnu, Sarika, Jayendra, Sudeshna, Hetu, Duli, Tarak, Subhrangshu and Rajesh (Satraj), for standing beside me through highs and lows. I also thank Kaushikda, Charan, Murali, Jayesh, Yogesh, Gowda, Sanjoy, Rajneesh, Ashoka and Morthekai. Thanks are also due to Shuklaji (Anil), Deshpandeji, Sheth (S.P.), Rajesh (P. K.), Gerelama, Neeraj (Srivastva) and Sudheer (A. K.).

I am out of words to express my gratitude toward my parents. Without their constant support and inspiring words, research wouldn't have been possible for me. I will always remember the confidence, which my younger brothers Vijayanand and Mahendra have shown towards me which helped me to progress even when I used to go out of energy. Smiles of Malkaush, Sohini, Bhumi and Indira have been the largest source of motivation for me. I thank my wife Deval for her love, patience and all the joy I have in life.

Chapter 1

INTRODUCTION

1.1 Background

The Earth's climate is controlled by the amount of solar radiation it intercepts and the fraction of that energy absorbed in the atmosphere. Average solar radiation received per square meter of the Earth is about 343 W/m^2 of which ~103 W/m^2 is reflected to space. The remaining 240 W/m^2 is radiated back to space in the form of infrared radiation to maintain equilibrium state. Black body radiation laws predict temperature of the Earth to be about 255 K for this amount of radiation, which is 18 degrees lower than the freezing point of water. Greenhouse gases present in the atmosphere keep the Earth warm at about 288 K and make it liveable (*Seinfeld and Pandis*, 1998). The climate, defined as the long term mean of weather is not always like the one which we experience currently. It is believed that during cryogenian period (800 to 600 million years ago) permanent sea ice covered almost the entire globe. Paleo-records show that past climatic and environmental changes on the Earth are correlated with atmospheric composition. Records from Vostok (Antarctica) ice core show that the lowest concentration for greenhouse gases such as CO_2 and CH_4 is observed during full glacial conditions. CO_2 and CH_4 concentration are found to be 190 ppmv and 0.35 ppmv respectively during the last glacial maximum, ~20 kyr BP. Increase in their concentration during deglaciation period is about 40% for CO_2 and 200% for CH_4. Ice core data also reveal that during ice age terrestrial and marine contributions to Antarctic aerosol deposition increased significantly. Concentration of calcium and sodium (crustal and marine primary aerosol reference elements, respectively) in Vostok ice were higher by factors of about 30 and 4 respectively, relative to Holocene values (*Wuebbles et al.*, 2003). Atmospheric composition affects climate as well as gets altered by climate. This feedback loop makes climate very sensitive to small perturbations in the atmospheric composition. For example, the warmer Earth

may sustain more water vapour in the atmosphere, which can absorb more infrared radiation making the earth further warm. The causes for natural variability of climate and atmospheric composition are yet to be fully understood. Mean while the present day concentration of greenhouse gases is unprecedented in the last 420 kyr. (*Petit et al.*, 1999) and likewise is the case for aerosols. Determining the influence of such large scale changes in the composition of the atmosphere on climate is the central objective of present day atmospheric science community. Complete understanding of emission rate of all atmospheric species, their transport and transformation, removal rate, seasonal variation, influence in radiation budget, and chemical and physical processes occurring in the atmosphere is key to acquire forecast ability for future changes of climate.

Rapid changes in atmospheric composition observed over the past century have been driven largely by increased usage of fossil fuel, intensive farming, industrial activities and biomass burning. One can deduce the anthropogenic contribution by comparing present day concentration with that of pre-industrial time (~1750 AD). Concentrations of CO_2 and CH_4 during pre-industrial time were ~280 ppmv and ~650 ppbv respectively, while the present day values are ~360 ppmv and ~1700 ppbv respectively. Similarly, sulphate concentration has increased from about 50 mg per tonne to about 200 mg per tonne of ice during the same period in ice core taken from Greenland (*IPCC*, 2001). Concentrations of CO_2 and CH_4 are global values whereas that of sulphate is more region specific. This is because greenhouse gases such as CO_2 and CH_4 have longer lifetimes and hence they are well mixed in the atmosphere whereas aerosols have shorter lifetime and hence their concentration shows gradient from source to remote region. Apart from large spatial variability, there are other complexities, such as poor understanding of the processes that link aerosol particles, precursor emissions and radiative effect, and lack of comprehensive global data set that can be used to verify models which contribute to large uncertainty in estimating the effect of aerosols on climate (*Huebert et al.*, 2003). Nevertheless, globally averaged anthropogenic aerosol

forcing is estimated, which is found to be equal to the forcing by anthropogenic greenhouse gases but opposite in sign (*IPCC*, 2001).

Atmospheric aerosols affect Earth's radiation budget in two different pathways, one is by directly scattering and absorbing the electromagnetic radiation and is called direct effect of aerosols. Aerosol particles can also modify the lifetime and microphysical properties of clouds. Increased concentration of aerosols increases the number concentration of cloud droplets but reduce their size. This leads to an increase in cloud reflectance. Also smaller size droplets have lower precipitation efficiency and hence lifetime of clouds increases. This results in increased global cloud cover. These effects of aerosol are known as indirect effects. Influence of parameters such as aerosols which affect the Earth's radiation budget is quantified by a quantity called radiative forcing. Radiative forcing is defined as the change in net irradiance at the tropopause due to an applied perturbation to a particular parameter while holding all other atmospheric variables fixed, and the stratospheric temperature is allowed to adjust to equilibrium value (*Haywood and Boucher*, 2000). Adjustment of stratospheric temperature is more important for computing radiative forcing by ozone depletion in stratosphere whereas it does not make any measurable difference for aerosols. Also, aerosol radiative forcing study is no more restricted to tropopause but more importance is given to vertical distribution particularly at lower altitudes (*Satheesh and Ramanathan*, 2000). Concept of radiative forcing was first used to deduce temperature changes for applied perturbations in 1 D models, but was found equally useful for 3 D models. Sign convention for radiative forcing is defined in a manner that positive forcing has warming effect and negative forcing has cooling effect. Until all the feedback effects such as changes in cloud, snow and ice cover, atmospheric water vapour, winds, ocean currents, etc are accounted for, exact effect of applied perturbation to radiation budget cannot be known, nevertheless concept of radiative forcing is useful for first order assessment of the impact of applied perturbation (*Ramaswamy et al.*, 2001).

Importance of aerosols in climate forcing of the Earth is well recognised for a long time. *Hansen et al.* (1990) estimate the global anthropogenic aerosol radiative forcing between -0.75 to -1.5 W/m^2. *Charlson et al.* (1992) estimate global anthropogenic sulphate forcing in the range of -1 to -2 W/m^2 including both direct and indirect effects. *Haywood et al.* (1999) have shown by comparing top of the atmosphere irradiance from general circulation model (GCM) and observations from Earth Radiation Budget Experiment (ERBE) satellite that annually and globally averaged tropospheric aerosol radiative forcing (including both natural and anthropogenic) is around -6.74 W/m^2 over oceans. *Haywood and Boucher* (2000) discuss in detail the anthropogenic aerosol radiative forcing and present range of values for sulphate (-0.26 to -0.82 W/m^2), mineral dust (+0.09 to -0.46 W/m^2), fossil fuel black carbon (+0.16 to +0.42 W/m^2) and organic carbon (-0.02 to -0.04 W/m^2), black carbon and organic carbon from biomass burning(-0.14 to -0.74 W/m^2), nitrate (-0.03 W/m^2) and indirect effect of aerosols (-0.3 to -1.8 W/m^2). Range of values span more than a factor of two for almost all the aerosol types. Such a large uncertainty is mainly because of insufficient data on inventories, poor understanding of mixing state of aerosols (whether aerosols are internally or externally mixed with other species), different schemes for cloud representation in sub grid level, lack of data on vertical distribution, etc. To reduce the uncertainty and enable better forecast for future climate change, world wide efforts have been made to measure aerosol properties by establishing permanent stations (*Subbaraya et al.*, 2000, *Holben et al.*, 1998) and through major field campaigns such as ISRO-GBP land campaign-1 (*Jayaraman et al.*, 2005), INDOEX (*Ramanathan et al.*, 2001 and 2002), TARFOX (*Russell et al.*, 1999), ACE (*Bates et al.*, 1998), SAFARI (*Campbell et al.*, 2003) etc.

INDOEX study has shown large aerosol radiative forcing existing over the Arabian Sea and the Indian Ocean during winter months when the winds are predominantly NE, blowing from the continents towards the ocean. Large latitudinal gradient is found in aerosol radiative forcing (Figure 1.1). Surface level

aerosol radiative forcing is found to very from -5 W/m^2 in southern Indian Ocean to -40 W/m^2 close to western coast of India (*Ramanathan et al.*, 2001).

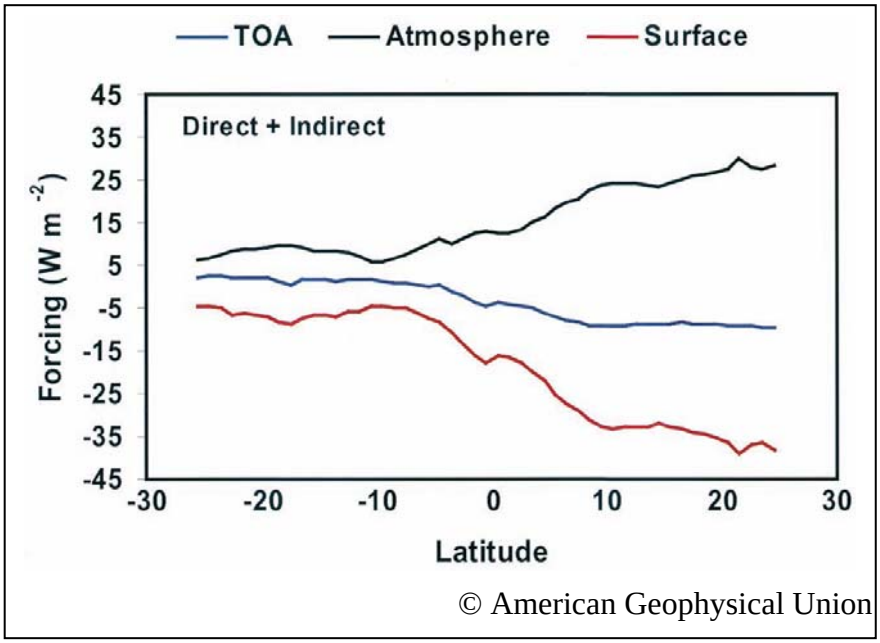

Figure 1.1. Latitudinal variation in aerosol radiative forcing (including both natural and anthropogenic) observed over the Indian ocean, averaged between 40^{0}E to 100^{0}E longitude. (source: *Ramanathan et al.*, 2001)

The modelling studies following INDOEX have identified significant consequences of the aerosol forcing in terms of variation in the spatial distribution of rainfall pattern over India and in modifying the amplitude and frequency of El Niño. Observed decrease in rainfall over India after 1950 is attributed to regional scale aerosol radiative forcing and further emphasized that if current trends in aerosol emission continue, draught frequency will double in coming decades (*Chung and Ramanathan*, 2004, *Ramanathan et. al.*, 2005). Latitudinal gradient in aerosol properties over the Arabian Sea and the Indian Ocean (*Jayaraman et al.*, 2001) suggest that major sources of aerosols lie over land. *Venkataraman et al* (2005) have shown that more 65 % of global black carbon from biofuel is emitted in Asia and about 25 % of that is emitted in India. The satellite data show large spatial and temporal variations of aerosol optical depth (AOD)

over land (Figure 1.2). AOD is high over northern and western part of India than peninsular India and the temporal variation is very high over Gujarat, Rajasthan and Gangetic basin of India.

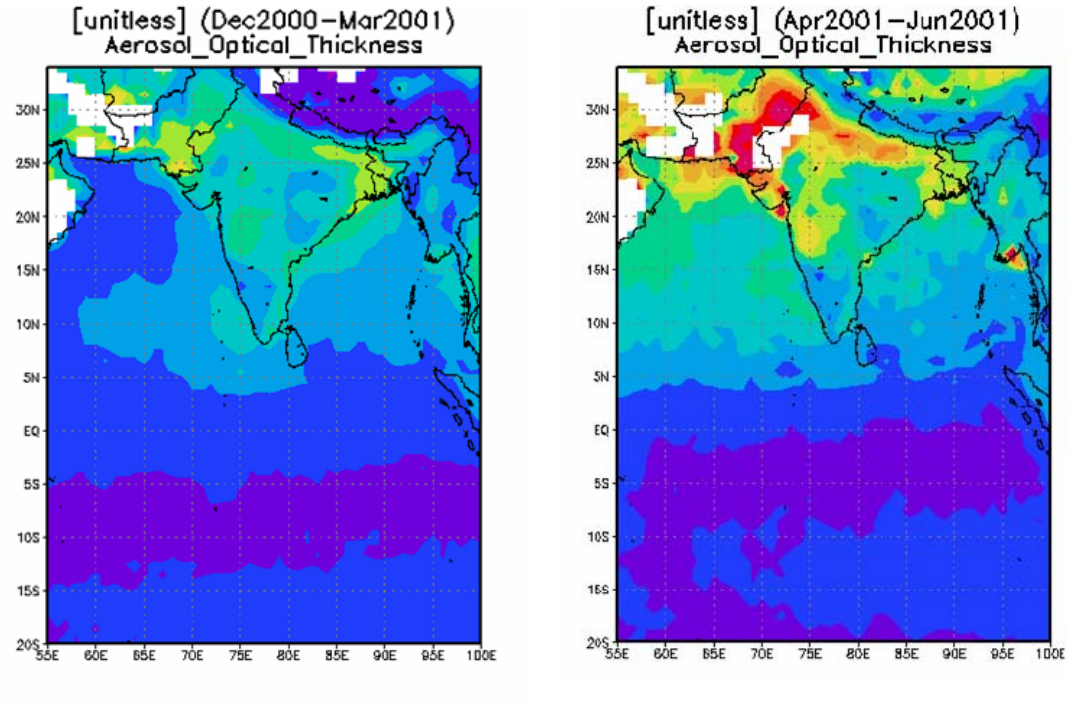

Figure 1.2. Satellite based observation of aerosol optical depth over Indian subcontinent. (source: MODIS; http://modarch.gsfc.nasa.gov/)

Detailed ground based observation for aerosol properties over land remains sparse. Measurements on vertical distribution of aerosol properties are further sparse. Even if radiation fluxes at the top of the atmosphere and surface level are correctly accounted for, the computed heating rate within the atmosphere can be erroneous if the vertical distribution of aerosols is not properly characterised. Depending on whether the aerosols occur above or below the cloud layer, the radiative forcing can be different for the same concentration and type of aerosols, hence accurate prescription of aerosol vertical profile is very important (*Haywood and Ramaswamy*, 1998, *Chung and Ramanathan*, 2004). Lifetime of aerosols depends, apart from their size, on the altitude of their occurrence. In the boundary layer, aerosol lifetime is of the order of few days, it is a few weeks in free troposphere

and few years in the stratosphere. Also satellite remote sensing of various parameters require knowledge on vertical distribution of aerosols (*Herman et al.,*1997, *Torres et al.*, 1998).

1.2 Scope of the present work

In the context of India, aerosol properties over ocean surrounding peninsular India are extensively studied and their impact on solar radiation fluxes reaching the surface and leaving the atmosphere have been reported (*Jayaraman et al.*, 1998, *Satheesh and Ramanathan*, 2000, *Rajeev and Ramanathan*, 2001, *Coakley et al.*, 2002, *Satheesh*, 2002, *Satheesh et al.*, 2002, *Satheesh and Lubin*, 2003, *Ganguly et al.*, 2005) but relatively a few measurements on land locations exist (*Ramachandran et al.*, 1994, *Devara*, 2000, *Niranjan et al.*, 2000, *Moorthy et al.*, 2001, *Moorthy et al.*, 2002, *Gupta et al.*, 2003, *Sagar et al.*, 2004, *Parameswaran et al.*, 2004). Measurements of vertical profiles of aerosol are further sparse (*Jayaraman et al*, 1996, *Parameswaran et al.*, 1998, *Devara*, 2000, *Ramachandran and Jayaraman*, 2003). The study of stratospheric aerosol have been carried out from Ahmedabad in the past (*Jayaraman et al.*, 1995a, 1995b, and 1996). *Ramachandran* (1995) has carried out observations of aerosol optical depth from 1991 to 1993 over Ahmedabad but for subsequent period AOD observations are not available over Ahmedabad. Though very important, no information exists on vertical distribution of aerosol in the lower troposphere over Ahmedabad where more than 90 % of aerosols reside during volcanically quiescent period.

Ahmedabad is an urban location in semi-arid region of western part of India (23^0 3'N, 72^0 52'E). Being an urban location, studies of aerosol is very important for long-term monitoring of environment degradation and source characterisation. Its proximity to Thaar desert of Rajasthan and the Arabian Sea allows one to study further the effect of changing airmass trajectory on aerosol properties and concentration. Present thesis focuses on the study of vertical distribution of aerosol in the troposphere. Vertical distribution of aerosol extinction coefficient has been studied using micro pulse lidar (MPL) system. More than 20 algorithms

have been surveyed for their feasibility to get extinction profile from lidar data and robustness of the solution for uncertainty in various assumptions. Chapter 2 of the thesis describes the instruments, data retrieval and important algorithms in detail. Seasonal variation in extinction profile, aerosol scale height and aerosol optical depth obtained by integrating extinction profile is presented in Chapter 3. Observations of aerosol absorption and scattering coefficients have been obtained for the first time over Ahmedabad. Their daily mean values for the period of about one year are also presented in Chapter 3.

Chapter 4 of the thesis discusses specific field observations made during special campaigns. Regions covered are highly heterogeneous such as Antarctica, Coastal Area of Gujarat, Rann of Kachchh, Central India, etc. Large difference in the aerosol properties is found from place to place. AOD over Antarctica is an order of magnitude lower than Ahmedabad, while vertical extent of aerosol over central India is found high by about one km in comparison to Ahmedabad.

Information gathered over Ahmedabad and other places has been used to study their impact on Earth's radiation budget. Results and details of radiative forcing calculations are presented in Chapter 5. Results of radiative forcing are discussed in the context of their seasonal as well as spatial variation and vertical distribution. Significant influence of surface reflectance is found on the aerosol radiative forcing. It is shown that sign of radiative forcing can flip from negative to positive depending on brightness of a surface. Chapter 6 presents the major conclusions and scope for future work.

Chapter 2

INSTRUMENTATION, OBSERVATION AND DATA REDUCTION

A state of the art mobile micro pulse lidar (MPL) is used extensively to study the vertical distribution of aerosols properties. The results obtained using this set-up are presented and discussed in more detail. In addition, results from other observations, using Sun-photometers, Aethelometer, Nephelometer, QCM-Cascade Impactor and Aerosol Size Spectrometer are also discussed and used in the aerosol radiative forcing estimation.

2.1 Aerosol Vertical Profiles

The knowledge of vertical profile of aerosol optical properties is very important for modelling the radiative effect as well as in computations related to the study of boundary layer stability, evaporation rate, sensible heat flux, convection, actinic flux etc. In the present work information on the vertical distribution of aerosol is obtained using the Micro Pulse Lidar (MPL).

2.1.1 Instrumentation

Lidar works on the principle similar to that of RADAR. Measurement of the intensity of the backscattered photons provides information on the properties of the scatterer. The time lapse between the transmitted and received signals is proportional to the distance of scatterer from Lidar. The Micro Pulse Lidar (MPL) used in the present study is a compact co-axial mono-static lidar system. Figure 2.1 shows the photograph of MPL mounted inside a mobile Lidar observatory of the Physical Research Laboratory (PRL) and Table 2.1 summarises important features of MPL. Laser, telescope and diode are housed in single tubular casing. The tubular casing is fixed on two stanchions with pivoting ring in the centre. This allows to change the viewing angle. Also, the arrangement is very useful for estimating the overlap correction (to be discussed later) unlike traditional lidar

system, which looks only at fixed angle. MPL uses a diode pumped Nd-YLF laser with second harmonic generation facility to give laser light of wavelength 523.5 nm. Advantage of diode pumped laser is that laser unit can be miniaturised and pulse repetition frequency can be increased greatly compared to conventional flash lamp pumped laser. This unit can be operated with pulse repetition rate from 1 to 10000 Hz. While a larger pulse rate is good for improving the signal to noise ratio (SNR) it decreases the power in individual laser pulses, which reduce the SNR. Hence it is necessary to find out the optimal value for the laser repetition rate. In the present case, it is operated with 2500 Hz pulse rate, which is found to be the optimum. Outgoing pulses are expanded by a telescope and sent to the atmosphere. Backscattered photons are received back by the same telescope, which is a 20 cm diameter Schmidt-Cassegrain telescope with field of view (FOV) less than 50 μrad. The small FOV reduces the background noise and complications arising out of multiple scattering to a great extent. A narrow band pass filter further reduces the background noise. MPL uses an interference filter of full width at half maximum (FWHM) equal to 0.1 nm centred at 523.5 nm to screen the incoming photons. Screened photons are detected with silicon avalanche photo diode (Si-APD) operated in counting mode. Si-APD has a quantum efficiency of about 40-50% at wavelength 523.5 nm and a larger dynamic range of detection limit. This enables MPL to work even in day light condition. The electrical pulses from Si-APD are counted by multichannel scaler (MCS) electronics as time gated signal. It is possible to set the binwidth as 200, 500, 1000 or 2000 ns, the time interval during which incoming photons will be summed and recorded in single memory location (bin). For the next same length of period, photons will be counted and recorded in consecutive bin. Binwidth essentially determines the range resolution of system (ΔR) which is equal to $BinWidth \times c/2$, where "c" is the speed of light. The factor two in the denominator is because the photon has to travel distance ΔR twice. In the present study, the bin width is set as 200 ns, which corresponds to a range resolution of 30 m.

Table 2.1. Features of Micro Pulse Lidar system operational at PRL, Ahmedabad

Laser	Diode pumped Nd-YLF
Wavelength	523.5 nm
Pulse repetition rate	2500 Hz (Typical)
Telescope	20 cm dia. Schmidt-Cassegrain
Field of view	50 μrad
Filter	Central wavelength: 523.5 nm FWHM: 0.1 nm
Detector	Si avalanche photo diode (Si-APD)
Data acquisition	Multichannel scaler
Bin width	200 ns (Typical)

Figure 2.1. Micro Pulse Lidar (MPL) fitted inside the mobile lidar observatory of the Physical Research Laboratory, Ahmedabad.

Pulse repetition frequency (PRF) determines the theoretical limit on the maximum range of a lidar. Time between two pulses is available to photons for travelling to and fro distance. In the case of PRF equal to 2500, this period is equal to 400 μsec. During this period maximum distance a photon can travel is 120 km. However, in actual practice the maximum altitude that is studied for aerosols is up to around 7 km, mainly determined by laser power and background sky radiation intensity but on perfect dark nights backscattered laser light could be detected up to about 20 km using the present system.

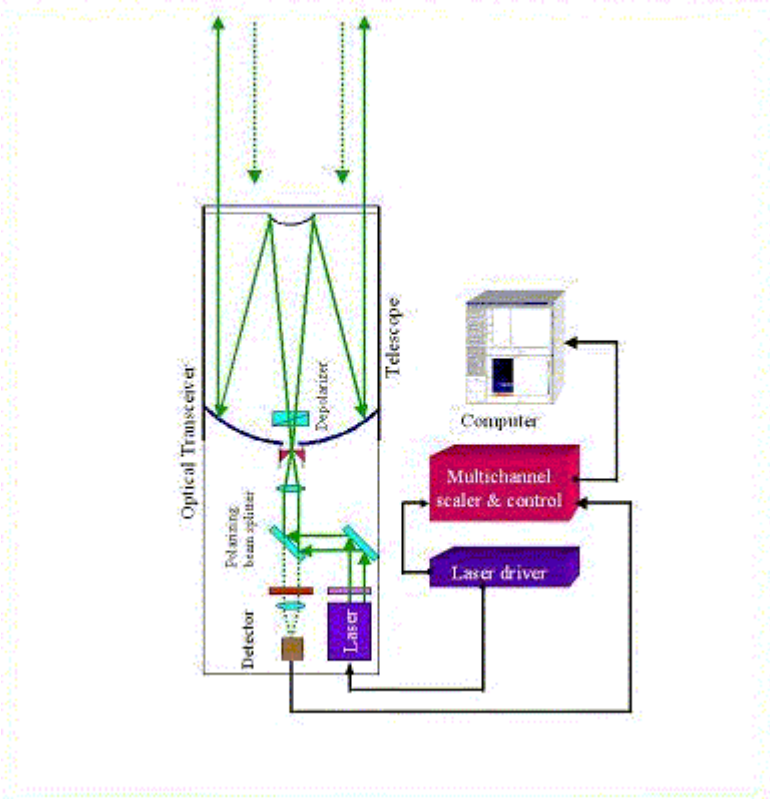

Figure 2.2. Block diagram of the micro pulse lidar system, described in Table 2.1 and shown in Figure 2.1.

2.1.2 Data reduction

Counts obtained using multi-channel scaler (MCS) are saved with one-minute average for 1000 bins. Each record is preceded with a header containing information on laser pulse energy, detector, laser and ambient temperatures, pulse

repetition rate, number of profiles summed, etc. This is called raw data record. Following paragraphs describe various corrections required to apply on the raw data.

MPL raw data counts can be related to extinction coefficient using following relation, known as the lidar equation:

$$P(r) = \frac{AE\beta(r)T^2(r)}{r^2} + P_{bg} + P_{ap}(r) \qquad 2.1$$

Here P is the actual count measured by the system. r is the range from lidar to target. A is an instrument constant, depends upon the size of telescope receiver, photo detector and optics efficiencies. E is the energy of the outgoing pulse. β is the volume back-scattering coefficient at laser wavelength by all the constituents of atmosphere at range r. T is the transmission of medium from lidar to range r. Since photons have to travel distance r twice, square of the transmission is taken. P_{bg} is the background due to ambient light sources. P_{ap} is the after-pulse count. In this equation range r can be calculated from bin number using the following relation:

$$r = Bin\ No \times Bin\ Width \times c/2 - Bin\ Width \times c/4 - \Delta t \times c/2 \qquad 2.2$$

where c is the speed of light. Bin number multiplied by bin-width gives the total time available for travelling the to and fro distance by photon and multiplying it with speed of light and dividing by two gives the distance of that particular bin with respect to Lidar. Since each bin has finite bin-width, distance calculated in this manner corresponds to a range (30 meter in present case). It is customary to designate distance of each bin with central value of range for that bin and the second term in above equation accounts for that. Laser trigger and MCS are synchronised using BNC cable. However there could be offset (Δt) between triggering of laser pulse and MCS. If triggering of laser pulse takes place before MCS starts recording, offset can be found only through laboratory experiments.

In the present case MCS starts data recording before the laser pulse is fired, hence offset can be directly found in the raw data. The bins, which are recording data before the laser is fired, contain only dark current and background noise. The present MPL system has 400 ns (in other words 2 bins) offset between MCS and Laser trigger. Last term in equation 2.2 accounts for this offset Δt.

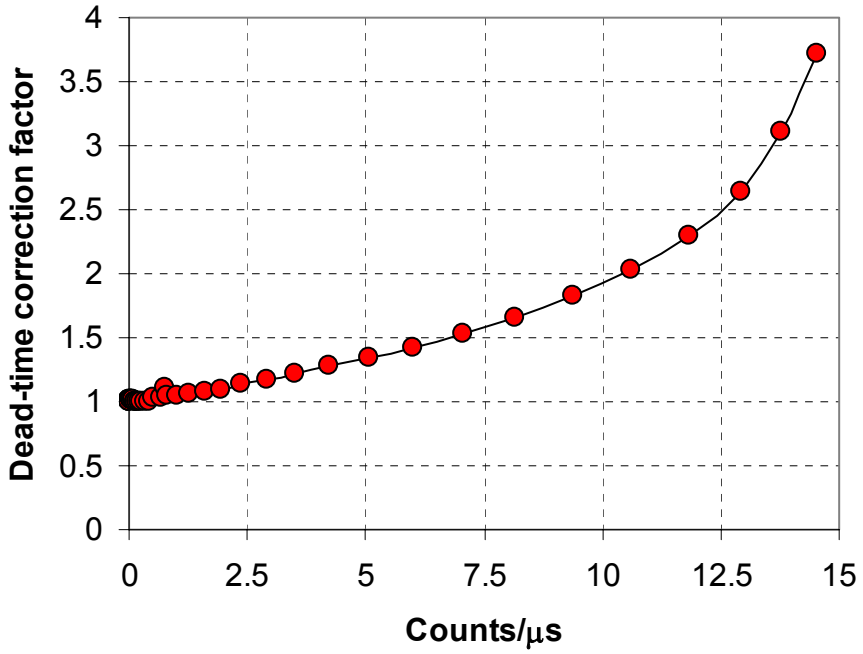

Figure 2.3. Dead-time correction factor for the MPL detector as a function of photon-counts

Avalanche photo diode has finite time for a single photon avalanche event. During this time interval it will not record another event if it occurs. This time interval is known as dead time of a diode. Overall effect of it will be an underestimation of the actual count rate. Correction of it is particularly important in the situation of high incident rate of photon. Dead-time varies from diode to diode, which can be estimated in laboratory by using standard light source. A lookup table supplied by the manufacturer listing the statistical approximation of dead-time correction factor as a function of photon events per μs is used in the present study. Figure 2.3 shows the dead-time correction factor used in the present study. The highest

incident rate of photons is immediately after the laser firing. This is because of internal reflection and atmospheric backscattering from the nearest range. Count rate for this case is always high and is typically around 5 counts/μs. Normally this bin is avoided in analysis. It is quite unlikely that atmospheric scattering can exceed this count rate. For the bins excluding third bin count rate normally remains less than 0.4 counts/μs and hence dead-time correction factor is very close to one. P(r) in the equation 2.1 is dead-time corrected.

Laser pulse before exiting the telescope encounters at least 6 surfaces (Figure 2.2) resulting in significant internal reflection of light that can reach to photodiode. This initial high count rate saturates the Si-APD and the exponentially decaying small leakage current from diode keeps on flowing even after the pulse is over. This current is known as after-pulse current. Since range is estimated from time elapsed after the pulse has been fired, after-pulse (P_{ap}) in that way is a function of range (Refer to equation 2.1). After-pulse can be estimated experimentally in dark room by pointing the lidar towards a black target. In this condition signal beyond the blocking point is after-pulse and dark current of detector. However, values of after-pulse also depend on the out-going pulse energy. Linear relationship between after-pulse and laser pulse energy is assumed (*Campbell et al.*, 2002). After-pulse correction factor is normalised with laser energy during the after-pulse calculation experiment.

$$P_{ap}(r) = P'_{ap}(r)\frac{E}{E_0} \qquad 2.3$$

In equation 2.3 $P'_{ap}(r)$ is the after-pulse factor obtained from the experiment. E_0 is the energy of laser pulse when $P'_{ap}(r)$ was estimated. E is the energy of laser pulse of the profile to which after-pulse factor is to be applied. In Figure 2.4, the after-pulse profile is shown by dotted line and total raw signal during night time using solid line. Dark current of the detector is also a limiting factor for higher altitude data as after 16 km total raw counts are very close to dark current counts.

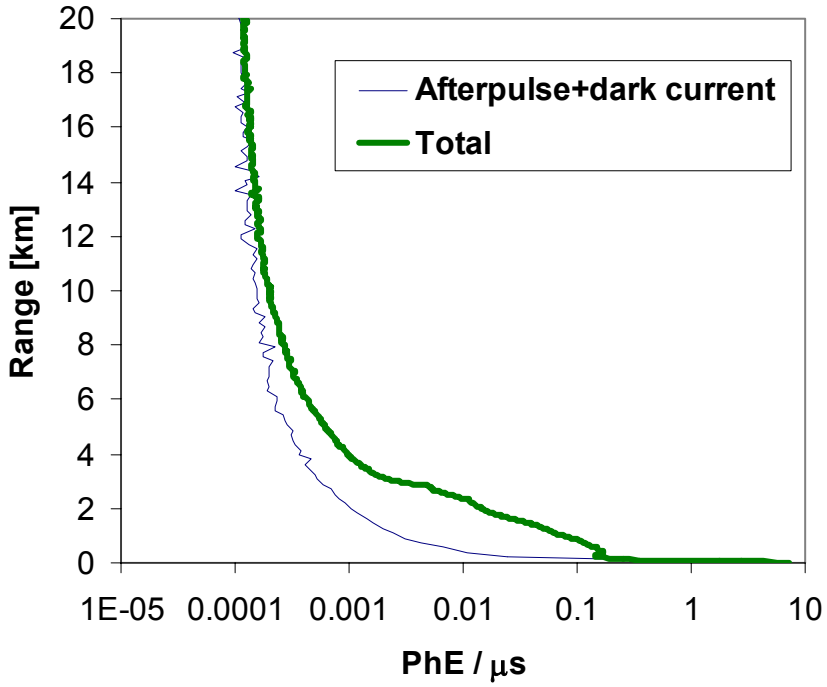

Figure 2.4. After-pulse effect in lidar signal. Thin line shows the after pulse and dark current photons and thick line shows the total photon counts obtained during nighttime.

Small field of view of telescope and narrow band-width of filter limits background light to a great extent but they do not completely eliminate it. MPL is operated with viewing angle in vertical direction. It is assumed that count measured for altitude range above 25 km may not contain back-scattered photons but only noise from after-pulse, dark current and sky background. Once the after-pulse and dark current are removed as described in previous section, background counts (P_{bg}) (equation 2.1) is calculated by averaging photon counts from the range 25 to 30 km. Sky background will be uniform over this range which is subtracted from lower bins.

In the equation 2.1, instrument dependent constant A is shown to be independent of range. However, for near range, it is a function of range for two reasons. First, the telescope has small field of view and laser beam is expanded to the size of telescope. In near range telescope will not see the entire image of the beam.

Secondly, rays coming from infinity are focused at focal point where pinhole is placed. However rays coming from near range are focused away from the focal point, and the pinhole blocks some part of ray reaching to the focal plane. If all the optical properties of the system are known overlap correction factor can be calculated theoretically (*Dho et al.*, 1997), however it is more advisable to obtain overlap correction factor experimentally.

When background and after-pulse corrections are accounted for and backscattered photon counts are normalized for laser energy, equation 2.1 takes the form:

$$P'(r) = \frac{O(r)\,A'\,\beta(r)\,T^2(r)}{r^2} \qquad 2.4$$

Here A in equation 2.1 is replaced with $O(r)$ and A'. Where $O(r)$ is range dependent part of A and A' is range independent part. $P'(r)$ is background and after-pulse corrected signal. Transmission of medium T is given by

$$T(r) = \exp\left(-\int_0^r \sigma(r')dr' \right) \qquad 2.5$$

Where σ(r) is the extinction coefficient of aerosol and air molecules. When system is pointed horizontally with no obstruction and if atmosphere is homogeneous, T(r) will be simply $T(r) = \exp(-\sigma r)$. Substituting this into equation 2.4 for range $r > r_0$ (where r_0 is the distance beyond that overlap correction factor is 1) and taking log on both the sides, we get the following relation:

$$\ln\left[P'(r)\,r^2 \right] = \ln\left[A'\beta \right] - 2\sigma r \qquad 2.6$$

which is the equation for straight line with slope equals to -2σ and intercept equals to $\ln[A'\beta]$. As shown in Figure 2.5, the coefficients are found by least square fitting for horizontal direction measurements and is used to estimate $O(r)$ for the range $r < r_0$.

$$O(r) = \frac{P'(r)\,r^2}{A'\beta \exp(-2\sigma r)} \qquad 2.7$$

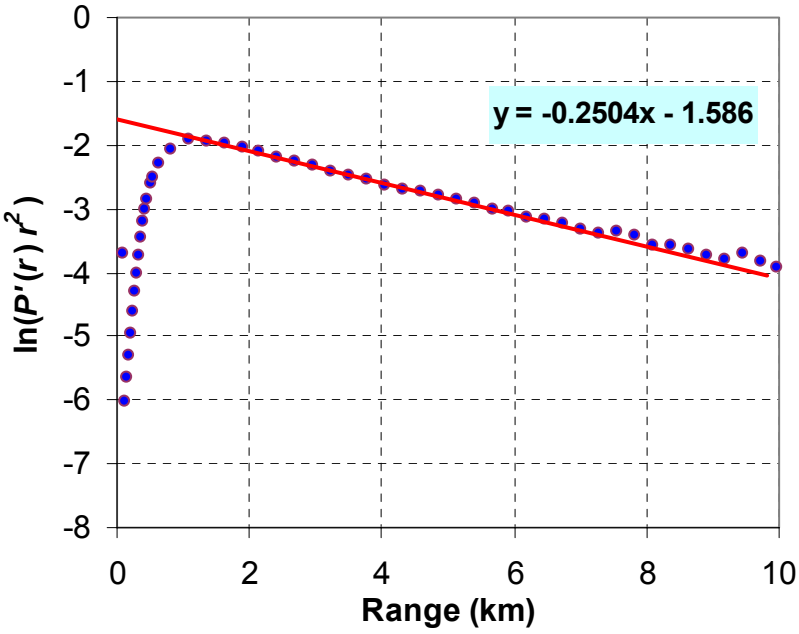

Figure 2.5. Result from an overlap correction experiment conducted at Mt. Abu, where lidar measurements are made in horizontal direction.

Over an urban region such as Ahmedabad, it is very difficult to get unobstructed horizontal view as well as a horizontally homogeneous atmosphere. So for overlap correction, at every 6 months MPL was taken to Mt. Abu observatory of PRL, situated on a hilltop at a height of 1.7 km from sea level, where the air is relatively clean. It can be seen in Figure 2.5 that for the range beyond 1.5 km overlap correction becomes one. After removing the instrument related artefact discussed above, data are further screened for presence of cloud and measurement timings. Cloud screening is not straight forward as cloud exhibits scattering features similar to that of aerosol except that cloud backscattered signal is stronger than aerosol. That is why most of the cloud-screening-algorithms rely on the threshold value (*Pal et al.*, 1992, *Sassen and Wang*, 1999, *Venema et al.*, 2000). One needs to be vary careful in selecting threshold value as it is quite possible that a smoke plume may

be screened out as a cloud or a thin cloud could be misunderstood as an aerosol layer. Often data contains large amount of random noise at the altitude where cloud occurs, which makes identification of cloud layer more difficult based on simple algorithm. In this work semi automatic approach is adopted for cloud screening. At first noise from the data is removed using wavelet transform (*Nanavati and Panigrahi*, 2004). Then based on threshold value, which is specific to particular instrument, clouds are screened out using a computer code. Threshold value is deliberately chosen higher so as optically thin clouds are not removed. The profiles are then checked one by one manually along with log-book description and further screening of data is done. Profiles for which cloud occurred above 10 km were retained for analysis. In case of partially cloudy day, if more than 25 % profiles contained the cloud then that day was removed from averaging. However exceptions were made for summer monsoon months i.e. July to September. For these months each profile was manually checked for cloud screening and the data for the day was retained after removing the cloud affected profiles. Since many aerosol properties show diurnal variation, for study of day to day or seasonal variation it is important that measurements done during the same period of the day to be compared. Observations done after sunset and within 3 hours after the sunset are considered for averaging purpose in case of Ahmedabad. There exist observations that are made outside this time limit on special occasions. Timing is explicitly mentioned whenever results from those observations are discussed. Data screened in such manner were used to create 30 minute average profile which were subsequently used to calculate Extinction values as described below.

2.1.3 Theoretical Basis for Extinction Calculation

Corrections discussed above are applied to the measured photon counts. These photon counts are further multiplied by the square of range and range corrected normalized photon counts are obtained. Lidar equation 2.1 for range corrected normalized photon counts will take the form:

$$r^2 P''(r) = A''\beta(r)\exp\left\{-2\int_0^r \sigma(r')dr'\right\} \qquad 2.8$$

where $P''(r)$ is the photon counts after all the corrections applied and A'' is the calibration constant. There are two approaches to solve equation 2.8 for backscattering or extinction coefficient. One way is to absolutely calibrate the lidar system for A'' using simultaneous measurements such as aerosol optical depth (AOD) as described in *Voss et al.* (2001). However this method has some limitations for example most of the lidar measurements exist during nighttime when sun-photometer measurements does not exist. Indeed many lidar systems are not able to take measurements in day light condition because of very sensitive photo detectors. Another problem comes form the fact that calibration constant A'' is not stable and is highly dependent on the conditions of optical parts, detector temperature, laser energy, etc. More popular approach is to calculate extinction or backscattering profile from lidar measurements by using relative calibration. This eliminates the need to evaluate A'' but involves certain assumptions. During the last two decades large amount of work has been carried out by several authors to develop algorithm for retrieving aerosol extinction profile and other properties from Lidar measurements, to name a few *Klett* (1981), *Ferguson and Stephens* (1983), *Fernald* (1984), *Mulders* (1984), *Klett* (1985), *Kaestner* (1986), *Balin et al.* (1987), *Gonzalez* (1988), *Kunz and Leeuw* (1993). *Kovalev* (1993), *Roy et al.* (1993), *Bissonnette and Hutt* (1995), *Devara et al.* (1995), *Kunz* (1996), *Rocadenbosch et al.* (1999), *Voss et al.* (2001), *Stephens et al.* (2001), *Sicard et al.* (2002), *Palm et al.* (2002), *Kovalev* (2003), etc. Algorithms given by *Stephens et al.* (2001) and *Palm et al.* (2002) are for lidar measurements from satellite based platform. These algorithms are discussed in Chapter 4 where aircraft based lidar measurements are discussed. Following paragraph describes the two algorithms *Klett* (1981) and *Kaestner* (1986) in detail. *Klett* (1981) algorithm is milestone in the field of lidar based aerosol study and many algorithms named above are originally variants of *Klett* (1981) algorithm. *Kaestner* (1986) algorithm is used in present study to retrieve the extinction profiles.

It is not philosophically different from *Klett* (1981, 1985), however mathematical treatment is quite different.

Equation 2.8 may be expressed in a system-independent form as follows:

$$S - S_0 = \ln\frac{\beta}{\beta_0} - 2\int_{r_0}^{r}\sigma dr' \qquad 2.9$$

where $S = \ln[r^2 P''(r)]$, $S_0 = S(r_0), \beta_0 = \beta(r_0)$ and r_0 is given constant reference range. Differentiating equation 2.9 with respect to r gives

$$\frac{dS}{dr} = \frac{1}{\beta}\frac{d\beta}{dr} - 2\sigma \qquad 2.10$$

Above equation can be solved only if we know the relationship between β and σ. Traditional way to account for dependency between β and σ is to assume a power law relationship of the form

$$\beta = B_0\sigma^k, \qquad 2.11$$

where B_0 and k are constants. Substituting this into equation 2.10 we obtain differential equation of the form:

$$\frac{dS}{dr} = \frac{k}{\sigma}\frac{d\sigma}{dr} - 2\sigma \qquad 2.12$$

The equation 2.12 is a nonlinear ordinary differential equation but it is of the form of Bernoulli or homogeneous Ricatti equation (*Weisstein E. W. at* http://mathworld.wolfram.com/RiccatiDifferentialEquation.html) and can be transformed to a first order linear form, solution to which is:

$$\sigma(r) = \frac{\exp[(s - s_0)/k]}{\sigma_0^{-1} - \frac{2}{k}\int_{r_0}^{r}\exp[(s - s_0)/k]dr'}, \qquad 2.13$$

where $\sigma_0 = \sigma(r_0)$. A priori knowledge of σ_0 is required to evaluate equation 2.13. The major drawbacks of equation 2.13 are that calculations of σ involve the ratio of two numbers that normally decrease with range due to attenuation and denominator is a subtraction of two big numbers. This makes solution of the form equation 2.13 highly unstable for small measurement errors. *Klett* (1981) has shown remarkably simple way out of this problem. One can get equivalent solution of equation 2.12 using reference range r_m so that solution generated for $r \leq r_m$ rather than for $r \geq r_0$ as before. New form of the solution will be

$$\sigma(r) = \frac{\exp[(s - s_m)/k]}{\sigma_m^{-1} + \frac{2}{k}\int_r^{r_m} \exp[(s - s_m)/k]dr'}, \qquad 2.14$$

where $S_m = S(r_m)$ and $\sigma_m = \sigma(r_m)$. These seemingly small changes contribute significantly to the stability of solution. The solution is in the form of two numbers that becomes progressively larger and larger. In order to get σ, one has to know σ_m a priori, which is usually not available. However, this is not a problem in case of vertical measurements from ground. This is because far end of profile (r_m) is in free troposphere or stratosphere where values of σ are very small and does not exhibit large day to day variability. One may start with a guess value or climatological value. Calculations for successive lower altitudes depend weakly on the choice of σ_m because of the form of the denominator in equation 2.14. In the end of this section it is shown that error due to guess value of σ_m is less than 1%. For the full discussion of sensitivity of solution with different guess values one may see *Klett* (1981). *Klett* (1985) has shown the improvement for air molecules scattering and variable backscatter-to-extinction ratio (i.e. B_0 in the equation $\beta = B_0\sigma^k$) and presented final equation (equation number 22 in *Klett,*1985) in the form of backscattering coefficient. For most practical purposes k is assumed to be equal to one. So extinction profile can be obtained by dividing backscattering profile with B_0. However, it is more advisable to get extinction profile straight from solution, as this is the physical quantity required for estimate of aerosol

radiative effect. *Kaestner* (1986) presents the solution of the lidar equation 2.8 in terms of extinction values. Following equations show the solution given by *Kaestner* (1986).

$$\sigma_M(r) = -\frac{\beta_R(r)}{B_M(r)} + \frac{Z(r)}{N(r)}, \qquad 2.15$$

with

$$Z(r) = \frac{r^2 \cdot P(r)}{B_M(r)} \cdot \exp\left\{2 \cdot \int_r^{r_m} \left[\frac{1}{B_M(r')} - \frac{1}{B_R}\right] \cdot \beta_R(r')dr'\right\},$$

$$N(r) = \frac{r_m^2 \cdot P_m}{\beta_{Rm} + B_{Mm}\sigma_{Mm}} + 2 \cdot \int_r^{r_m} Z(r')dr',$$

where P is equal to P" in equation 2.8 and hence forth double prime are dropped for sake of brevity. Subscript M denotes the aerosol (Mie scattering) and R denotes the gaseous (Rayleigh scattering) extinction or backscattering as the case may be. Subscript m denotes the quantity at range r_m (maximum range). σ and β are volume extinction and backscattering coefficients respectively and B is backscatter-to-extinction ratio equivalent to B_0 in equation 2.11. To get the aerosol extinction using equation 2.15 two assumptions are required, one on aerosol extinction at maximum range and another on backscattering-to-extinction ratio, inverse of which is known as lidar-ratio. Henceforth lidar-ratio will be denoted with symbol '*L*'. Lidar ratio remains to be the largest source of systematic error in retrieving aerosol extinction (*Hughes et al.*,1985, *Kovalev,* 1995). Value of the lidar ratio ranges from 20 to 80 sr over time and space as shown by *Young et al.* (1993), *Marenco et al.*(1997), *Anderson et al* (2000), *Welton et al.* (2000), *Voss et al.* (2001), *Liu et al.* (2002), *Welton et al.* (2002), *Sakai et al.* (2003) depending upon aerosol type, size distribution and relative humidity. As far as regional variability is concerned *L* value of about 40 sr for arid and semi arid region, around 30 sr for maritime aerosol and around 60 sr for urban and biomass burning are reported. Ahmedabad is an urban semi-arid region. We have used the constant lidar ratio 40

sr for extinction calculation through out the period. Lidar ratio was found to be 44 sr during one of the experiment carried out over Mt Abu (a hill-station about 250 km north of Ahmedabad) following *Young et al.* (1993). One check for correctness of algorithm is how well observations made by one type of instrument matches with other type of instrument. Aerosol optical depth measurements using sun-photometer and aerosol optical depth measurements by integrating extinction profile are measurements of same quantity using two different methods. Correlation between them is checked and slope of the line is found close to one (Figure 2.6).

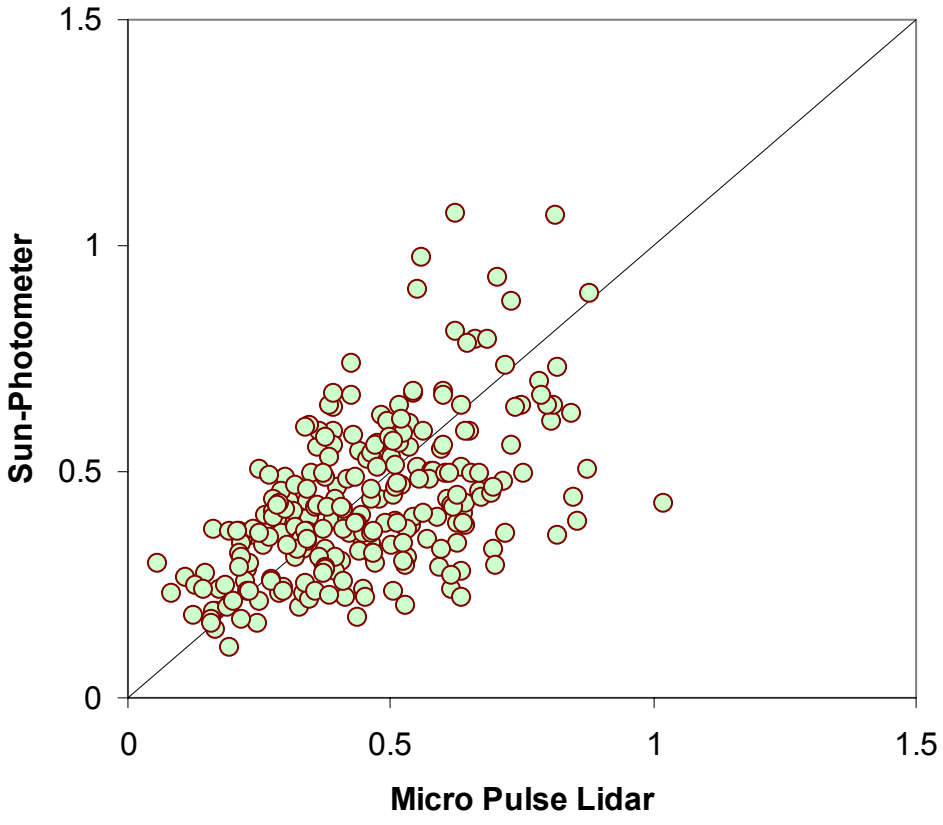

Figure 2.6. Scatter plot between sun-photometer derived AOD and micro pulse lidar derived AOD. Solid line through the middle of data point is 1:1 line.

In Figure 2.6 scatter of data points arise because of the fact that sun-photometer measurements are mainly during afternoon hours whereas lidar measurements are

mainly after sun-set hours. Also, scatter in data points due to error in lidar-ratio cannot be ruled out completely. In the absence of measurements of lidar-ratio it is justified to use constant lidar-ratio for all seasons because single scattering albedo (SSA) which is like lidar-ratio depends on aerosol type, does not show systematic variation with season over Ahmedabad (discussed in Chapter 3).

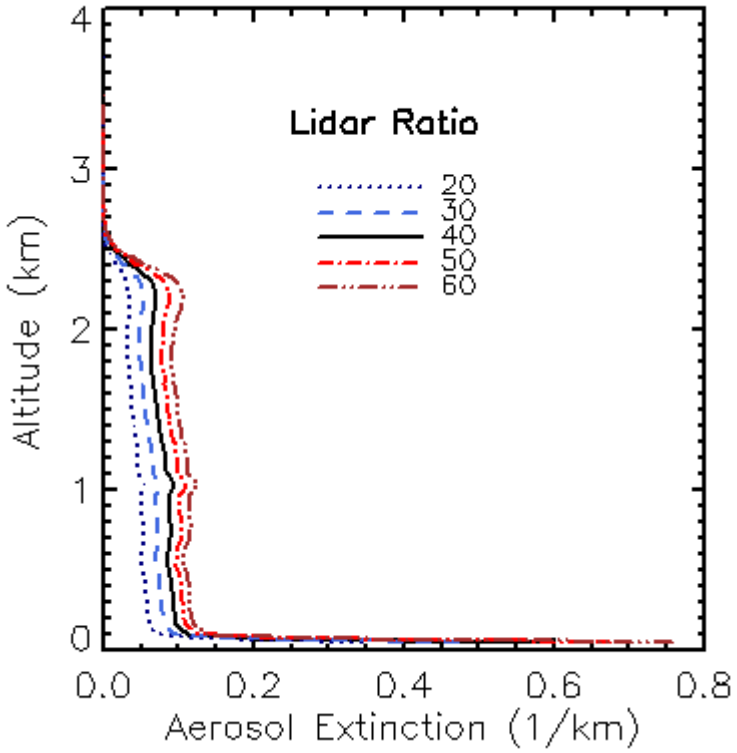

Figure 2.7. Aerosol extinction profiles obtained by using different values of lidar ratio for the observation made on 15 Feb 2002.

Errors in the extinction profile are mainly because of various assumptions involved rather than instrument precision and noise. Assumption related to boundary condition i.e. extinction value at far end (σ_{max}) is found not to affect the accuracy of extinction profile. We carried out calculations of extinction profiles using different values of σ_{max} for the same set of measurements. When σ_{max} varied from 0 to 10^{-3} km^{-1} changes in the extinction coefficient in the boundary layer is found to be less than 1%. The average extinction coefficient in the altitude range 7

to 10 km (i.e. where guess value σ_{max} is required) observed by SAGE-II (http://www-sage2.larc.nasa.gov) satellite is 5 x 10^{-4} km^{-1}.

Similar sensitivity analysis was also carried out for lidar ratio. Figure 2.7 shows the calculations of extinction profiles for different values of lidar ratio for the same set of measurements done on 15 February 2002. As described earlier extinction calculations for data analysis were carried out using lidar ratio 40, however lidar ratio for Ahmedabad like stations can be in the range of 30 to 50. Changing lidar ratio in the range of 30 to 50 changes the extinction profile in boundary layer by 15 to 20 %. Changes due to change in Lidar ratio are like shifting the whole profile by a constant value. Hence even if error is of the order of 20% it will not affect the conclusions regarding relative distribution of aerosol with height. In the absence of independent measurements to calibrate, error in extinction profile is quoted 25%.

2.2 Total Columnar Aerosol Optical Depth

Aerosol optical depth (AOD) is one of the key aerosol optical property and an important input to climate modelling studies. It critically depends upon the amount, size-distribution and chemical composition of aerosols. It is a measure of the attenuation of radiation while passing from top of the atmosphere to surface by aerosol. The loss of intensity *F* over the infinitesimal slice *dx* as a result of light absorption or scattering is (*Seinfeld and Pandis,* 1998):

$$dF = -\sigma_i F dx \qquad 2.16$$

where, σ is extinction coefficient (m^{-1}) of the medium. For a finite path between x_1 and x_2, integration of equation 2.16 is gives

$$F(x_2) = F(x_1)\exp(-\tau) \qquad 2.17$$

where τ is the optical thickness (dimensionless) between x_1 and x_2 and is given by

$$\tau = \int_{x_1}^{x_2} \sigma(x)dx \qquad 2.18$$

This result is known as the *Beer-Lambert law of extinction*. When x is measured vertically in the atmosphere the optical thickness is referred to as *optical depth*.

2.2.1 Instrumentation

AOD is calculated by integrating aerosol extinction profile obtained using lidar as evident from equation 2.18. Results pertaining to AOD over Ahmedabad, which are discussed in present work, are mainly obtained in this way. However, AOD can also be measured directly by using a Sun-Photometer. Observations of AOD during field campaigns and also over Ahmedabad were also made using Sun-Photometer, which are used in the calculation of radiative forcing discussed in Chapter 5. Present section describes the Sun-Photometers in detail.

Table 2.2. Characteristics of the Sun-Photometers used in the present study. Last column shows the total optical depth due to Rayleigh scattering by air-molecules (τ_{ray}) and molecular absorption (τ_{mol}) for standard atmosphere.

Instrument	Central Wavelength (nm)	Full Width at Half Maximum (FWHM; nm)	Optical Depth ($\tau_{ray} + \tau_{mol}$)
Sun-Photometer (in-house make)	400	15	0.366
	497	13	0.156
	668	12	0.058
	750	9	0.030
	875	12	0.015
	954	18	0.010
	1058	25	0.007
Microtops-II (columnar ozone and water vapour)	300	2	---
	305.5	2	---
	312.5	2	---
	937	10	---
	1021.8	11	---

Instrument	Central Wavelength (nm)	Full Width at Half Maximum (FWHM; nm)	Optical Depth ($\tau_{ray} + \tau_{mol}$)
Microtops-II (aerosol optical depth)	380	~10	0.435
	440	~10	0.235
	500	~10	0.138
	675.6	11	0.037
	871.5	10	0.011

There are three different Sun-Photometers used in present study. Table 2.2 summarizes the major characteristics of these Sun-Photometers. A filter Sun-Photometer built in PRL, was used for the measurement of AOD over Maitri-Antarctica (*Gadhavi and Jayaraman*, 2004), Gujarat, Mt. Abu, Indore (*Gupta et al.*, 2003) and over Ahmedabad until a commercially available Sun-Photometer (MICROTOPS-II) from Solar Light Co. acquired. A Sun-Photometer can also be used for ozone and water vapour measurements by selecting appropriate wavelengths. One such Sun-Photometer is used to measure columnar ozone and water vapour concentrations. Ozone and water vapour measurements are used for correcting AOD measurements as well as radiative forcing calculations.

2.2.2 Theoretical Basis and Calibration of the Sun-Photometer

Figure 2.8 shows the block diagram of the Sun-Photometer developed at PRL. A Sun-Photometer essentially measures the sun light intensity at selected wavelengths. Baffle in front of photo detector is used to minimize diffuse radiation by reducing the field of view (FOV) of Sun-Photometer. FOV of PRL built Sun-Photometer is around 4^0 whereas that of Microtops is 2.5^0. Equation 2.17 may be rewritten in following form as discussed in *Gupta et al.* (2003)

$$\tau(\lambda) = -\frac{1}{\mathrm{m}}\left\{\ln\left(\frac{I(\lambda)}{I_0(\lambda)}\right) - 2\ln\left(\frac{r_0}{r}\right)\right\} \qquad 2.19$$

where τ is total optical depth, I is the instantaneous solar radiation intensity measured at ground level. I_0 is a top of the atmosphere (TOA) radiation intensity. I and I_0 need not be in absolute unit (W/m²), instead they can be in the form of voltages or current output of the Sun-Photometer as only the ratio of intensities are used. Symbol 'm' denotes relative airmass, a ratio of path length light beam has actually travelled in the atmosphere to that it would have travelled in vertical direction, and depends upon solar zenith angle. Symbols r and r_0 in second term of equation 2.19 are Sun-Earth distances when measurements of I and I_0 were made. In plane parallel approximation m can be obtained by taking inverse of cosine of zenith angle. However, this approximation can introduce significant error in airmass calculation at high solar zenith angle because of curvature of the Earth and refractive index of air.

Young (1994) has given one approximate formula to calculate airmass from true solar zenith angle that accounts for the effects of refractive index and curvature of the Earth.

$$m = \frac{1.002432\cos^2(\theta) + 0.148386\cos(\theta) + 0.0096467}{\cos^3(\theta) + 0.149864\cos^2(\theta) + 0.0102963\cos(\theta) + 0.000303978} \qquad 2.20$$

where θ is the solar zenith angle. Precision given in the coefficients in equation 2.20 is intended only to prevent round-off errors near horizon; it does not indicate either the true accuracy of the formula or the precision of individual coefficients. Calculations of airmass using equation 2.20 are better than 1 % even at horizon and taking into account the changes in meteorological conditions such as temperature, pressure etc. Solar zenith angle can be calculated from latitude, longitude of the place and time of measurements by astronomical formulae. Computer code to calculate solar zenith angle is prepared from the algorithm given by *Meeus* (1991). Left side of equation 2.19 is total optical depth, which is sum of optical depths by aerosol, scattering by air molecules and absorption by gases at that particular wavelength.

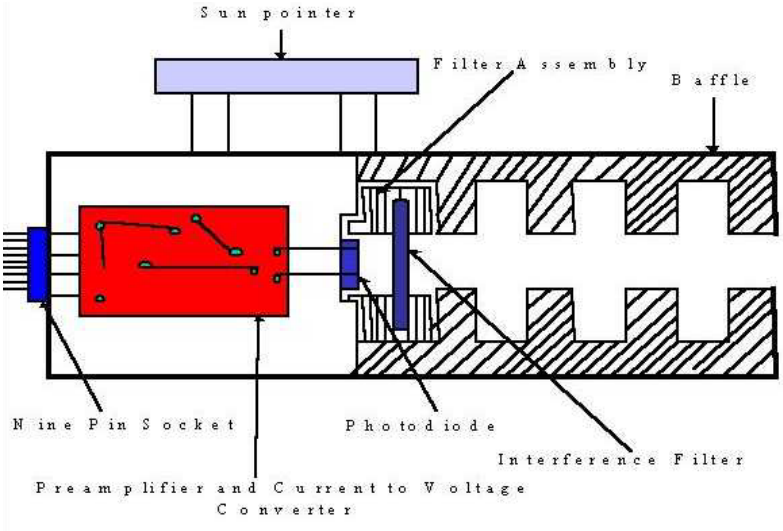

Figure 2.8. Block diagram of the Sun-Photometer developed at PRL.

I_0 in equation 2.19 can be calculated from ground based measurements using Langley method (*Liou*, 2002). In this technique log of intensity measured at ground level is plotted as a function of airmass. A line is fitted to data points by least square fitting. Intercept of line on Y-axis gives $\log_e(I_0)$. Ideally I_0 should remain constant over different places and time however because of deterioration in detector or filter characteristics value of I_0 can change. Hence, Sun-Photometers are repeatedly calibrated. Figure 2.9 shows a typical Langley plot for data obtained over Maitri-Antarctica on 21st February 2001 for 400 nm.

Inaccuracy in I_0 is the largest and most difficult to define source of systematic error (*Shaw*, 1983). Another sources of error in AOD measurements are radiometric uncertainties due to bias and precision of instrument that is around 5 %. Optical depth is calculated by *Beer-Lambert law* that ignores the contribution of forward scattering to the measured flux. Forward scattering in FOV of a Sun-Photometer tends to decrease the measured AOD. *Jayaraman et al.* (1998) estimates less than 8% decrease in AOD for 400 nm and less than 4% in case of 1058 nm wavelength for the Sun-Photometer used in the present study. Errors for Microtops II would be certainly less than this as they have smaller FOV. Overall error estimated for hand held Sun-Photometer built in PRL is around 15%.

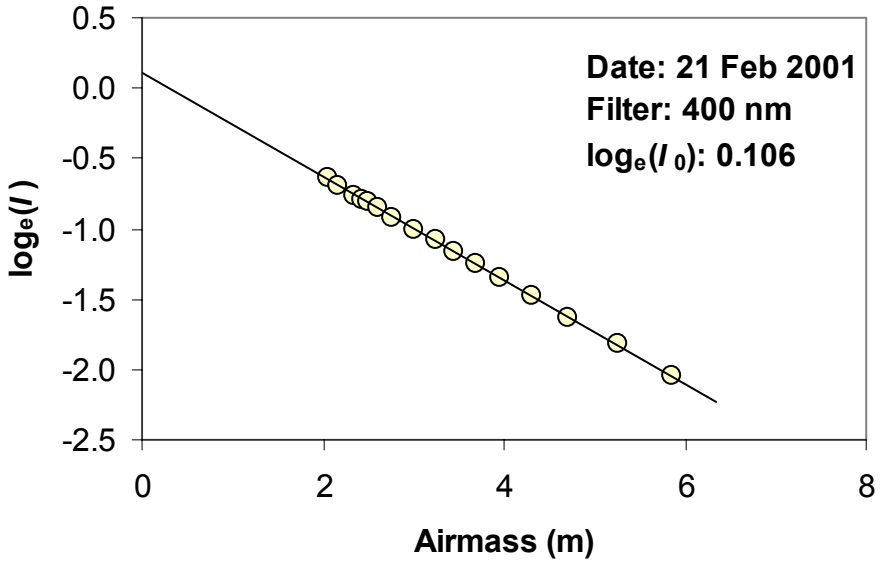

Figure 2.9. Calculation of I_0 by Langley plot technique for filter 400 nm from data obtained over Maitri-Antarctica on 21 Feb 2001.

AOD is obtained by subtracting the Rayleigh optical depth and molecular absorption optical depth from total optical depth. For Rayleigh optical depth, average scattering cross-section for air molecules is calculated using an empirical formula given by *Nicolet* (1984).

$$\sigma_{RS} = 4.02 \times 10^{-28} \Big/ \lambda^{4+x} \; cm^2 \qquad 2.21$$

where

$$\begin{aligned} x &= 0.389\lambda + 0.09426/\lambda - 0.3228; \qquad 0.2\mu m < \lambda < 0.55\mu m \\ x &= 0.04; \qquad\qquad\qquad\qquad\quad 0.55\mu m \le \lambda < 1.0\mu m \end{aligned} \qquad 2.22$$

and λ is wavelength expressed in μm. One can calculate Rayleigh optical depth by multiplying σ_{RS} to columnar number density of air molecules. It is 2.153 x 10^{25} molecules/cm^2 for standard atmosphere at mean sea level. However, it can change due to change in pressure, which is accounted by multiplying Rayleigh optical depth calculated for mean sea level by ratio of measured ambient pressure with

that of standard atmospheric pressure. Further, to account for finite bandwidth of filters, transmission weighted mean of optical depth is used. Optical depth due to molecular absorption is calculated using radiative transfer code SBDART (further discussed in Chapter 5). Important gases for molecular absorption for the present filters of the Sun-Photometers are Ozone, Water vapour and Oxygen. Ozone and Water vapour are variable gases in the atmosphere. Values of columnar ozone concentration are obtained from MICROTOPS-II measurements and substantiated by *TOMS* satellite data whenever measurements were not available. Columnar water vapour measurements were done using one of the MICROTOPS-II and substantiated by *NCEP* reanalysis data whenever measurements of water vapour were not available. Selection of filters for AOD measurements is done in such a manner that highest contribution of molecular absorption optical depth is less than 10 %. Last column in Table 2.2 shows the sum of typical optical depth due to Rayleigh (τ_{rayleigh}) and molecular absorption (τ_{mol}), which needs to be subtracted from total optical depth in order to get AOD (Equation 2.23). Rayleigh optical depth is calculated for standard atmosphere. Molecular absorption in case of hand held sun-photometer is calculated for average condition over Maitri-Antarctica and that of Microtops-II is for tropical atmosphere.

$$\tau_{aero} = \tau_{total} - \tau_{rayleigh} - \tau_{mol} \qquad 2.23$$

2.3 Aerosol Scattering and Absorption Coefficients

In addition to extinction profile and AOD, other optical properties of aerosol, which are important for modelling aerosol radiative forcing are single scattering albedo (SSA) and asymmetry parameter (g). Single scattering albedo is a measure of the proportion of scattering and absorption in the light extinction by aerosol. It is defined as a ratio of scattering coefficient to extinction coefficient

$$\omega = \frac{\sigma_{scat}}{\sigma_{ext}} \qquad 2.24$$

where, σ_{scat} is the scattering coefficient (m^{-1}) and σ_{ext} is the extinction coefficient (m^{-1}). Extinction coefficient is a sum of scattering coefficient and absorption coefficient.

2.3.1 Instrumentation

Observations of scattering coefficient are carried out using Nephelometer (Model M903, Radiance Research) at wavelength 530 nm. Nephelometer measures light scattering in an airflow that passes through the scattering chamber of the instrument. Air volume is illuminated by diffuse light source from side. Photomultiplier tube views the dark trap through a scattering conical volume define by baffles with a hole in centre. Baffles are arranged in such a manner that photomultiplier tube does not see any surfaces. This geometry is chosen because light measured by photomultiplier is nearly proportional light scattered in all directions. So by calibrating Nephelometer volume scattering coefficient in the unit of m^{-1} is obtained.

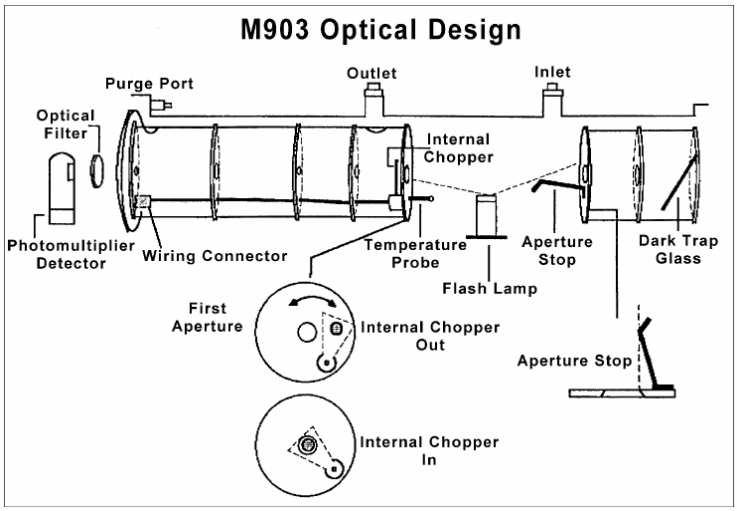

Figure 2.10. Block diagram of the Nephelometer (model M903 Radiance Research, USA).

Calibration of nephelometer involves two steps known as zero calibration and span calibration. Zero calibration of nephelometer is done by measuring the scattering by particle free air. Measured scattering for particle free air is recorded

for subtraction from sample air. Scattering by air molecules will depend upon pressure, temperature and relative humidity (RH). Nephelometer has in-built pressure, temperature and relative humidity sensors. Since operating condition and calibration condition were same within 3% of pressure, no special correction is applied for the change in pressure. Sample air is pre-heated before measuring the scattering coefficient and hence very small differences are possible in temperature and RH between calibration and actual measurements. Span calibration is done using CO_2 gas whose scattering coefficient is higher by a factor of 2.61 than that of particle-free air. There are two sources of errors in scattering coefficient measurements. One is called wall scattering, which defines all type of stray light entering into Photomultiplier tube. However, this is not a serious problem for nephelometer, which is calibrated regularly, and stray light is expected to be same for particle-free air and aerosol-laden air. Another serious error occurs because of very nature of aerosol scattering i.e. Mie Scattering. Integrating nephelometer cannot measure scattered light at angles close to 0 and 180 degrees. For small particles, this is not a problem as very little light is scattered in forward direction than compared to bigger particles where large amount of light is scattered in forward direction. This error is known as truncation error. Since there is no direct way to correct this error and any indirect way may involve assumptions, which not necessarily improve the results, truncation error in measurements are ignored. Rest of the error in scattering coefficients are in the range 3 to 4 %.

Measurements of absorption coefficients are carried out using Aethalometer (Model AE-42, Magee Scientific) at seven wavelengths i.e. 370, 450, 520, 590, 660, 880 and 950 nm. Aethalometers are primarily used to measure black carbon (BC) or soot concentration in air. Measurements of soot particles are carried out using optical attenuation method. Sample air with constant flow rate for a known period is passed through a quartz filter paper and change in attenuation of light beam is monitored. Soot particles have one of the largest broad-spectrum absorption cross-sections approximately 10 m^2/gm at wavelength 550 nm. This absorption is proportional to the wavelength of the incident light. Change in attenuation is

calibrated to mass concentration of BC. However there are other aerosol species in the atmosphere who have absorption in visible wavelength e.g. mineral dust, iron, etc. Hence, measurement of BC may be overestimated or can be corrected by studying the spectral dependence of absorption. However, error in BC mass is not a problem for this work since aethalometer measures the attenuation coefficient that is indeed required to calculate SSA. It is found that error due electronic noise, optical noise, and flow rate inaccuracy is less than 1%. Manufacturer of aethalometer states the accuracy in the range of 2 to 3 % by showing results from simultaneous measurements with other instruments, which uses different mechanism to measure attenuation of BC concentration.

2.4 Aerosol Size Distribution

Asymmetry parameter (*g*) of aerosol depends on aerosol size distribution and refractive index of particles. It is a ratio of photons scattered in forward direction to total scattered photons. Value of *g* ranges from -1 to +1. When photons are completely back-scattered, *g* is -1 and for completely forward scattering *g* is +1. For symmetrical scattering *g* will be 0. For ISRO-GBP land campaign (discussed in Chapter 4) calculations of *g* were carried from size distribution. For rest of the places measurements of size distributions are used as a proxy to constrain the model estimates of *g*.

2.4.1 Instrumentation

A quartz crystal microbalance cascade impactor (QCM) manufactured by California Measurements Inc, USA is used to measure the mass size-distribution of aerosols (*Gadhavi and Jayaraman*, 2004). The instrument has 10 stages with each stage sensitive to a specific size range of particles. The radii at which the collection efficiency is maximum are 8.64, 4.26, 2.24, 1.08, 0.55, 0.29, 0.16, 0.07 and 0.03 μm respectively for the stags 2 to 10. The full width at half maximum of efficiency changes from 7 to 0.03 μm for stages 2 to 10. As the name implies QCM works on the principle of cascade impactor but unlike the traditional cascade impactors, which use filter paper, QCM uses quartz crystal to give the aerosol mass size

distribution in near real time (*Wood*, 1979). In the cascade impactor several stages are cascaded and each subsequent stage has smaller size of nozzle. Quartz crystals are placed opposite to nozzles. Air stream coming out of nozzle takes sharp turn because of the crystal. Depending upon the size of the particle (smaller or bigger) either it will take turn with air stream or it may get impacted on crystal. Crystal surfaces are greased to capture the impacted particles. Quartz crystals have property that their resonance frequency is changed with change in their mass. Hence, by monitoring change in frequency the mass accumulated in given time over crystal is calculated. Since subsequent stages have smaller size of nozzle, speed of air coming out of nozzle will be increased and hence particles which were able to escape with airflow in previous stage, now will be impacted on crystal. There are several sources of error for example re-entrainment of particle from crystal surface, wall loss, change in relative humidity, electronics noise, etc. Error is estimated to be ~15% by running QCM with collocated Anderson impactor (*Jayaraman et al.*, 1998).

TEMPORAL VARIATION OF AEROSOL PROPERTIES OBSERVED OVER AHMEDABAD

3.1 Aerosol Vertical Profile

Daily mean aerosol extinction profiles for clear sky are calculated from 30 min averaged extinction profiles observed within 3 hours after the sunset (see Chapter 2). Monthly mean aerosol extinction profiles are calculated by taking average of daily mean extinction profiles for that month. Figure 3.1 to 3.6 show monthly mean extinction profiles from January to December. Extinction profiles for the years 2002, 2003 and 2004 are shown with black (solid), red (dotted) and blue (dashed) lines respectively. Horizontal bars over data points show standard deviation from the mean. Total period covered is from February-2002 to November-2004. There are only limited number of profiles in Feb-2004 as the micro pulse lidar (MPL) was taken out for field campaign (to be discussed in Chapter 4).

There is a large day to day variability observed in the daily mean aerosol profiles. It has resulted in large standard deviation found in almost all the months. Standard deviation is high in boundary layer than in free troposphere where extinction values are also high. Exception to this are months of June, July and August, where standard deviation is high near the top of boundary layer than lower altitude. Around altitude level 1 km, standard deviation is in the range of 17 % to 67 %. This is because of short residence time of aerosol and inhomogeneous distribution of sources of aerosol near the measurement site. *Jayaraman et al* (2001) have found that variability in columnar and surface aerosol properties are high near the coastal India than over southern Indian Ocean. In the southern Indian Ocean there is no major source of aerosols except sea salt particle produced by breaking of waves, which are uniformly distributed with respect to measurement location. Hence, air parcel coming from any direction may contain similar aerosol

concentration. But urban agglomeration, big factories, thermal power stations, etc constitute point sources in comparison to ocean and hence depending upon the transport and other meteorological history of airmass, it may contain high or low aerosol concentration resulting in large variability of aerosol properties.

Seasonal and inter-annual variations are so pronounced that they can be discerned in spite of large standard deviations. Comparison of the monthly mean aerosol extinction values in the boundary layer for the year 2003 shows that they are higher than the year 2002 for corresponding months. Average extinction in altitude range 0.7 to 1 km during February 2003 is about 0.171 km^{-1} which is about factor of two higher than February-2002 values. Similar magnitude of difference is observed between September 2002 and 2003, where 2003 extinction value is 0.307 km^{-1} and 2002 extinction value is 0.17 km^{-1}. Figure 3.7 shows the comparison of average extinction values in the range 0.7 to 1.0 km between the year 2002 and 2003. In case of July, year 2002 and 2003 extinction values are comparable up to altitude 1.5 km but 2002 extinction values are higher between 1.5 and 3.5 km (Figure 3.4). During the last two months of the year i.e. November and December, extinction values are comparable between the 2002 and 2003. In November average extinction value for 2003 in the altitude range 0.7 to 1 km is 12% higher than 2002, whereas for December, extinction values in same altitude range for 2003 are 14% lower than 2002 (Figure 3.7). Extinction values during year 2004 are more or less comparable to 2003 but 2003 values are slightly higher than 2004 values. Low values during February 2004 needs to be ignored since they consist very few numbers of data and may not be overall feature of the month. Difference in extinction values in the altitude range 0.7 to 1 km between 2003 and 2004 is within 20% for most of the months.

(a)

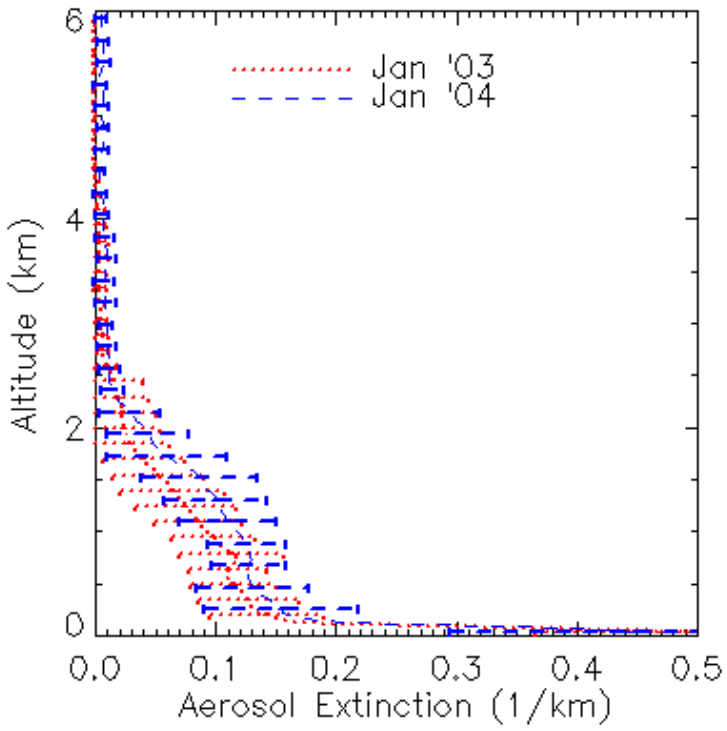

(b)

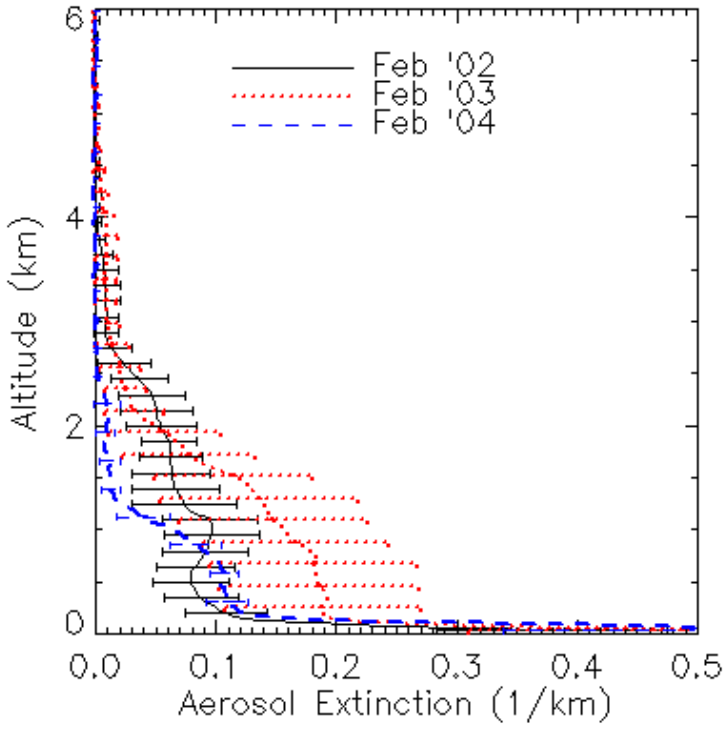

Figure 3.1. Monthly mean extinction profiles during (a) January and (b) February for the years 2002 , 2003 and 2004. Horizontal bar over data points show ±1 standard deviation from the mean.

(a)

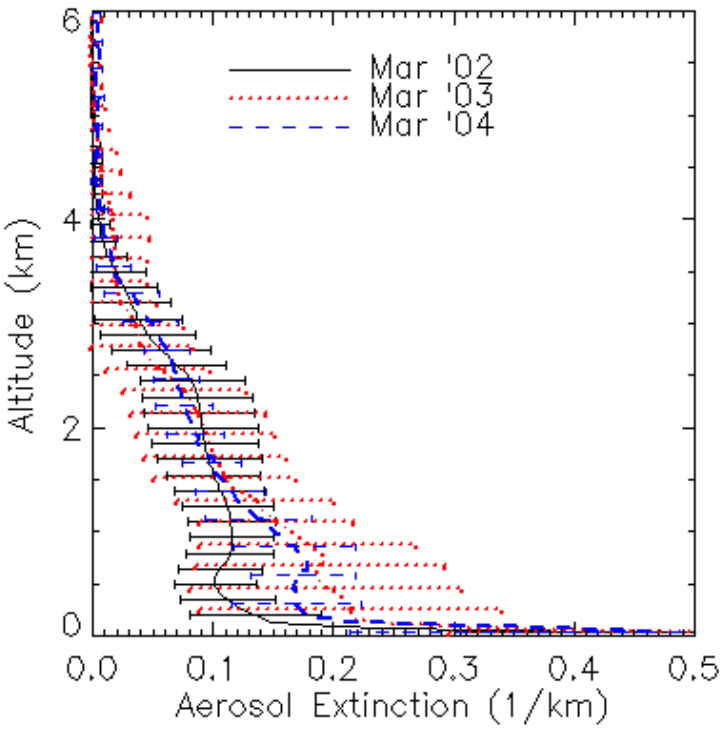

(b)

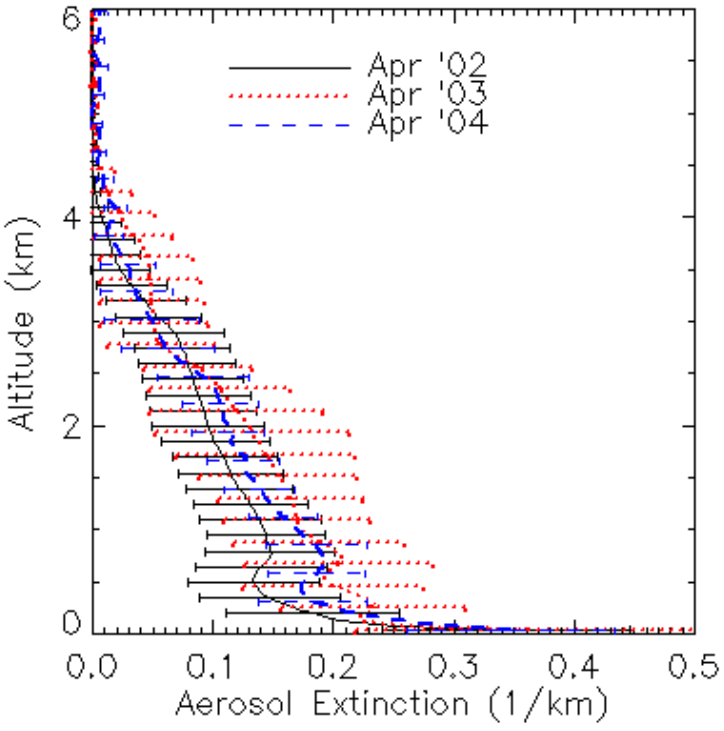

Figure 3.2. Monthly mean extinction profiles during (a) March and (b) April for the years 2002, 2003 and 2004. Horizontal bar over data points show ±1 standard deviation from the mean.

(a)

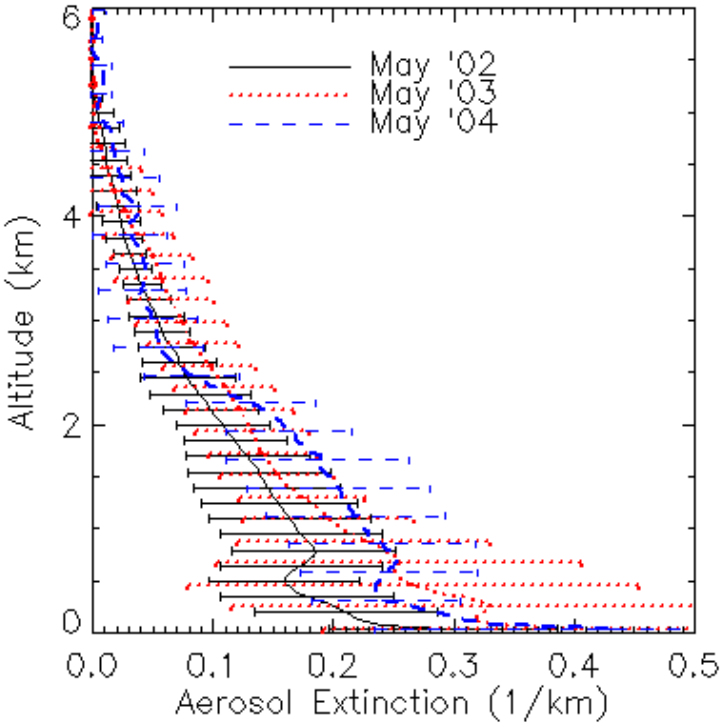

(b)

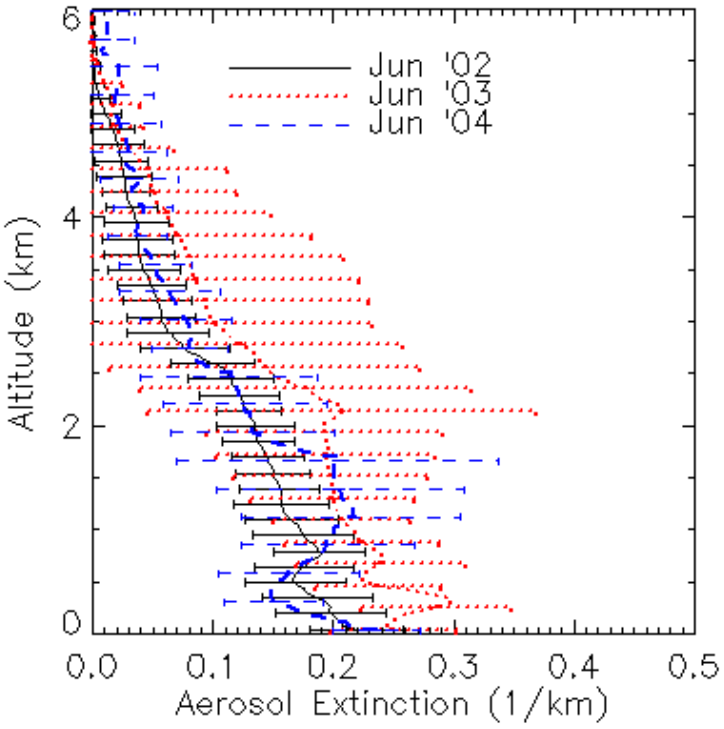

Figure 3.3. Monthly mean extinction profiles during (a) May and (b) June for the years 2002, 2003 and 2004. Horizontal bar over data points show ±1 standard deviation from the mean.

(a)

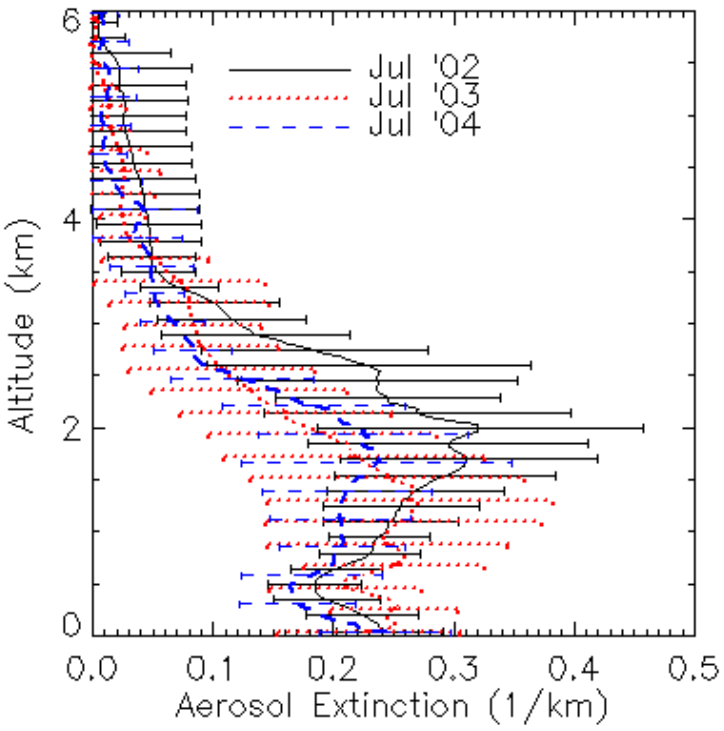

(b)

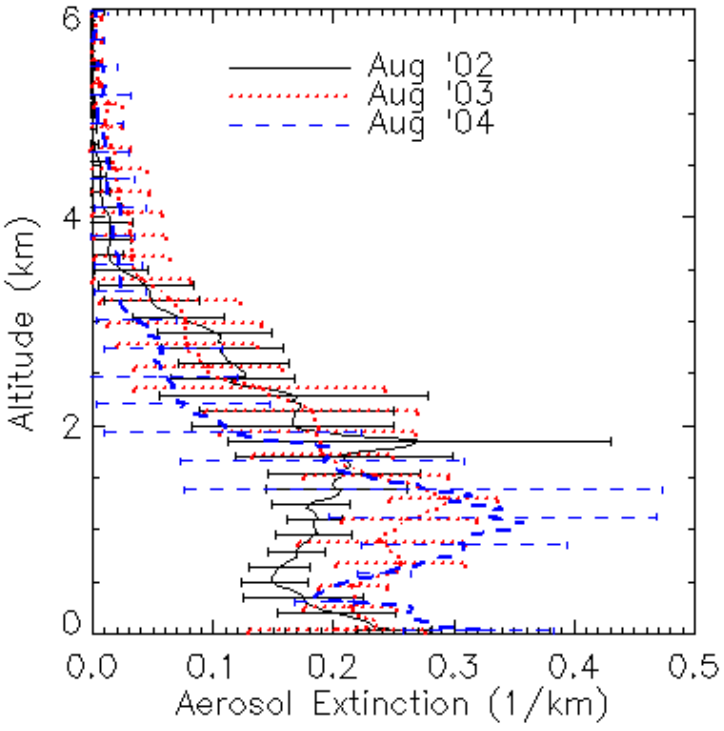

Figure 3.4. Monthly mean extinction profiles during (a) July and (b) August for the years 2002, 2003 and 2004. Horizontal bar over data points show ±1 standard deviation from the mean.

(a)

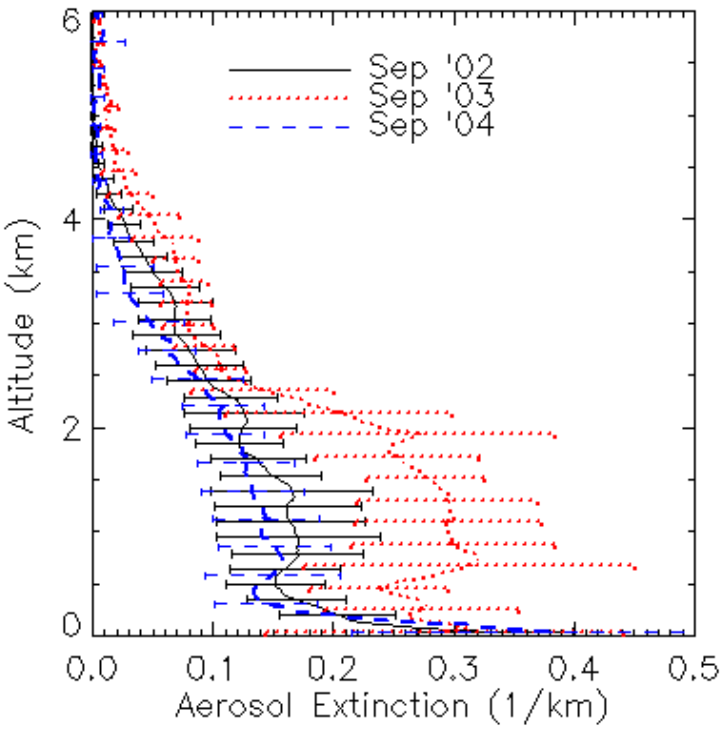

(b)

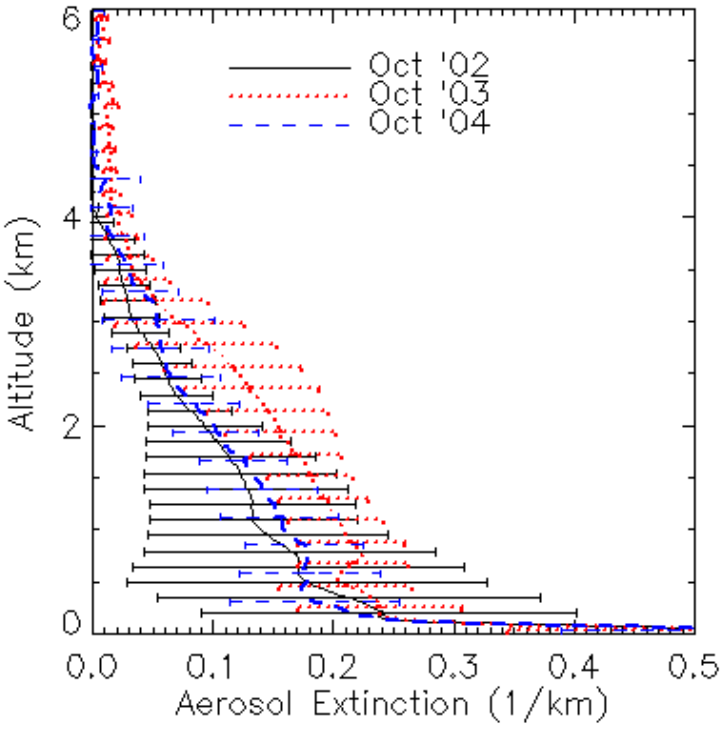

Figure 3.5. Monthly mean extinction profiles during (a) September and (b) October for the years 2002, 2003 and 2004. Horizontal bar over data points show ±1 standard deviation from the mean.

(a)

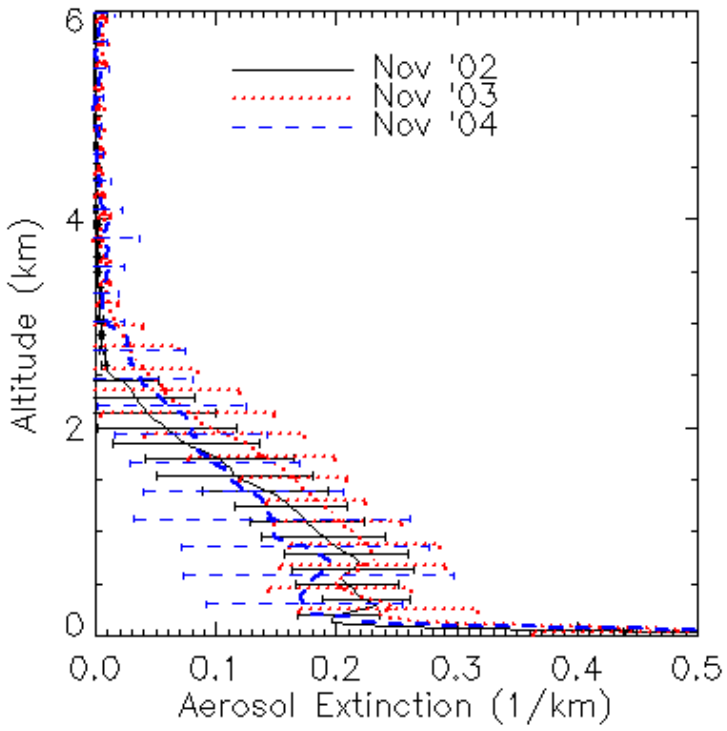

(b)

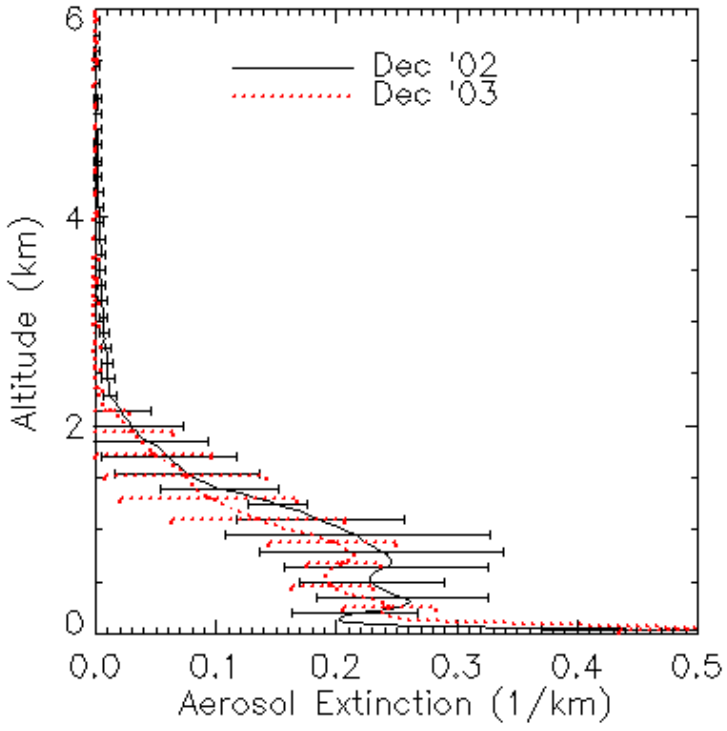

Figure 3.6. Monthly mean extinction profiles during (a) November and (b) December for the years 2002, 2003 and 2004. Horizontal bar over data points show ±1 standard deviation from the mean.

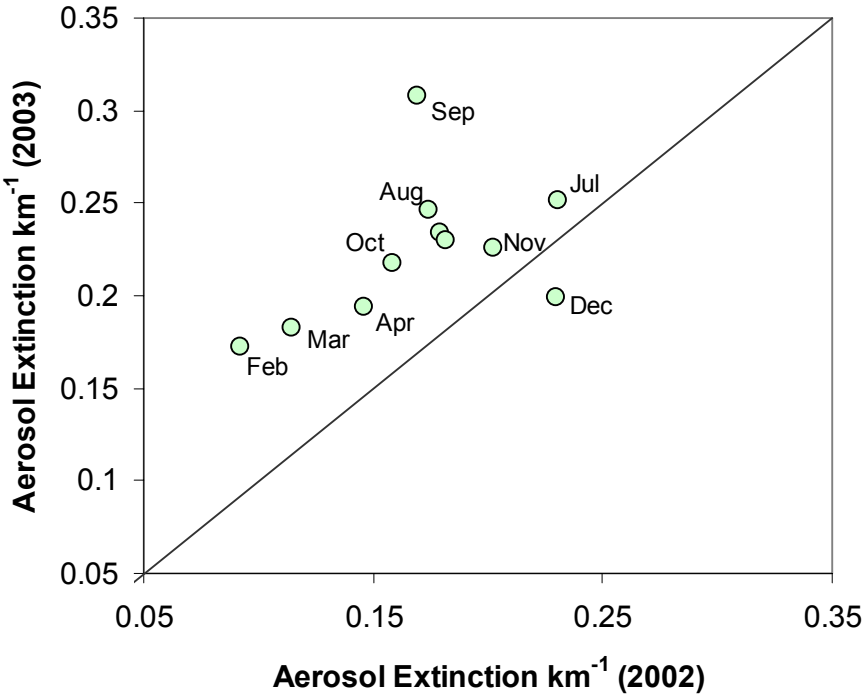

Figure 3.7 Average aerosol extinction in the altitude range 0.7 to 1.0 km is compared between year 2002 and 2003.

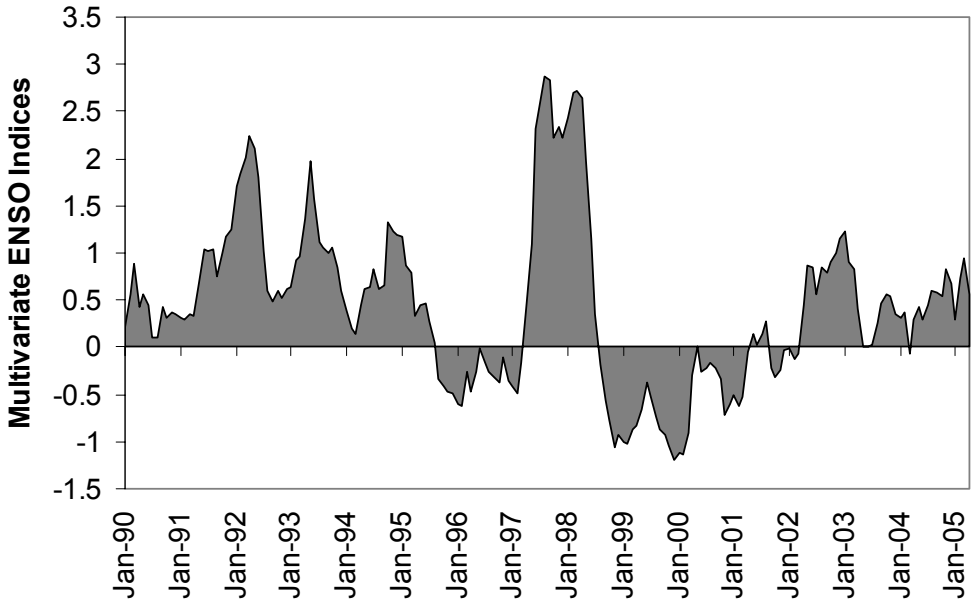

Figure 3.8. Multivariate El Niño/Southern Oscillation indices. (Data source: http://www.cdc.noaa.gov/people/klaus.wolter/MEI/)

Inter-annual variability appears to be associated with global phenomena such as the El Niño/Southern Oscillation (ENSO). Figure 3.8 shows the multivariate ENSO Index (MEI) (*Wolter and Timlin*, 1993 & 1998) from the year 1990 to 2005. Data are obtained from the web-site http://www.cdc.noaa.gov/people/klaus.wolter/MEI/. Positive value represents the warm ENSO phase (El Niño) and negative value cold ENSO phase (La Niño). Year 2002 is transition period from La Niño to El Niño phase whereas year 2003 and 2004 are more or less El Niño years. It is not clear through what mechanism ENSO affects the aerosol distribution over Ahmedabad but effect of ENSO in past is noted by other researchers over different regions of the world. *Moorthy et al.* (2001) observed high AOD during 1999 in comparison to 1998 over Trivandrum (8.5^0N, 77^0E), Mysore (12.3^0N, 76.5^0E), Visakhapatnam (17.7^0N, 83.3^0E) and Minicoy (8.3^0N, 73.04^0E) which they attribute to inter-annual variability in the position of Inter Tropical Convergence Zone (ITCZ) and associated circulation pattern. *Moorthy et al.* (2001) further note that effect of circulation pattern on aerosols is different at different locations; more will be near the equator than the northern latitudes. *Jayaraman et al.* (2001) also observed high AOD during 1999 in comparison to 1998 over the Indian Ocean, Arabian Sea and Coastal India. *Eck et al.* (2001) observe that AOD over Kaashidoo (4.966^0N, 73.466^0E) island during January to April - 1999 is higher by more than factor of two in comparison to 1998 values. As shown in Figure 3.8, year 1998 was El Niño year and 1999 was La Niño.

In order to understand the effects of season on extinction profiles it is necessary to consider the overall features of extinction profiles. Extinction profile over Ahmedabad can be divided into three layers. The lowest layer (also known as surface layer) where extinction values are usually very high and decreases rapidly with altitude up to 200 to 300 meter. Second layer starts from the top of the lowest layer where sharp changes in extinction values as function of altitude can be noticed. Extinction values decreases rather slowly in the second layer. This layer extends up to 2 to 5 km depending upon season. Extinction values in the second

layer are mainly governed by boundary layer dynamics. Third layer extends from top of the second layer, where extinction values are very low and more or less representative of free troposphere. Detail investigation of this layer (i.e. third layer) reveals that extinction values are decreasing exponentially. Aerosol extinction values for the lowest layer i.e. first layer are usually more than 0.5 km^{-1} for Jan to Apr (Figure 3.1 and 3.2) and come down to less than 0.3 km^{-1} during May to August (Figure 3.3 and 3.4). From the September onward, it rises again and becomes more than 0.5 km^{-1} for the months of October, November and December. In the second layer, the trend is reverse i.e. from January to April extinction values are low between 0.1 and 0.2 km^{-1} and increase to 0.2 to 0.3 km^{-1} during May, Jun, Jul and Aug, which again decreases to less than 0.2 km^{-1} for the last quarter of the year. It appears that the first layer is made of bigger size dust particles injected into atmosphere from the surface by action of wind or by anthropogenic activities. A study of rainwater carried out over Ahmedabad by *Rastogi and Sarin* (2005) indicates that dust particles or crustal sources dominant its chemical composition. Most of the precipitation over Ahmedabad occurs during summer monsoon, from June to September. When land surface becomes wet, it significantly curtails the supply of dust particles from land to atmosphere, which is responsible for the observed decrease in extinction value during monsoon months in the lowest layer. Figure 3.9 shows the comparison of extinction profile observed over Ahmedabad during March and June 2003 with that of observed over the Arabian Sea during March 1999. Data over Arabian Sea are obtained from INDOEX web-site; http://www-indoex.ucsd.edu/. Data shown for the Arabian Sea are mean of measurements done on-board R/V Ron Brown between the latitudes 5^0 N to 20^0 N and longitude 67^0 E to 75^0 E. Complete detail on measurements is given in *Welton et al.* (2002). Extinction values are low in the first layer over oceanic locations and increases with altitude up to 500 meter. The shape is somewhat similar but different in magnitude to what has been observed during monsoon months over Ahmedabad. Ocean surface as a source of aerosols per

square meter area is far smaller in strength than semiarid land region during dry season.

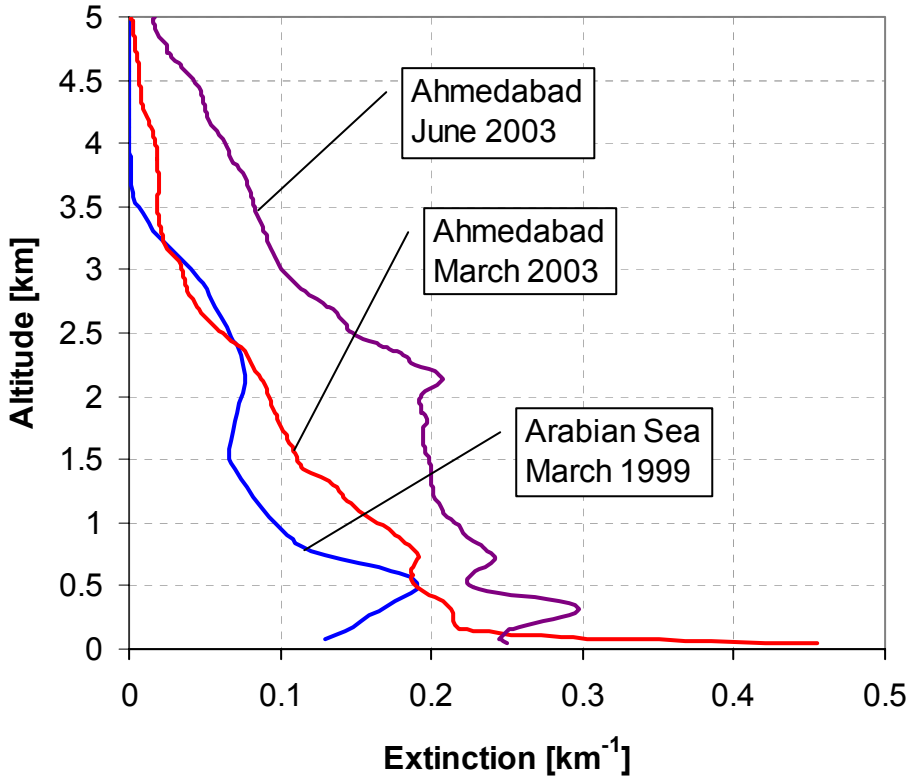

Figure 3.9. Comparison between average extinction profile over Arabian Sea and monthly mean extinction profile over Ahmedabad shows excessive aerosol in lower altitude over Ahmedabad during winter months. Data for Arabian Sea are obtained from INDOEX web-site (http://www-indoex.ucsd.edu/).

However, monsoon months are also characterised by high temperature and wind speed, which increase the boundary layer height. Aerosols that were trapped near the surface get distributed over larger spatial extent. This could also be the reason for reduction in the concentration of aerosols near the surface and increase at higher altitude. Increase in extinction values in the second layer during monsoon months could also be due to increase in relative humidity (Figure 3.13). During the monsoon months, winds are predominantly from Arabian Sea, whereas during rest of the months winds are of continental origin. Hence, the influence of transport

and increased rate of gas-to-particle conversion cannot be ruled out as possibilities for observed increase in the extinction during monsoon months in the second layer. More discussion on influence of relative humidity and wind is discussed in the section 3.2.

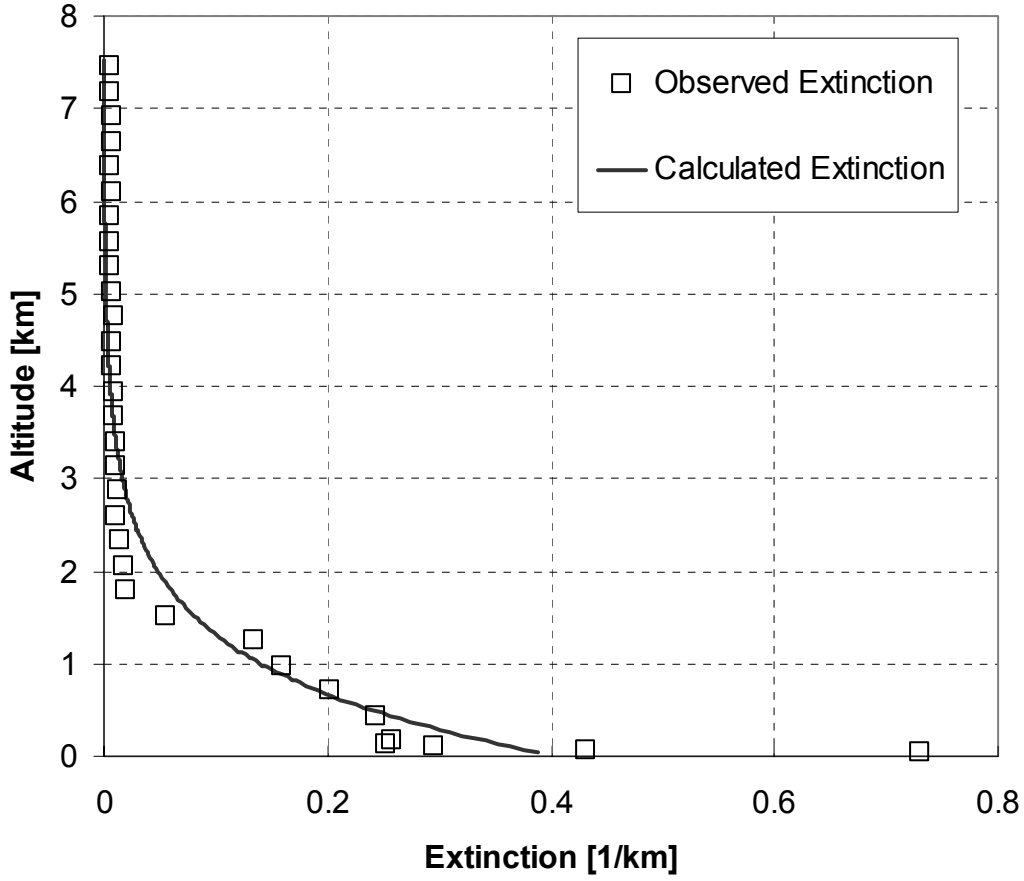

Figure 3.10. A sample aerosol extinction profile, observed on 10 Dec 2002. Squares show the observed values. Solid line is exponential curve fit to observed data. Scale height estimated for this day is 0.7 km.

3.1.1 Temporal variation of scale height of tropospheric aerosol over Ahmedabad

Though very important, measurements of extinction profiles exist only at very few locations. In such a situation, often extinction profiles are assumed to be exponentially decreasing with height, where scale height is calculated from AOD

and visibility measurements. Integrated extinction profile and scale height are good parameters for quantitative comparison of observed vertical profile, which is otherwise very difficult owing to their complex shape and high variability. Scale height (*H*) of aerosol is calculated from observed extinction profile by fitting a curve of the form $\sigma(z) = \sigma(0)\exp\left(-\frac{z}{H}\right)$, where σ is the extinction coefficient and z is the altitude from ground. Fitting of the curve was done using gradient expansion algorithm (*Press et al.*, 1998). One sample fitting is shown in Figure 3.10. Quality of fitting is not expected to be same for all the days, still scale height parameter remains to be a very good indicator of vertical distribution of aerosol.

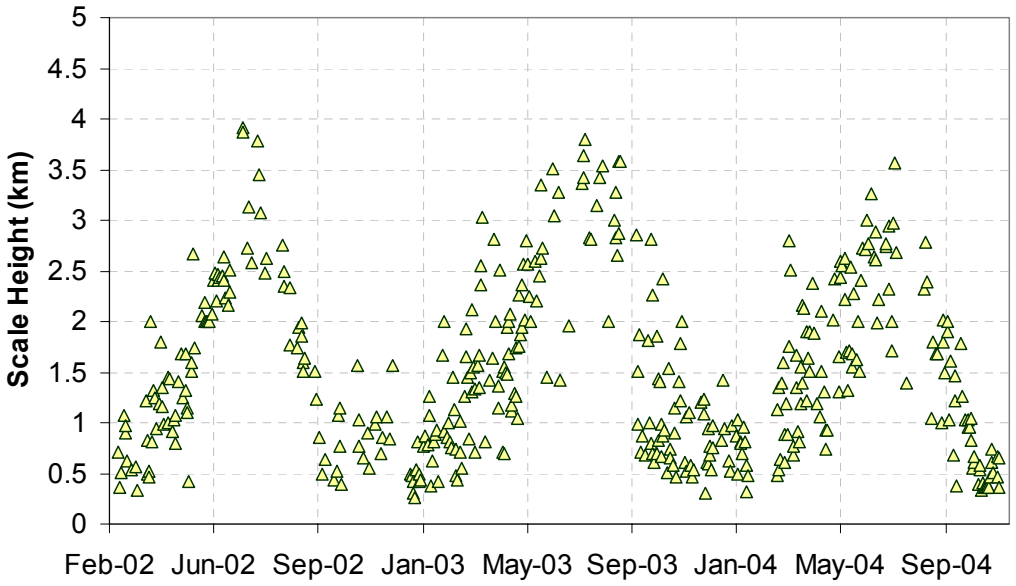

Figure 3.11. Scale height calculated from daily mean extinction values by fitting an exponentially decreasing profile.

Figure 3.11 shows scale height of aerosol calculated from daily mean extinction profiles. Prominent annual cycle can be observed for scale height variation. During winter months i.e. December to February scale height is low around 0.5 km. It increases from March onward and attains peak during July, with a value around 3.5 km. During summer months boundary layer height is more when air in contact with surface of the earth rises aloft and carries with it aerosols to higher altitudes.

There is not much inter-annual variability in magnitude and timing of peak/low scale height. This means that interannual variability observed for the extinction profile and discussed in previous section varied in same proportion at all altitudes otherwise the observed scale height variability would have been different. During intermediate period i.e. April and May, year 2003 and 2004 have higher scale height about 2 to 2.5 km in comparison to year 2002. During September and October 2003 scale height is high whereas 2004 values are comparable to that of 2002.

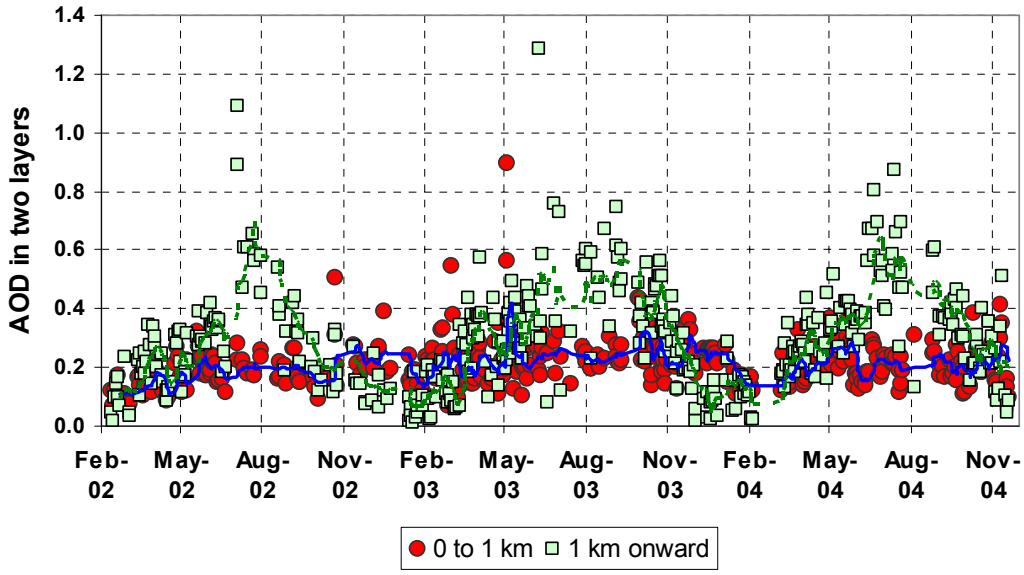

Figure 3.12. Aerosol optical depth computed for two layers, one below 1 km (circles) and the other above 1 km (squares). Lines through the data points represent 7 point running average values.

3.2 Aerosol Optical Depth

To study variation in magnitude of aerosol extinction, good parameter would be integration of extinction profile, which gives the aerosol optical depth. As shown earlier (Chapter 2) AOD can also be measured using a Sun-Photometer, but present section describes AODs that are obtained by integration of lidar measured extinction profiles. Like scale height, AOD also exhibits very prominent annual cycle. AOD over Ahmedabad are low during winter and high during summer.

During January and February AOD is between 0.1 and 0.2, while from February onwards it increases and attains a peak value of around 0.8 in Jun-July.

Similar trend was also observed in the past over Ahmedabad and other places of world. *Ramachandran et al.* (1994) observed a factor of 4 increase in AOD from Jan to May, which is of the same magnitude observed in the present study. Similar trend has been observed over places in India such as Indore (22^{0}41' N, 75^{0}52' E ; *Gupta et al.*, 2003), Visakhapatnam(17.7^{0}N, 83.3^{0}E ; *Niranjan et al.*, 1997), Trivandrum (8.5^{0}N, 77^{0}E, *Moorthy et al.*, 2001), Manora-Peak Nainital (29^{0}22' N, 79^{0}27' E; *Sagar et al.*, 2004),Kanpur (26^{0}26' N, 80^{0}20' E; *Singh et al.,* 2004), etc. However, seasonal trend observed in the Russian Arctic by *Shahgedanova and Lamakin* (2005) is opposite i.e. winter time increase and summer time decrease in AOD is found. *Shahgedanova and Lamakin* (2005) note that increase during winter time is mainly anthropogenic as there is decrease in natural sources of aerosols during winter in polar region.

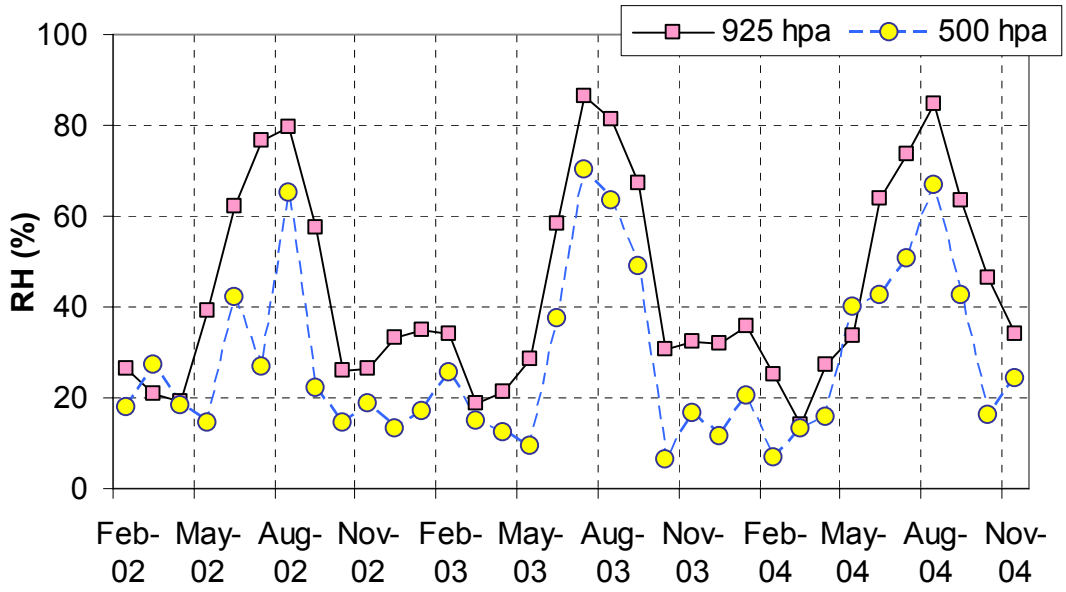

Figure 3.13. Monthly mean relative humidity over Ahmedabad at two different altitude levels. Data are obtained from Air Resource Laboratory, USA.

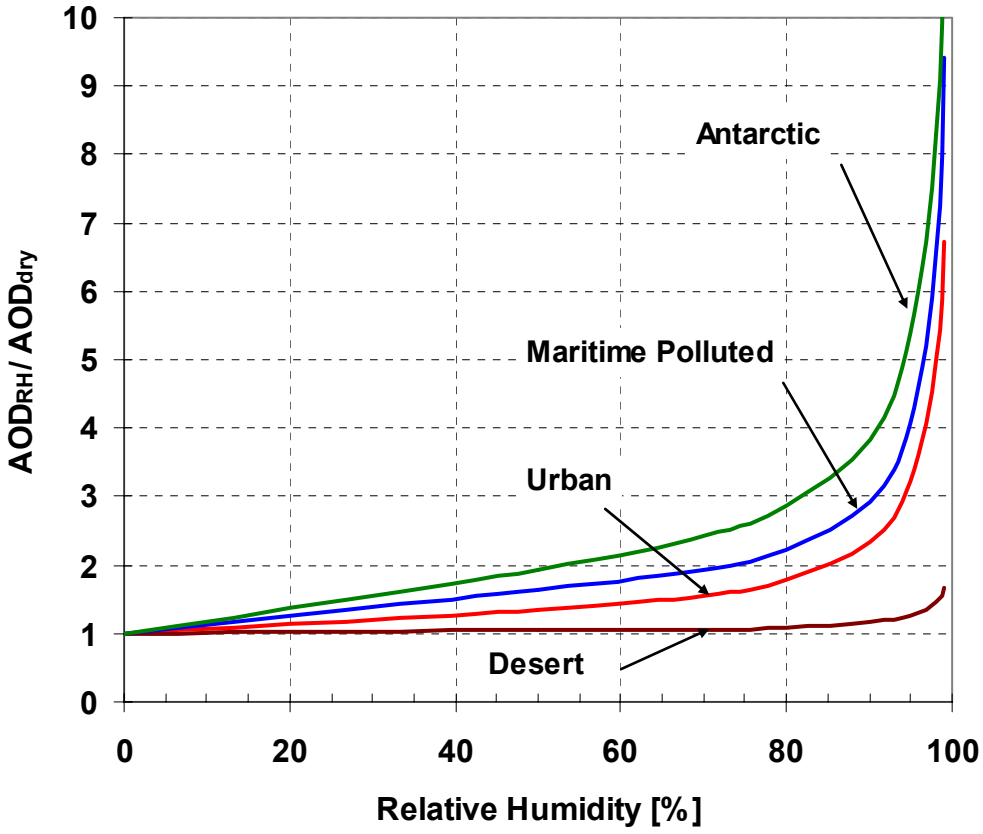

Figure 3.14. Variation of AOD with relative humidity (RH) for different aerosol models as defined in *Hess et al*. (1998) and *Gadhavi and Jayaraman* (2004). On the Y axis shown is the ratio of AOD at particular RH with AOD at 0% RH for the same amount of aerosol.

The summer time increase of AOD over Ahmedabad is found to be well correlated with relative humidity variation. Figure 3.13 shows the monthly mean variation of relative humidity observed over Ahmedabad. Data for relative humidity are obtained from Air Resource Laboratory, USA. Relative humidity (RH) at 925 hpa pressure level is shown with squares and at 500 hpa with circles. Pressure levels 925 and 500 hpa correspondence to approximately 0.8 and 5.8 km above mean sea level. At both the altitudes, trend of RH is similar. RH increases from 20 % in winter to around 80 % in summer. This variation in RH can increase AOD by factor of two to three (Figure 3.14). However, observed increase in AOD over Ahmedabad is more than this. In an interesting study carried out over

seven European cities under the European Aerosol Research Lidar Network (EARLINET) by *Wandinger et al.* (2004), it is found that summer time AOD is 10 – 30 % higher than winter time AOD over Aberystwyth (52.4^{0}N, 4.1^{0}W), Munich (48.2^{0}N, 11.6^{0}E), Hamburg (53.6^{0}N, 10.0^{0}E), Paris (48.6^{0}N, 2.2^{0}E), Leipzig (51.4^{0}N, 12.4^{0}E), Minsk (53.9^{0}N, 27.4^{0}E) and Belsk (51.5^{0}N, 20.5^{0}E) when data of same airmass history are grouped. Increase in AOD during summer irrespective of airmass history about RH emphasis the fact that there are changes taking place in production or removal mechanism of aerosols during summer apart from the increased RH and change in wind direction from continental to marine over Ahmedabad. This has serious implication for aerosol modelling studies which are largely based on various emission inventories, as this results call for better understanding of hygroscopic growth of aerosol, seasonal variation in aerosol sources and boundary layer dynamics.

In order to investigate the altitude range that contributes maximum to seasonal variation in AOD, extinction values are grouped in different altitude range. It is found that AOD in altitude range 0 to 1 km does not show any systematic variation with season whereas altitude range above 1 km shows strong seasonal variation (see Figure 3.12). AOD in 0 to 1 km remains around 0.2 whereas AOD above 1 km is low around 0.02 during winter and increases to 0.6 and more during summer. Large amount of aerosol in the lowest layer may be locally produced primary aerosols that could be wind blown mineral dust, or soot from automobile which are non hygroscopic. Secondary aerosols, which are produced by gas-to-particle conversion, are in general hygroscopic. Precursor gases released at surface can get mixed up to higher altitude say above 1 km faster than primary aerosols and hence altitude range above 1 km may be dominated by secondary aerosol, this could be reason for different response of two layers to change in relative humidity.

3.3 Aerosol Single Scattering Albedo

Single Scattering Albedo (SSA) of aerosol is computed from scattering and absorption coefficient measurements (see Chapter 2). Figure 3.15 shows aerosol

absorption coefficient observed over Ahmedabad at 520 nm. Daily mean values for year 2003 are shown with circles and that of 2004 with squares. Absorption coefficient show seasonal variation. It peaks during winter months and decreases during summer months. Average absorption coefficient from April to September is (0.92 ± 0.39) x 10^{-5} m^{-1} and from October to March it is (3.68 ±1.32) x 10^{-5} m^{-1}. Average of all data point is (2.1±2.0) x 10^{-5} m^{-1}.

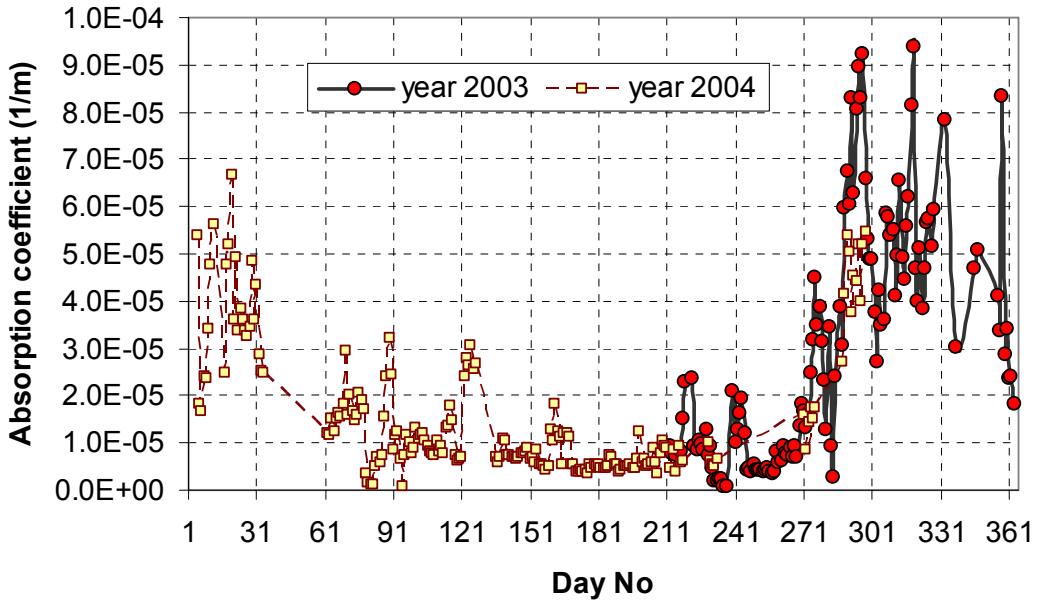

Figure 3.15. Daily mean aerosol absorption coefficient measured over Ahmedabad for year 2003 (circles) and 2004 (squares).

Reddy and Venkataraman (2000) have shown similar seasonal variation for black carbon and other anthropogenic species through a modelling study carried out based on emission inventories and observed meteorology. Seasonal variation is negatively correlated with AOD but positively correlated with extinction values in lower levels. As discussed earlier it appears that local meteorology plays important role for observed seasonal variations. During winter the Earth surface is generally cool which increases the stability of atmospheric profile and reduces the height of boundary layer. Pollutants such as soot emitted near the surface will not get easily

dispersed to higher altitude in stable boundary layer. This will result in increased concentration of pollutant near the surface.

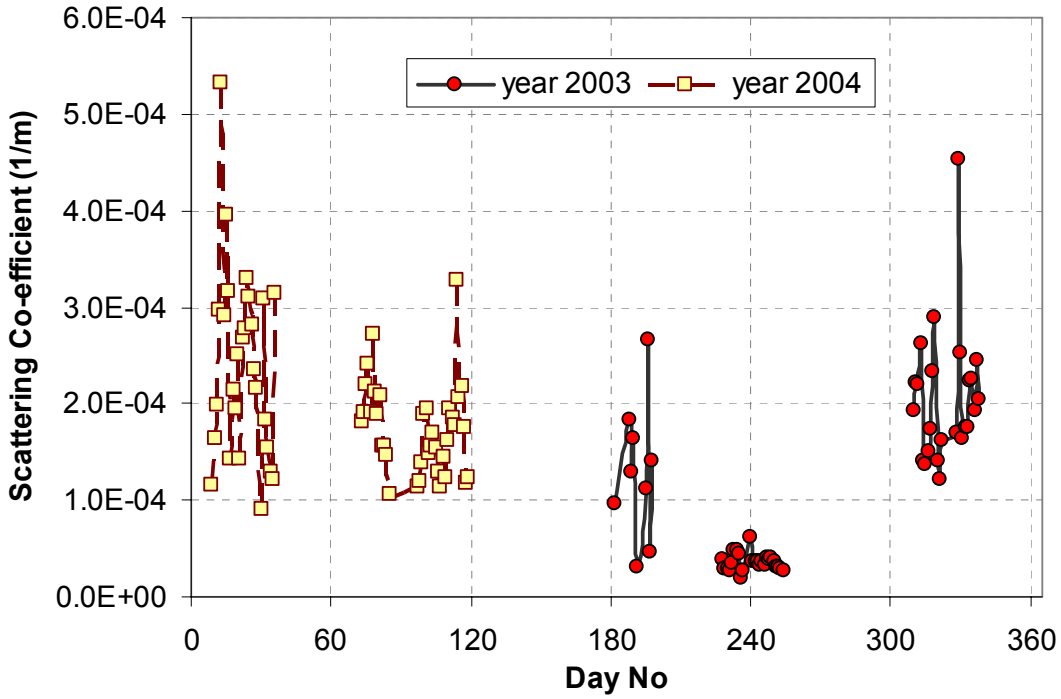

Figure 3.16. Daily mean aerosol scattering coefficient measured over Ahmedabad for the years 2003 (circles) and 2004 (squares)

Figure 3.16 shows the aerosol scattering coefficient observed over Ahmedabad at 530 nm. Like absorption coefficient scattering coefficient also shows seasonal variation i.e. low during summer and high during winter. However, seasonal variation is not pronounced as in the case of absorption coefficient During the summer months along with relative humidity, wind speed also increases. Increased wind speed results in faster removal of aerosols by advection, while it can also bring in aerosols from other locations. Black carbon, which is responsible for absorption mainly originate from anthropogenic sources. Over urban location like Ahmedabad advection will remove the existing aerosols and will bring in new aerosols, which may be significantly devoid of black carbon if they are of natural origin. This could be the reason for different seasonal response between

absorption and scattering coefficients. Average scattering coefficient observed is (1.63±0.96) x 10^{-4} m^{-1}.

Scattering coefficient is an order of magnitude higher than absorption coefficient. In order to calculate SSA small difference between wavelength for absorption and scattering coefficient is ignored. Ignoring wavelength difference, which is about 10 nm, will result in error less than 1%. While extinction coefficient can also be obtained from lidar observation, for the sake of consistency, here it is calculated by summation of absorption and scattering coefficients discussed above.

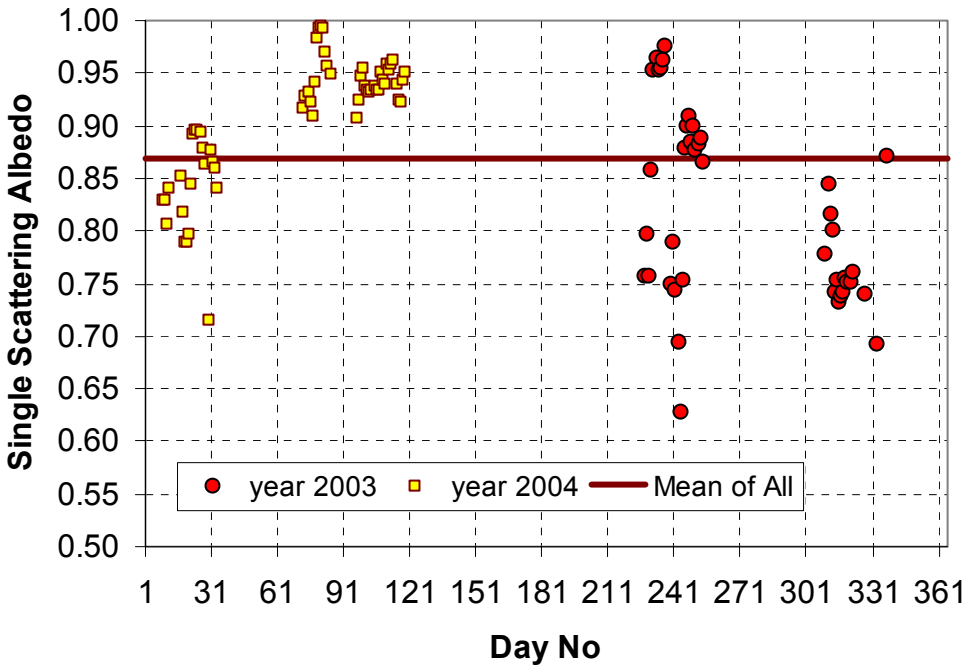

Figure 3.17. Daily mean single scattering albedo for Ahmedabad for the years 2003 (circles) and 2004 (squares).

Figure 3.17 shows the computed single scattering albedo (SSA) over Ahmedabad. Daily mean values for year 2003 are shown with circles and that of 2004 with squares. SSA is calculated only for those days when measurements of both scattering and absorption coefficients were available. Average SSA over Ahmedabad is around 0.87±0.09 which is quite close to 0.84 of continental

average aerosol model (*Hess et al.*, 1998) but somewhat lower than observed over Kanpur (26.45^0 N, 80.35^0 E), an urban location in Gangetic plain of India (*Singh et al.*, 2004). *Singh et al.* (2004) report 0.9±0.03 SSA at 471 and 673 nm over Kanpur. SSA over Ahmedabad is comparable to that found over Arabian Sea and coastal India (0.8 to 0.9) but considerably lower than Indian ocean (>0.95) (*Jayaraman et al.,* 2001).

Table 3.1. Nadir surface reflectance over Ahmedabad at seven wavelength bands from MODIS satellite data.

Wavelength Band (nm)	Nadir Reflectance (Annual Mean)	Standard Deviation
459 – 479	0.074	0.013
545 – 565	0.113	0.018
620 – 670	0.141	0.031
841 – 876	0.289	0.017
1230 – 1250	0.339	0.022
1628 – 1652	0.326	0.042
2105 − 2155	0.256	0.053

3.4 Surface Reflectance over Ahmedabad

Though surface reflectance is not an aerosol property, it is very important in determining the magnitude and sign of aerosol radiative forcing. Since all the aerosol properties are investigated here are further used to compute the aerosol radiative forcing, discussion of surface reflectance will be in order here. Land discipline of NASA provides surface reflectance data derived from Moderate-Resolution Imaging Spectroradiometer (MODIS) on board Terra and Aqua satellite (http://modis.gsfc.nasa.gov/about/index.html). Reflectance data provided are nadir bidirectional reflectance distribution function (BRDF) adjusted at mean solar zenith angle for a 16-day period (*Vermote and Vermeulen*, 1999, *Vermote et al.*, 1997). These data are available at every 16 days for 7 wavelength bands in the sinusoidal projection. Spatial resolution of the data is 1 km x 1 km. Central wavelengths of these bands are 469 nm, 555 nm, 645 nm, 858.5 nm, 1240 nm, 1640 nm and 2130 nm. Their full-width-half-maximum ranges from 20 nm to

50 nm. Reflectance values for region 10 x 10 km around the site of measurements were extracted and mean of these values was calculated. Reflectance for two wavelength-bands 555 nm and 2130 nm is shown in Figure 3.18. Reflectance at other wavelength is also similar to that shown in Figure 3.18. There is not much seasonal variation except September when there is a decrease in surface reflectance. This decrease could be because of the fact that the monsoon rain renders the surface wet and there is increased vegetation for a while. Decrease in reflectance at 555 nm is very small. Annual mean reflectance at 555 nm is 0.11±0.02. Annual mean surface reflectance and their standard deviation at other wavelength bands are shown in Table 3.1.

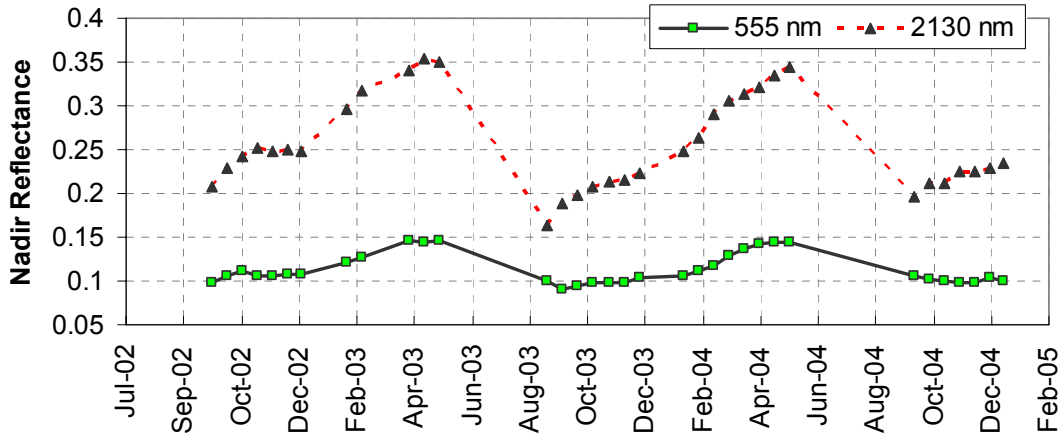

Figure 3.18. Surface reflectance observed over Ahmedabad by Moderate Resolution Imaging Spectroradiometer (MODIS) onboard Terra and Aqua satellites.

FIELD CAMPAIGN RESULTS

Aerosol not only exhibits large temporal variability but also high spatial variability. Different field campaigns have been undertaken as a part of this study to examine the spatial variability in aerosol properties and its consequences to aerosol radiative forcing.

4.1 Twentieth Indian Antarctic Expedition

During the 20th Indian Antarctic expedition conducted in January–February 2001, a detailed study on the aerosol spectral optical depth, mass concentration and size-distribution along with columnar ozone and water vapour concentrations was made from the Indian station, Maitri (70.77° S, 11.73° E) (*Gadhavi and Jayaraman*, 2004).

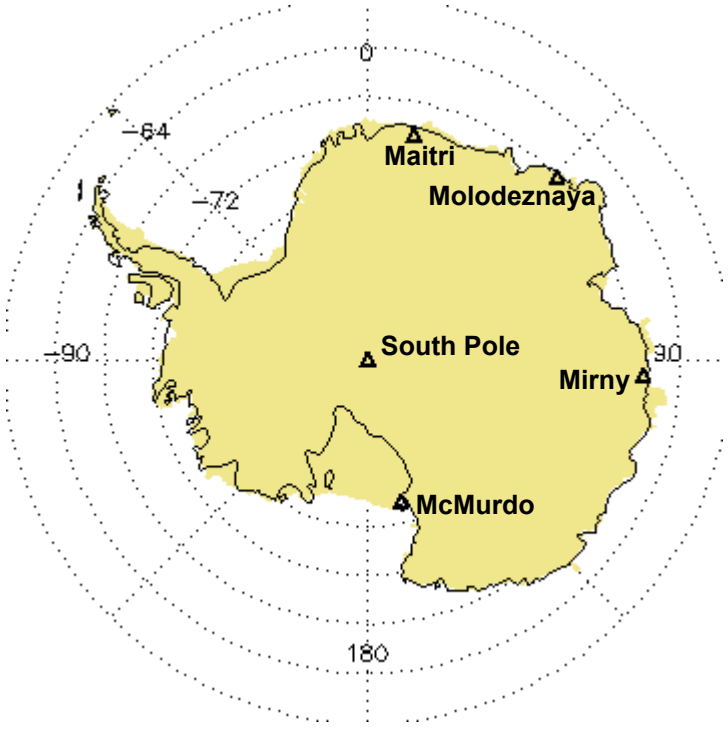

Figure 4.1. Indian station Maitri and other stations in Antarctica.

Over continents the amount of aerosol is generally large compared to that over the interior oceanic regions because the particles are produced over continents due to natural processes such as windblown dust, accidental forest-fires, etc. as well as due to man-made activities such as industries, vehicular traffic and biomass-burning. Over the oceans, the source of aerosols is mainly the sea-salt particles produced by breaking of air bubbles by surface winds and to a lesser extent, sulphate particles produced from dimethyl sulphide emitted by phytoplankton. However, the Antarctic region is unique. Its 96 % land surface is covered with snow and does not have indigenous population. In the absence of any major local aerosol source, the air is generally pristine and is only influenced by the long-range transport of sub-micron-size particles and gaseous pollutants from other parts of the globe. In the last few decades there has been a considerable increase in anthropogenic activities both in developed and developing nations, which is responsible for an overall increase in the aerosol burden around the globe. Aerosol and radiative-forcing studies over sites such as Antarctica will help in estimating the background-level aerosol forcing over a pristine site, which could be compared with results obtained over polluted regions. Also, such a study helps in establishing a database that could be used in future for studying the long term impact of continuous human activities in increasing the background-level aerosol concentration. Factors like high surface albedo and unique solar insolation cycle over Antarctica also make the study an interesting one. The present field study made at Maitri (70.77°S, 11.73°E; Figure 4.1) provides the continuity to aerosol optical-depth measurements made over Antarctica by other groups e.g. *Shaw* (1982), *Herber et al.* (1993 and 1996), *Sharma and Sharma* (1999), etc.

The 20th Indian Antarctic expedition was launched from Goa on 28 December 2000. The team arrived at Maitri on 14 January 2001. Aerosol studies were carried out from 18 January to 23 February 2001. A hand-held sun-photometer was used to measure the aerosol optical depth and a quartz crystal microbalance (QCM) cascade impactor was used to measure the surface-level aerosol mass-concentration and size-distribution. Measurements of columnar ozone and water

vapour were carried out using Microtops-II. AOD observations were made at five wavelength regions centred around 400, 497, 668, 875 and 1058 nm at approximately 15 min interval whenever clouds were not obscuring the sun or are not in the vicinity of about 30 degrees around the sun. A total of about 220 measurements were made for each wavelength region during the campaign period. The QCM was kept about 225 m away in a wooden hut, in a northward direction from the main station to avoid contamination from any localized sources such as power generator, kitchen, etc. Air sample was drawn at a height of 2 m from the ground level. The sampling arrangement is configured vertically such that there is negligible loss of particles within the sampling tube. About 3 to 4 measurements were taken every day. Prior to the starting of the measurement, drift if any, in the crystal frequency was checked each day, and was found to be negligible and random.

4.1.1 Meteorological conditions

Routine meteorological observations were made at the site. Additional data necessary for calculation of air back-trajectory analysis, etc. were obtained from Air Resource Laboratory (ARL) and NOAA–CIRES Climate Diagnostics Center, USA. The daily mean air temperature at Maitri during the campaign period was in the range of 0 to –10°C, with an average value of –3°C. A decreasing trend in daily mean temperature is observed from January to February, with cloudy days recording lower temperature than the mean trend. The relative humidity (RH) is found to be around 78 ± 7%, with a decreasing trend from January to February. Decreasing trends observed in both temperature and RH are indicative of the air becoming drier, typical of the transition from summer to winter season in southern hemisphere. The average surface-level wind speed was 7.1 m/s, but was highly variable and often reaching values of 12 m/s and above. However, no systematic trend in wind speed was observed during the campaign period. It should be noted that Maitri is located at the edge of the Antarctic continent and hence experiences wind from both ocean and inland, intermittently. This altering

airmass has an important effect on the aerosol, ozone and water vapour content over Maitri, as discussed in the following sections.

4.1.2 Aerosol Optical Depth over Maitri-Antarctica

Daily variation in the mean AOD for the campaign period is shown in Figure 4.2 for two selected wavelengths of 400 and 1058 nm. Except for the two high values recorded on 18 and 19 January, remaining days the values are in the range 0.01 to 0.1 for all wavelengths (*Gadhavi and Jayaraman*, 2004). High values of AOD and high day-to-day variations are seen in the extreme wavelengths of 400 and 1058 nm compared to the intermediate wavelengths. Figure 4.3 shows the average AOD spectrum obtained for the whole period. Vertical bars over the data points represent the standard deviation from the mean. The high values recorded on 18 and 19 January are not included for the estimation of the average spectrum. The AOD value at 400 nm is high compared to those at longer wavelengths, with a mean value of 0.036 ± 0.018 and also exhibiting larger daily variability. The average AOD spectrum indicates two modes, one peaking at a lower wavelength of 400 nm or below and the other at a higher wavelength of 1058 nm or above.

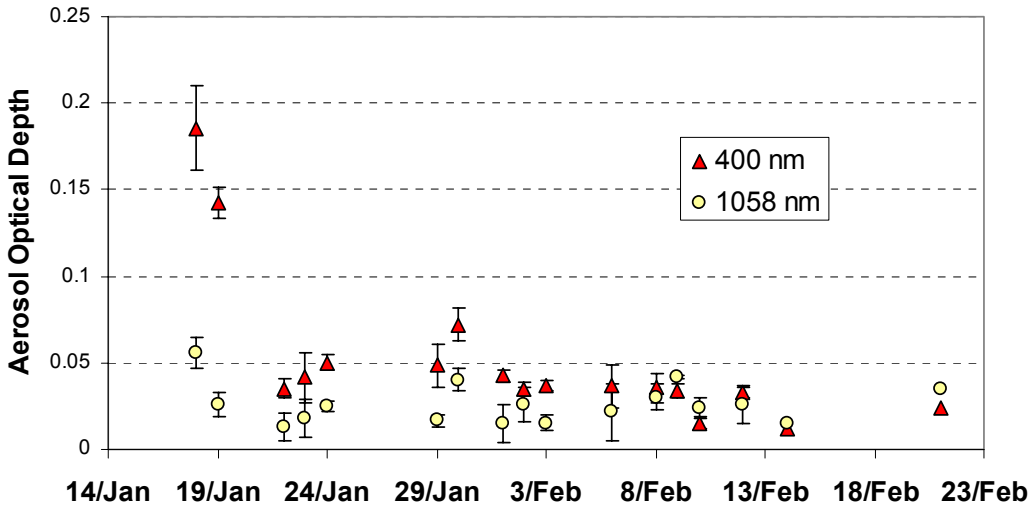

Figure 4.2. Day to day variation in mean AOD at two-selected wavelengths over Maitri-Antarctica during Jan-Feb 2001 (modified from *Gadhavi and Jayaraman*, 2004).

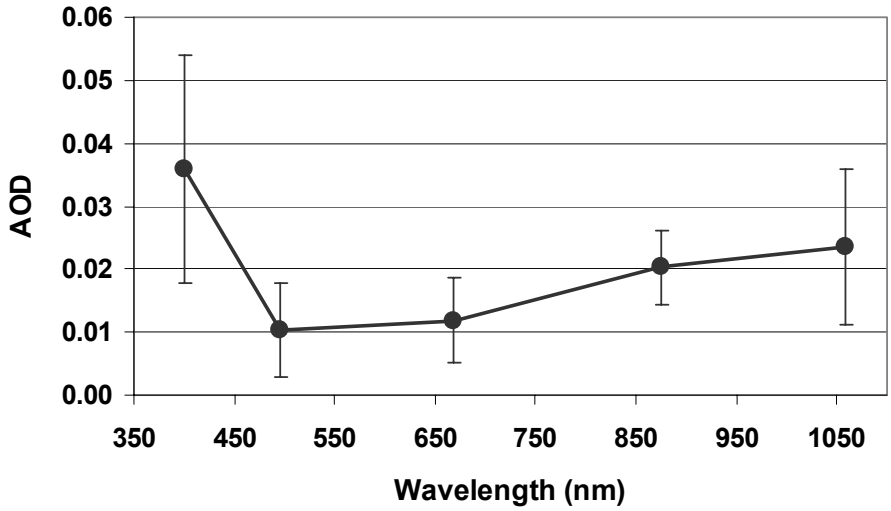

Figure 4.3. Mean AOD spectrum for the entire campaign period. The high AOD values obtained on 18 and 19 January (shown in Figure 4.2) are not included in the mean spectrum (modified from *Gadhavi and Jayaraman*, 2004).

This kind of feature is typical of an optically clean region where the AOD at the visible wavelength region is the minimum. The higher AOD at shorter wavelength is caused due to nucleation-mode particles, which are of sub-micron size. These particles are produced mainly in-situ within the atmosphere by gas-to-particle conversion mechanism from precursor gases such as oxides of sulphur, nitrogen, etc. Owing to their small size, they have a longer residence time in the atmosphere compared to bigger particles. Also, the residence time increases with increasing altitude and in the free troposphere, these submicron particles have residence time of the order of a few weeks to a month, sufficient to sustain long-range inter-continent transport from their source origin to the polar region. Higher AOD values seen in the longer wavelength region is produced mainly by bigger size particles, which are of local and natural origin and composed mainly of sea-salt particles from the ocean and dust debris from the underlying land. *Shaw* (1982) has reported a value of 0.025 ± 0.010 for AOD over McMurdo station (77.85°S, 166.67°E) and 0.012 ± 0.005 over the South Pole for 500 nm. *Herber et al.* (1993) report a value in the range of 0.02 to 0.025 at 1000 nm during the volcanically

quiescent period at George Forster, which is near to Maitri. Further, *Herber et al.* (1993) found very little difference between the AOD values obtained for this wavelength at stations George Forster, Mirny (67°S, 93°E) and Molodeznaya (68°S, 46°E). However, *Herber et al.* (1993) reports higher AOD about 0.035 to 0.045 at 500 nm compared to those reported by *Shaw* (1982) at stations McMurdo and South Pole (Figure 4.1).

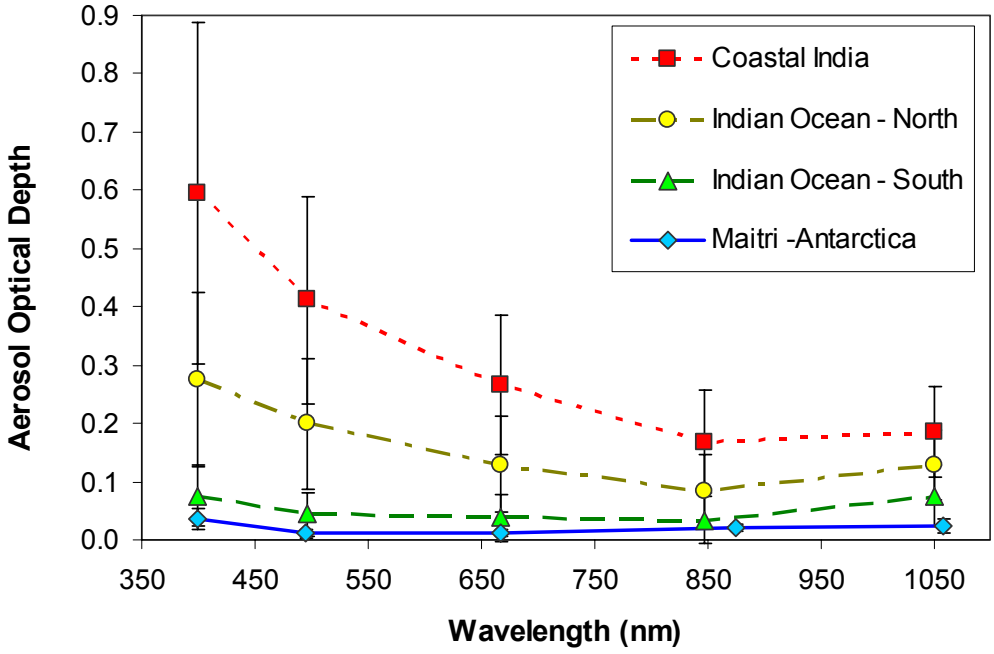

Figure 4.4. Comparison of mean AOD spectrum obtained over Maitri with those over other regions obtained during INDOEX cruises. Vertical bars represent ± 1 standard deviation from the mean. See text for explanation of the regions.

The AOD values obtained over Maitri are lower than those obtained over other regions, including the clean Indian Ocean region. Figure 4.4 compares the mean AOD spectrum obtained over Maitri with those measured over other regions, obtained from similar sun-photometer observations made on-board ship cruises. In Figure 4.4, coastal India represents data collected along the west coast of India, Indian Ocean-North represents data collected over the Indian Ocean but north of the inter-tropical convergence zone (ITCZ), and influenced by continental air from the north, and Indian Ocean-South represents data collected south of the

ITCZ, which has relatively less anthropogenic influence. The data shown are for the period January to March, similar to the present study, but are the average for the years 1996 to 1999. AOD at all wavelengths is the lowest over Antarctic and increases as we move towards the north, with the highest value obtained near coastal India. The interesting observation is that the increase in AOD from the pristine polar site to the polluted site is not uniform at all wavelengths, which is indicative of the change in columnar aerosol size-distribution and composition with latitude. For example, if one compares the Maitri data with the Indian Ocean-South data, though AOD values are high at all wavelengths over the Indian Ocean-South; the increase is more at wavelengths longer than 400 nm, indicating that the increase in the number of bigger particles is higher than that of the smaller particles. Smaller particles have longer residence time in the atmosphere and they are well mixed compared to coarse particles. Also, over the Indian Ocean the concentration of sea-salt particles is more compared to that over Maitri, and this contributes to the observed higher AOD at longer wavelengths. Between the AOD spectra over the Indian Ocean-South and the Indian Ocean-North, the major difference is in the lower-wavelength AOD indicating an increase in the concentration of smaller particles that are mainly transported from the continents towards the ocean. A more or less similar shape observed in the AOD spectra over Indian Ocean-North and coastal India shows that the aerosols are well mixed in these regions, except that the concentrations are higher in the coastal region.

4.1.3 Aerosol Mass Concentration and Size Distribution over Maitri-Antarctica

The average mass concentration of the ambient aerosol particles of size less than 10 μm (denoted as PM_{10} particles) at Maitri for the entire campaign period is 9.1 $\mu g/m^3$, with a standard deviation of 6.0 $\mu g/m^3$. The relatively large variation shows the extent of the day-today variability in the surface-level aerosol mass concentration over Maitri. Of the average total mass, the coarse particles having size between 1 and 10 μm contribute 5.8 $\mu g/m^3$, which is 63% of the total (Figure 4.5). Similarly, the accumulation-mode particles having a size between 0.1 and 1

μm contribute 1.9 μg/m^3, which is 21% of the total and the nucleation-mode particles having a size less than 0.1 μm contribute 1.5 μg/m^3, which is 16% of the total.

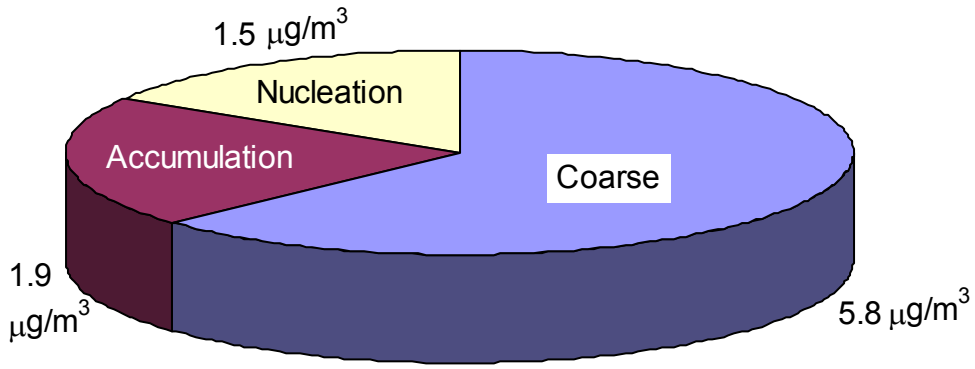

Figure 4.5. Average mass concentration of aerosol (PM_{10}) particles at Maitri during the campaign period, of the total 9.1 μg/m^3, the coarse mode particles (r > 1 μm) contribute 5.8 (63%); the accumulation mode (0.1 < r < 1 μm) particles 1.91 (21%); and the nucleation mode (r < 0.1 μm) particles 1.47 (16%) μg/m^3.

The mass values shown are for the ambient measurements, meaning that they also contain water. If we correct for the water content, the dry (0% RH) PM_{10} aerosol mass becomes 6.97 μg/m^3 and at 50% RH, it becomes 7.9 μg/m^3. The major contribution to the total aerosol mass is from the coarse particles which have local origin, such as the sea-salt particles brought from the nearby ocean region as well as dust from the underlying surface. The aerosol mass concentration over Maitri is at least an order of magnitude low compared to those found in anthropogenically affected regions (*Jayaraman et al.*, 2001 and *Ramachandran and Jayaraman*, 2002). However, in comparison with other Antarctic stations such as McMurdo (77°51' S, 166°40' E), the Maitri value is high. *Mazzera et al.*, (2001) have found average PM_{10} in the range 3.2 to 4.8 μg/m^3 between the years 1995 and 1997, at two different locations over McMurdo station. Also over Maitri, an increasing trend is observed in the total mass value from January to the end of February. Other explorers (*Hall*

and Wolff, 1998 and *references there in*) have also observed increase in surface level aerosol concentration as austral winter progresses. *Hall and Wolff*, (1998) have explained this seasonal increase by the effect of temperature on salinity of brine formed over newly-formed sea-ice surface. *Richardson* (1976) has demonstrated through laboratory experiments that original sea-water salinity of 35‰ increases to 122‰ when temperature decreases from 0 to –8°C, and the surface brines formed are much better sources of sea-salt aerosol than sea-water.

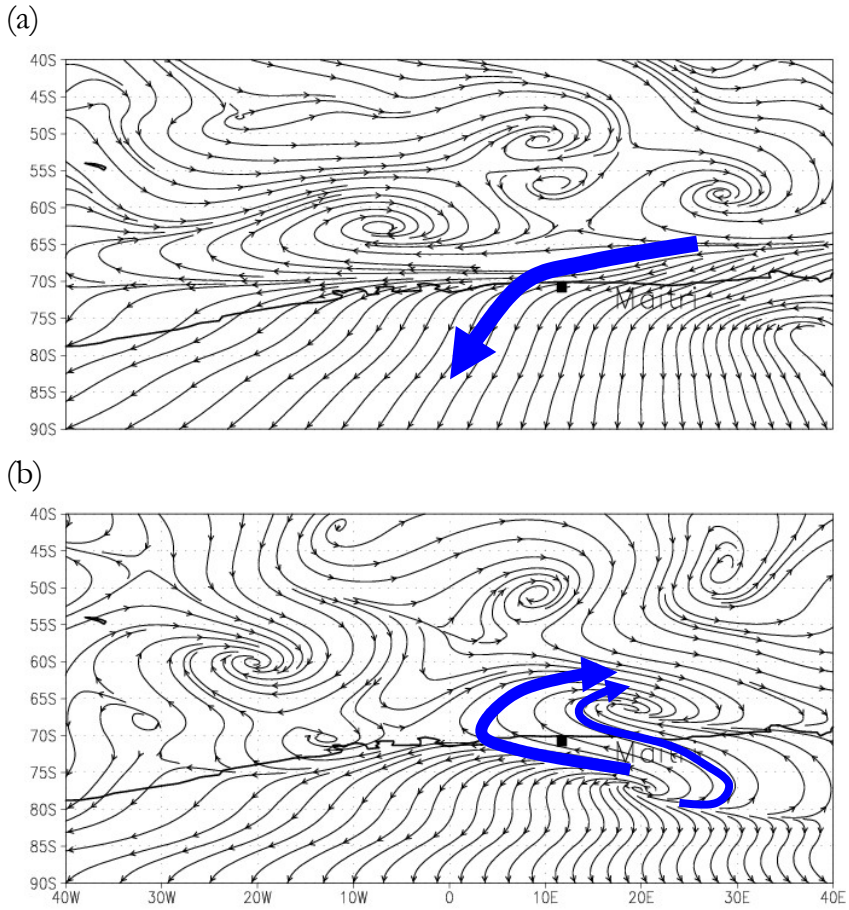

Figure 4.6. Wind streamline over Maitri on 19 January 2001 (a) and 29 January 2001 (b). Arrow shows the wind direction and the location of Maitri is marked.

Over Maitri, the observed mass increase is however not monotonous, but with substantial decrease in values during 29 January to 2 February 2001, and on 6 February 2001. This is explained in terms of changing wind direction. Figure 4.6 shows wind stream line calculated from NCEP reanalysis data for 19 and 29

January 2001. On 29 January 2001, the wind is predominantly from the interior continent compared to 19 January 2001. The inland continental air brings less aerosols to the measurement site than the wind from the ocean side, which remains the main source of aerosols over Antarctica.

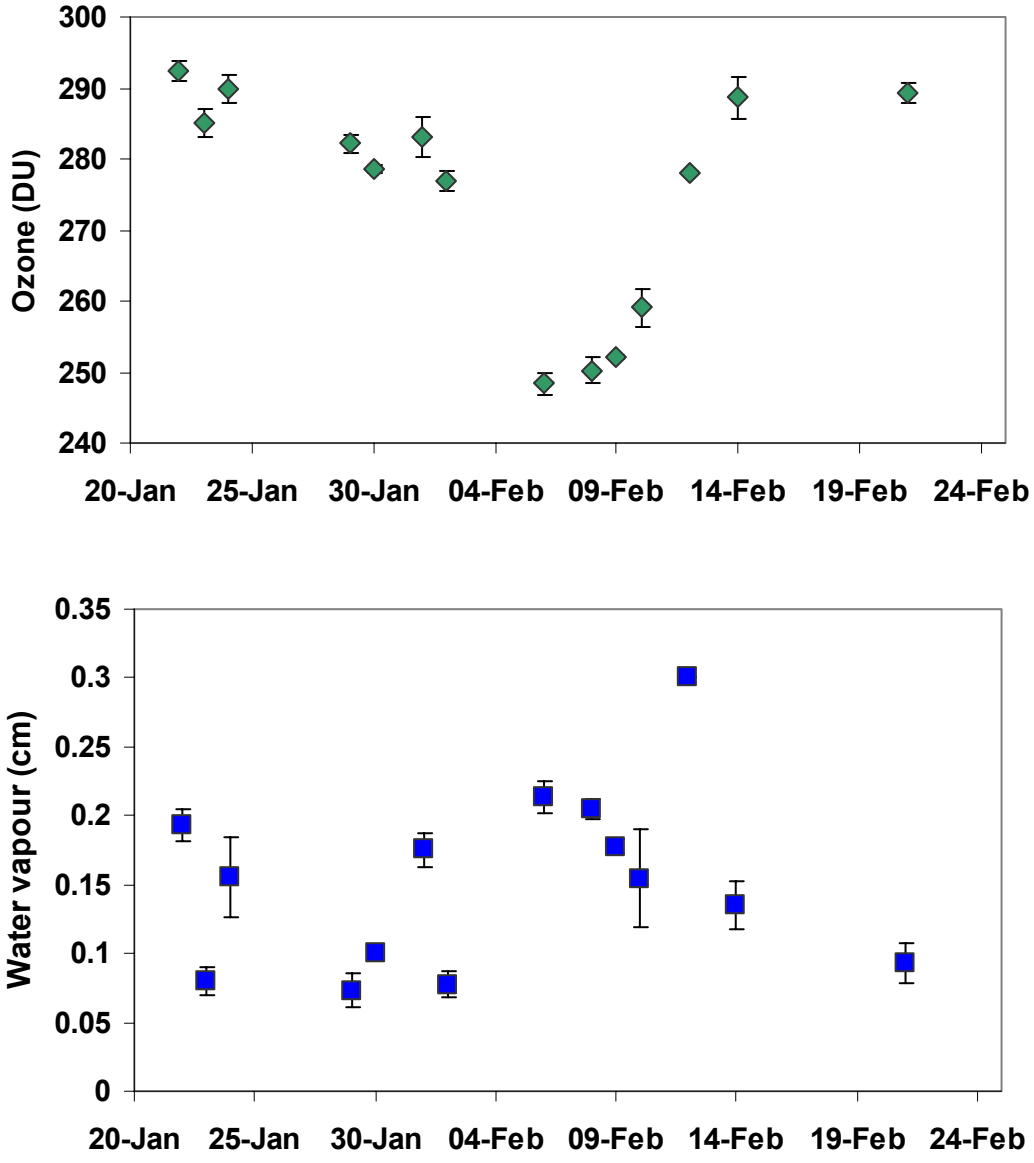

Figure 4.7. Daily mean columnar ozone (a) and total precipitable water-vapour (b) over Maitri, Antarctica. Vertical bar over data points represents standard deviation from the daily mean.

4.1.4 Columnar Ozone and Water Vapour concentrations over Maitri-Antarctica

In spite of the pristine atmosphere, large day-to-day variations in both aerosol parameters as well as column concentrations of ozone and water-vapour are recorded over Maitri. Though the ozone and water-vapour measurements are made to correct the AOD for the estimation of the radiative forcing over Maitri, which is the main objective of the present study, because of the large variations observed in the column ozone and water-vapour, it is found appropriate to present the results here. Figure 4.7 shows the daily average values of the measured integrated vertical columnar ozone and water vapour concentrations, and the vertical bar over data points are standard deviation for that day. During the period from 3 to 11 February 2001, an episodic decrease in ozone concentration by about 40 DU was observed from the normal background value of about 285 DU.

Jain et al. (2004) have also observed sudden changes of similar magnitude for column ozone concentration in 1997 and 2002 during January and February; however, they report changes of much higher magnitude during September and October when ozone hole is recovering. Comparison of this observed decrease with TOMS satellite data revealed that the decrease was localized mainly over the Maitri region. Atmospheric dynamics plays a major role in controlling the ozone concentration over this region, located at the edge of the polar vortex (*Jain et al.*, 2004). Air back-trajectory analysis using HySPLIT (*Draxler and Rolph*, 2003, and *Rolph*, 2003) model shows that during the low ozone period, airmass came from low altitude and rose while reaching Maitri. Figure 4.8(top) shows the geographical location of the air parcel, whereas Figure 4.8(bottom) shows its altitude variation with time. From the three air trajectories arriving at altitudes 10, 15 and 20 km, it is seen that the air at low altitude, which is ozone deficit, is replacing the ozone-rich upper air and causing a local ozone minimum over the site. Figure 4.7-b shows the daily mean value of the total precipitable water vapour which is found to vary between 0.05 and 0.2 cm, with high values during the period when ozone minimum is observed. This further corroborates the earlier conclusion that the

mixing between the lower and upper atmospheric air is responsible for the observed ozone minimum. In the case of water-vapour, its concentration is more at lower altitude and the vertical mixing from the airmass has resulted in an increase in the total columnar content during the above period.

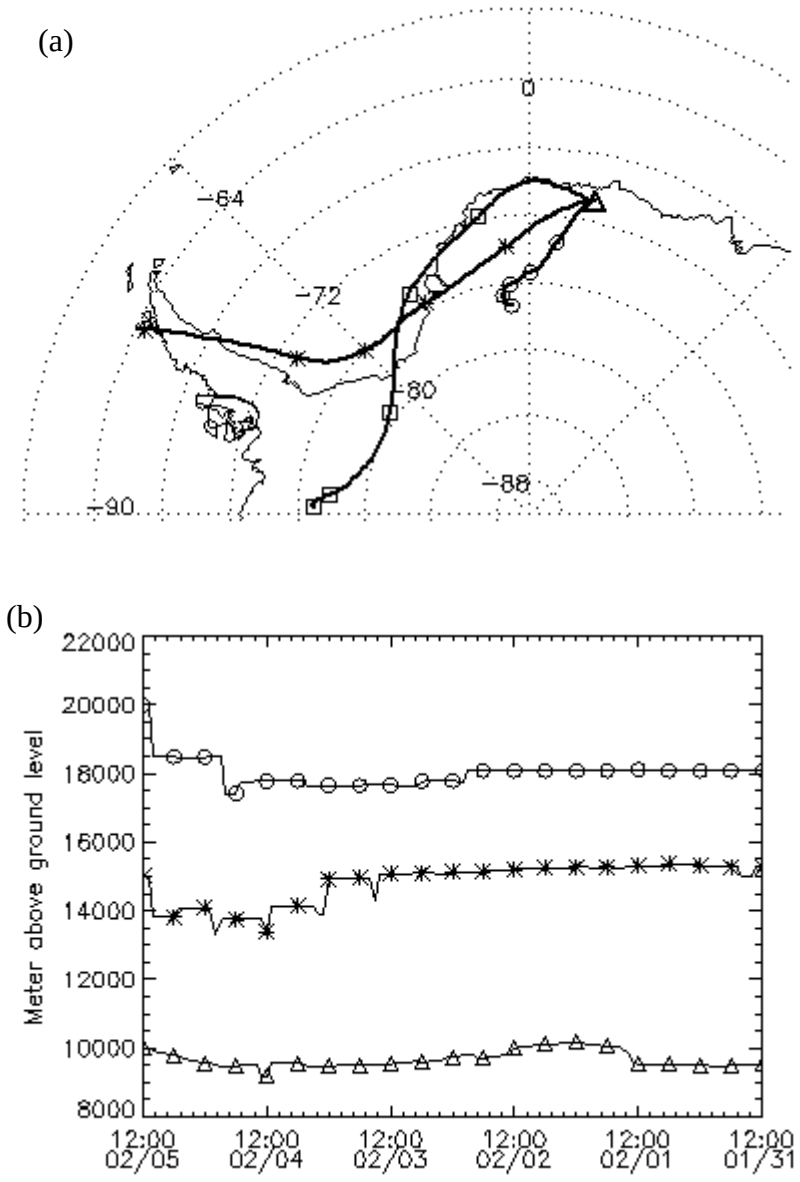

Figure 4.8. Five days air back-trajectory made for 5 February 2001 over Maitri, Antarctica. Top panel shows Geographical location of air parcel and the bottom panel shows altitude variation of air parcel with time. Height is given in metre above ground level.

4.1.5 Aerosol Model for Maitri-Antarctica

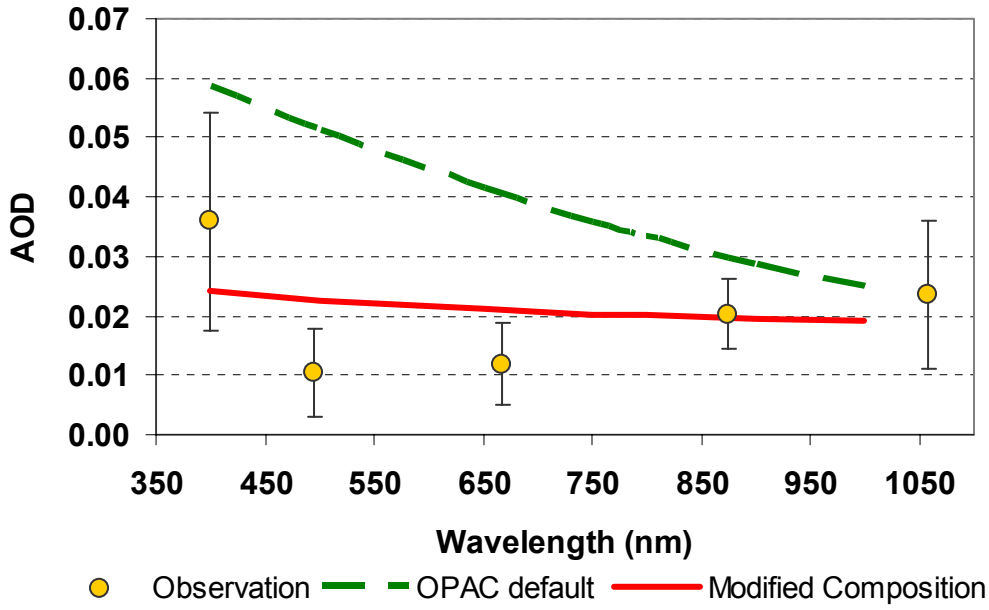

Figure 4.9. Comparison of the observed mean AOD spectrum over Maitri with that of the OPAC model computed at 50% relative humidity (broken line) and using the modified values proposed in the present study (solid line).

Analysis of the spectral dependence of AOD provides a rough estimation on the aerosol size-distribution and chemical composition. Model AOD spectrum is computed using OPAC (Optical Properties of Aerosol and Cloud) software (*Hess et al.*, 1998) for the default values prescribed for Antarctica. OPAC describes ten aerosol components that are representative of different origins, with internally mixed chemical composition. The components could be externally mixed to get different aerosol types. Antarctic aerosol type in OPAC is same as that suggested by *d'Almeida et al.* (1991), in which the major component is sulphate aerosol. In terms of mass, at 50% RH, sulphate contributes 91%, sea-salt accumulation 4.5% and mineral transported 4.5% to the total mass at the surface-level, which is about 2.2 μg/m^3. In the OPAC model, Antarctic AOD is calculated assuming an exponentially decreasing aerosol profile, with a scale height of 8 km. With this default aerosol profile and composition, the computed AOD is found to be high at lower wavelengths compared to that observed using Sun-Photometer. The mass

concentration computed based on the OPAC parameters for particles of size less than 7.5 μm is lower compared to that measured by QCM, indicating that there is underestimation of the amount of bigger particles in the model. Also, the default Antarctic aerosol model could not explain the observed size-distribution. In order to have a better comparison and consistency between the measured data and the model, using information available on the chemical composition from earlier studies (*Mazzera et al.*, 2001, *Wagenbach et al.*, 1998 and *Kerminen et al.*, 2000) we propose modifications to the Antarctic aerosol model prescribed in the OPAC model (see Table 4.1).

Table 4.1. Values prescribed in the OPAC model for Antarctic aerosols and suggested modifications proposed in the present study to better explain the observed AOD spectrum and aerosol mass size-distribution

	Number density (cm^{-3})				
Component	**OPAC model**	**Suggested modification**	r^*_{mod} **(μm)**	σ	ρ^* **(g/cm^3)**
Sea-salt accumulation mode	0.047	-	0.336	2.03	1.29
Sea-Salt coarse mode	-	0.015	2.82	2.03	1.29
Mineral transported	0.0053	0.1	0.5	2.2	2.6
Sulphate	42.9	0.05	0.0983	2.03	1.25

r_{mod} and σ are respectively, mod radius and width parameter for log normal size-distribution

ρ is density of aerosol particles.

*At 50% RH.

The important change is to increase the concentration of the bigger particles while reducing the amount of the submicron (sulphate) particles. With this proposed modification, the computed AOD spectrum compares better with measurements (Figure 4.9). The dashed line represents the calculated AOD at 50% RH using the aerosol composition suggested in the OPAC model, while the continuous line represents the calculated AOD for the modified composition at 50% RH. With the proposed new model composition, the total mass for particles of size less than 7.5 μm becomes 5.6 $\mu g/m^3$, which is in better agreement with the

measured mass value. Other aerosol properties like single scattering albedo and asymmetry factor are calculated using Mie theory, and are further used to calculate the aerosol direct radiative forcing.

4.2 Mobile Lidar Road Campaign in Western Gujarat

From 26 Dec 2002 to 13 Jan 2003 a field campaign was carried out over western part of Gujarat using the mobile micro pulse lidar (MPL) and sun-photometer to study the spatial variations in distribution of aerosol optical properties. A variety of geographical regions were covered which included urban inland, urban coastal, rural inland, rural coastal, desert, etc. Starting from Ahmedabad observations were carried out approximately at every 50 km for an hour or more. At one of the locations (Narayan Sarovar), long observations were also carried out to study the variation in nocturnal boundary layer. During some of the measurements, clouds were present which are not discussed here. Also at some stations data could not be saved because of instrument failure. Remaining stations are described in Table 4.2 with their names, latitude, longitude, time duration, and average AOD. Our broad objective for this land campaign was to obtain data on spatial variability at sub-regional scale and if wind directions are favourable to study the cross boundary transport of aerosols. Figure 4.10 shows the route map taken during this land campaign. Borders and places shown in the map are only approximate. During onward journey coastal route was followed and during the return journey part of the route was retraced but Somnath onwards a different inland route was taken.

Table 4.2. Locations where observations made, their latitude, longitude, date, time and AOD obtained by integration of mean extinction profile during this period is shown.

Sr. No.	Station Name	Lat ^{0}N	Lon ^{0}E	Date	Time (IST*)		AOD
					From	To	
1	Ahmedabad	23.04	72.54	23/12/2002	18:00	19:42	0.319
2	Dholka	22.91	72.49	26/12/2002	14:54	15:54	0.454
3	Mota Bora	22.47	72.34	26/12/2002	16:07	19:40	0.262
4	Bawalia	22.08	72.11	27/12/2002	05:09	06:13	0.200
5	Mamsa Patia	21.66	72.14	27/12/2002	08:47	09:44	0.271
6	Gopnath Mahadev	21.21	72.11	27/12/2002	12:05	13:06	0.662
7	Madhia	21.05	71.68	27/12/2002	18:18	19:21	0.303

Sr. No.	Station Name	Lat ^{0}N	Lon ^{0}E	Date	Time (IST*)		AOD
					From	To	
8	Rajula	21.03	71.44	28/12/2002	05:01	06:01	0.214
9	Una	20.83	71.05	28/12/2002	09:18	10:18	0.260
10	Diu	20.71	70.93	28/12/2002	12:51	13:51	0.295
11	Vikrameshwar Mahadev	20.90	70.50	28/12/2002	17:46	18:46	0.242
12	Kesod	21.31	70.25	29/12/2002	05:26	06:27	0.114
13	Nr. Porbander	21.44	69.80	29/12/2002	09:08	11:07	0.399
20	Sarvad	22.98	70.69	30/12/2002	22:17	23:17	0.220
21	Samkhiyali	23.31	70.43	31/12/2002	07:21	08:22	0.274
22	Mokhana	23.29	70.01	31/12/2002	09:39	10:44	0.505
23	Bhuj	23.24	69.67	31/12/2002	20:05	23:26	0.153
24	Black hill	23.93	69.81	01/01/2003	16:44	17:22	0.136
25	Mandvi	22.86	69.39	02/01/2003	14:51	15:52	0.250
26	Sabharai	23.01	69.11	02/01/2003	17:28	18:28	0.218
27	Suthari	23.02	68.89	02/01/2003	19:49	20:43	0.158
28	NarayanSarovar	23.67	68.54	03/01/2003	06:22	07:30	0.174
29	Koteshwar	23.67	68.54	03/01/2003	10:28	11:29	0.192
30	K-to-L-1*	23.69	68.53	03/01/2003	12:05	12:35	0.282
31	K-to-L-2*	23.70	68.62	03/01/2003	13:14	13:29	0.308
32	K-to-L-3*	23.78	68.67	03/01/2003	14:58	15:35	0.405
33	Lakhpat	23.82	68.76	03/01/2003	17:42	23:42	0.200
34	Narayan Sarovar	23.67	68.54	04/01/2003	18:00	21:00	0.173
35	Ravapur	23.52	69.06	05/01/2003	12:29	13:29	0.471
38	Adipur	23.07	70.08	06/01/2003	15:35	16:36	0.489
39	Bhachau	23.29	70.39	06/01/2003	19:15	20:54	0.176
40	Sarvad	22.98	70.70	07/01/2003	06:27	07:26	0.074
41	Nr. Jodia	22.65	70.37	07/01/2003	09:19	10:19	0.178
42	Nr. Sikka	22.43	69.91	07/01/2003	14:59	16:00	0.349
43	Nr. Vadtara	22.21	69.56	07/01/2003	17:44	19:10	0.142
44	Kuthali	22.06	69.15	08/01/2003	08:33	09:36	0.235
45	Mool Dwarka	21.72	69.51	08/01/2003	11:11	12:14	0.569
46	Mokha (Porbandar)	21.34	69.89	08/01/2003	14:53	16:00	0.241
48	Gundaran	21.05	70.56	09/01/2003	14:24	15:29	0.379
49	Somnath	20.88	70.41	09/01/2003	18:18	19:26	0.303
50	Gir	21.17	70.50	10/01/2003	11:29	12:31	0.350
51	between Junagadh & Jetpur	21.62	70.50	10/01/2003	15:42	16:42	0.359
52	between Gondal & Rajkot	22.05	70.78	10/01/2003	18:19	19:15	0.375
53	Chotila	22.42	71.15	11/01/2003	09:44	10:47	0.409
54	Nr. Limbdi	22.56	71.65	11/01/2003	12:21	12:56	0.454
55	Bagodara	22.64	72.20	11/01/2003	14:05	15:05	0.441
56	Ahmedabad	23.04	72.54	13/01/2003	18:18	20:10	0.342

*IST – Indian Standard Time

*K-to-L – on the way Koteshwar to Lakhpat

4.2.1 Meteorological Condition during Western Gujarat Road Campaign

Meteorological data during the land campaign are obtained from Air Resources Laboratory (ARL), NOAA, USA and Climate Diagnostic Center (CDC), NOAA, USA. Temperature was usually low between 20 to 26 degree centigrade and wind speed was from calm to moderate. Average wind speed during the campaign period was 4.4 m/s. Figure 4.11 shows monthly mean wind field at 925 hpa pressure level over India and adjacent region. An anticyclone is found to prevail over north India and wind direction over Gujarat is somewhat undefined but in general from continent to sea. On 29 December 2002, drizzle was experienced near Dwarka. For subsequent one or two days clouds were visible in the sky otherwise sky remained clear during campaign period.

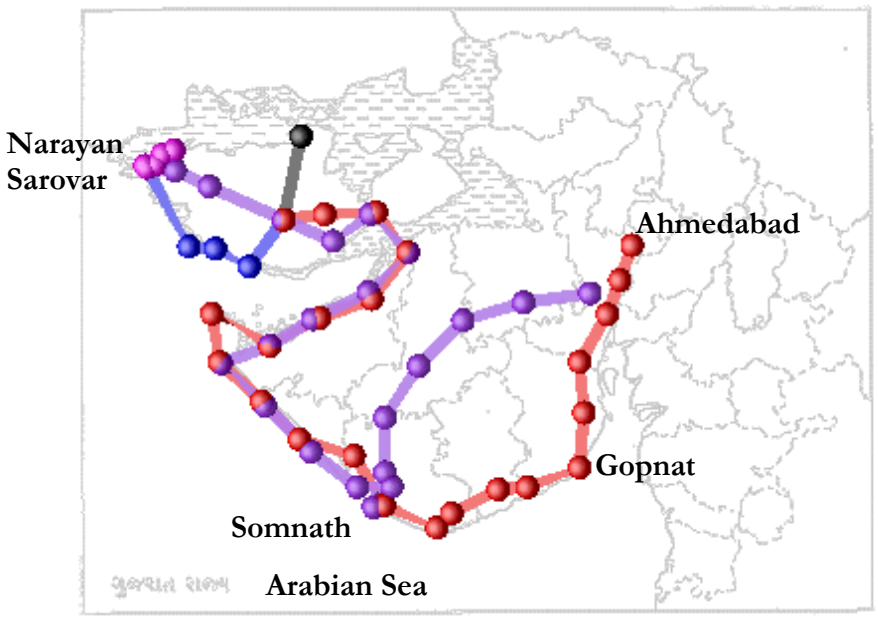

Figure 4.10. Route map of western Gujarat road campaign. Borders and location marks are approximate.

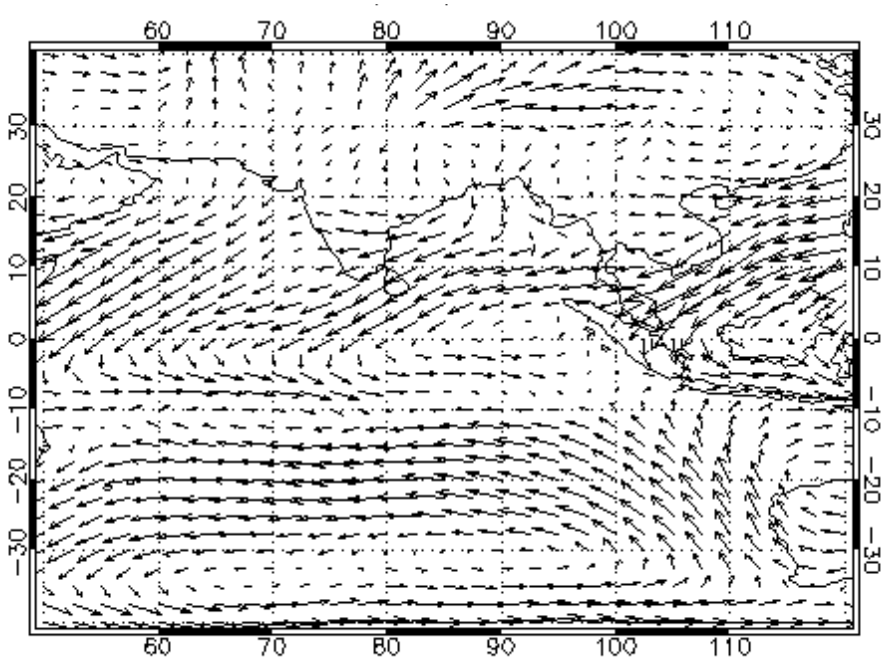

Figure 4.11. Monthly mean wind field over India and adjacent region during January 2003 at 925 hpa pressure level. Anticyclone is prevailing over India during this period. Data for wind fields are obtained from CDC, NOAA, USA.

4.2.2 Results and Discussion

Aerosol optical depths (AOD) are obtained from both the methods, using sun-photometry and by integrating lidar measured extinction profile. AOD at 497 nm wavelength observed by the sun-photometer is found to vary from 0.08 (Black Hill of Kachchh) to 0.57 (Gopnath-Bhavnagar). AOD calculated by integrating extinction profiles also showed similar trend from station to station (see Table 4.2). However, significant difference between two AOD calculations was found in one to one comparison. This could be because of usage of constant lidar ratio value of 40 sr to retrieve extinction profile at all the location. An attempt was made to calculate lidar ratio when sun-photometer AOD and lidar measurements are available simultaneously. Lidar AOD is calculated as function of lidar ratio and using bisection iteration it matched to the sun-photometer AOD at 497 nm. It is found that lidar ratio varies from 14 to 41 sr. Since sun-photometer AOD measurements are not available during night time and also the difference between

lidar derived AOD and the sun-photometer derived AOD is random, in the present discussion only lidar derived AOD is used.

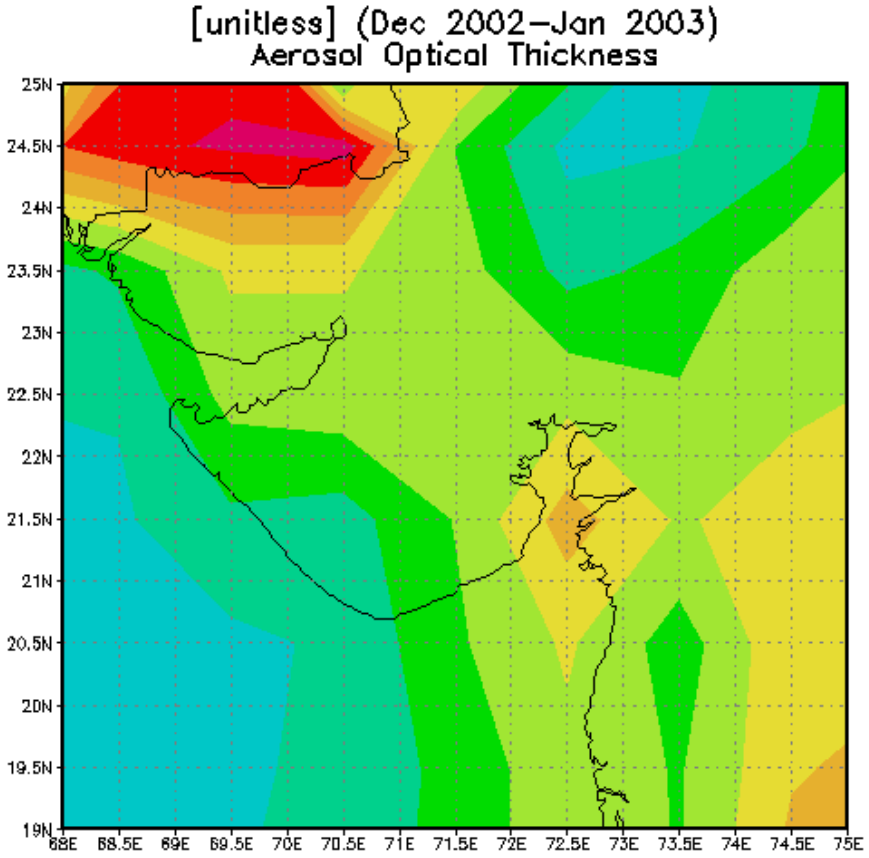

Figure 4.12. Mean MODIS derived AOD data from December 2002 to January 2003 showing accumulation of aerosols over gulf of Khambhat.

Though Gopnath is neither an urban location nor it is close to big industry, we observe very high AOD there. It is likely that geography of Gopnath is playing major role in increasing the AOD. Figure 4.12 shows mean AOD from December 2002 to January 2003 obtained from MODIS. AOD over gulf of Khambhat is more than any other place of Gujarat. On the one hand gulf of Khambhat is downwind of urban and densely populated locations such as Ahmedabad, Kheda, Nadiad, etc, on the other hand eastern coast of gulf is highly industrialized area of Gujarat. Interesting observation is that AOD over gulf of Khambhat is higher

than the locations claimed as source of aerosol over gulf of Khambhat. *Chand and Lal* (2004) have also observed ozone concentration higher than Ahmedabad close to gulf of Khambhat though sources for precursor gases are claimed to be over Ahmedabad and other cities upwind. In the absence of data on micrometeorology close to gulf of Khambhat it is presumed that diurnal cycle of differential heating between sea and land surface may have significant role for stagnation of pollutants over gulf of Khambhat. Also relative humidity over gulf of Khambhat is expected to be more in comparison to upwind locations that can also contribute to the observed high AOD.

Figure 4.13 and Figure 4.14 show aerosol extinction profiles at selected coastal and inland stations. Only those profiles are selected which are obtained approximately same time of the day that is within two hours of sunset. Significant difference between inland and coastal stations particularly in low altitude range (0 to 300 meter) is seen. Over inland stations aerosol extinction is very high (0.4 to 0.9 km^{-1}) in this low altitude layer, whereas in the case of coastal station it is difficult to distinguish between this layer and the layer above it. Aerosol extinction in lower layer is in the range of 0.06 to 0.2 km^{-1} for the coastal stations as shown in Figure 4.13. Similar shape and magnitude of extinction profile over Ahmedabad is observed only during the monsoon months (Figure 3.4). Coastal stations experience more dew formation throughout the year in comparison to inland stations, which renders surface wet and minimize supply of particle from the Earth's surface. In other words, first layer is mainly characterised by the dust from the surface injected into the atmosphere by action of wind or anthropogenic activity. A subtle difference is observed in the height of boundary layer between inland stations and coastal stations. In general, coastal region have a deeper boundary layer, as it experiences sea breeze and day-night reversal of wind, which raises the height of boundary layer. Difference in boundary layer height may be the feature peculiar to winter months as ocean and land surfaces respond differently to solar insolation received.

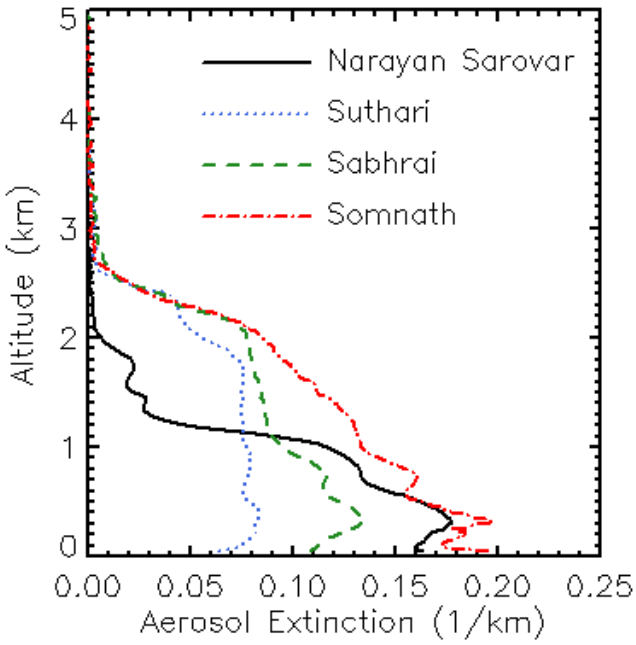

Figure 4.13. Aerosol extinction profiles obtained close to coastal region, showing low aerosol extinction value at lower altitudes.

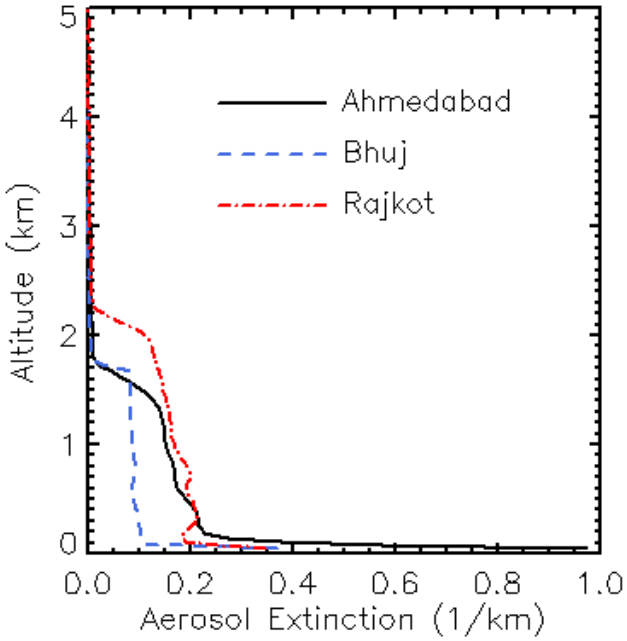

Figure 4.14. Aerosol extinction profiles obtained over inland region showing higher aerosol extinction value at lower altitudes.

4.3 ISRO-GBP Road Campaign

Under the Indian Space Research Organization's Geosphere Biosphere Program of (ISRO-GBP) a road campaign was undertaken from Ahmedabad to Hyderabad and back during February 2004 to study the spatial distribution of aerosol and trace gases in the central/peninsular India. Henceforth this road campaign will be referred to as LC-1. Apart from PRL, about nine other institutes/universities participated in LC-1. Teams from all the institutes started journey from their headquarters to Hyderabad and made observations en-route. At Shaadhnagar (a small town about 60 km south of Hyderabad) intercomparison exercise for various instruments was carried out for 5 days. Also, over Hyderabad aircraft based measurements for extinction profile, trace gases and black carbon were also carried out on explorative basis. More detail on aircraft based measurements is presented in next section. PRL team covered wide range of locations ranging from urban and highly industrialized areas like Surat to interior rural areas. Campaign started from Ahmedabad on 7th February 2004 and first measurements were carried out close to Kheda. Table 4.3 shows the latitude, longitude of the stations along with their name and duration of observations. Places of observations were chosen in upwind direction at least 3 km from the road and at least 10 to 15 km away from town or city. Aerosol related measurements were made for vertical profile, optical depth, absorption and scattering coefficient, mass concentration, and number and mass size distribution. In addition, meteorological parameters were also recorded using portable automatic weather station. Observations were normally carried out continuously between 10:00 and 17:00 hrs. However during return journey because of high temperature and low solar zenith angle, lidar measurements were carried out only in morning and evening hours, while other measurements were taken continuously. Travelling was done during the late evening and early morning hours. At the places of stay, observations of vertical profile of aerosol were carried out for about an hour in night. Figure 4.15 shows the map of the route taken during LC-1. Open circles show the locations during onward journey and filled circles show the locations

during return journey. As far as possible, same locations were selected during onward and return journey. In the background of the route shown is composite surface reflectance over India. Surface reflectance is observed by moderate resolution imaging spectroradiometer (MODIS) on board Terra and Aqua satellite and data are provided by land discipline for MODIS of NASA, USA. Image is created using reflectance at three wavelength bands namely 645, 555, and 469 nm for red, green and blue colours, and gamma corrected. Area covered is mainly arid and semi arid region.

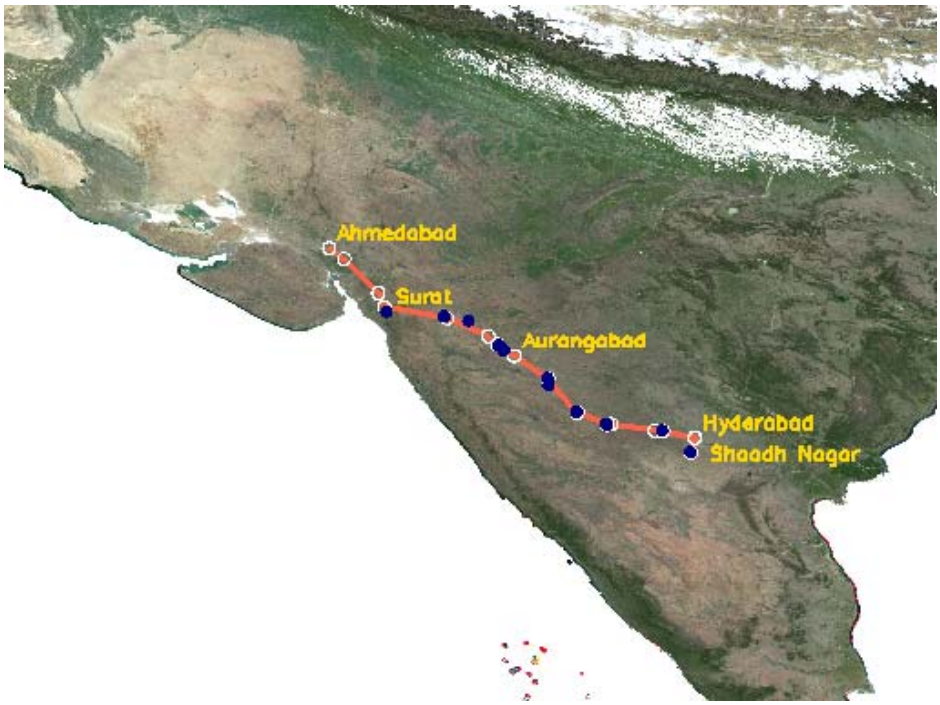

Figure 4.15. Route map of Land Campaign-1. In the background is the surface reflectance obtained from MODIS. Background image is created from reflectance at three wavelengths viz. 645 (Red), 555 (Green) and 469 (Blue) nm. Figure is gamma corrected. Open circles show the stations during onward journey and filled circles show the stations during return journey.

Table 4.3. Latitude, longitude of the location, time duration of the lidar measurement and average AOD observed for that station.

Sr. No.	Place	Lat ^{0}N	Lon ^{0}E	Date	Time (IST*)		AOD
					From	To	
1	Ahmedabad	23.04	72.54	06/02/2004	00:00	03:00	0.277
2	Antroli	22.73	72.73	07/02/2004	13:30	16:15	0.449
3	Bharuch	21.73	73.03	07/02/2004	22:19	23:25	0.183
4	Chorasi gaon	21.31	72.96	08/02/2004	11:24	16:30	0.391
5	Sakri	20.99	74.29	09/02/2004	10:49	16:41	0.485
6	Chalisgaon	20.46	75.00	10/02/2004	23:27	00:29	0.387
7	Palana	20.21	75.10	10/02/2004	12:27	16:43	0.515
8	Aurangabad	19.88	75.34	11/02/2004	00:26	01:32	0.457
9	Khandvi	19.20	75.81	11/02/2004	11:56	17:00	0.690
10	Osmanabad City	18.19	76.04	12/02/2004	23:50	01:16	0.416
11	Osmanabad-Outskirt	18.22	76.06	12/02/2004	10:04	17:00	0.542
12	Omarga	17.85	76.59	13/02/2004	00:13	01:24	0.403
13	Madaj	17.86	76.69	13/02/2004	11:09	16:53	0.808
14	Jahirabad	17.68	77.62	14/02/2004	23:35	00:33	0.439
15	MagdumPalli	17.66	77.80	14/02/2004	10:41	16:49	0.810
16	Hyderabad-City	17.47	78.45	15/02/2004	17:10	19:46	0.534
17	Shaadhnagar	17.03	78.19	18/02/2004	19:37	21:11	0.357
18	Shaadhnagar	17.03	78.19	19/02/2004	21:32	22:35	0.402
19	Shaadhnagar	17.03	78.19	20/02/2004	21:00	23:59	0.486
20	Shaadhnagar	17.03	78.19	21/02/2004	06:45	09:45	0.451
21	MagdumPalli	17.66	77.80	23/02/2004	11:58	17:32	0.502
22	Omarga	17.85	76.59	24/02/2004	00:12	01:13	0.424
23	Gunjoti	17.82	76.59	24/02/2004	10:18	17:05	0.641
24	Osmanabad	18.19	76.04	25/02/2004	23:38	01:32	0.390
25	Osmanabad-Outskirt	18.22	76.06	25/02/2004	09:50	12:45	0.612
26	Beed	19.00	75.75	25/02/2004	21:52	23:20	0.465
27	Khandvi	19.20	75.81	26/02/2004	10:22	10:59	0.736
28	Ellora	20.02	75.18	27/02/2004	00:13	01:20	0.533
29	Hatnoor	20.18	75.13	27/02/2004	10:58	17:26	0.740
30	Dhule	20.89	74.77	28/02/2004	05:45	07:05	0.585
31	Sakri	21.02	74.26	28/02/2004	12:09	17:23	0.720
32	Surat	21.16	72.96	01/03/2004	00:15	01:03	0.552

*IST – Indian Standard Time

4.3.1 Results and Discussion

Figure 4.16 shows the aerosol extinction profile during daytime (a) and night time (b) over few selected stations. Altitude shown on the Y-axis is height above

ground level. In Figure 4.16 (a) profile shown with solid line is for Kheda, the first station after leaving Ahmedabad (Figure 4.15).

(a)

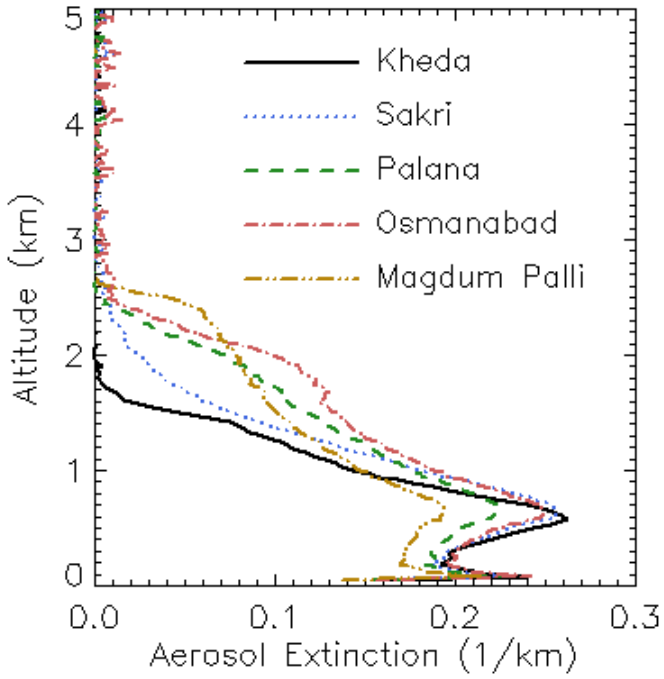

(b)

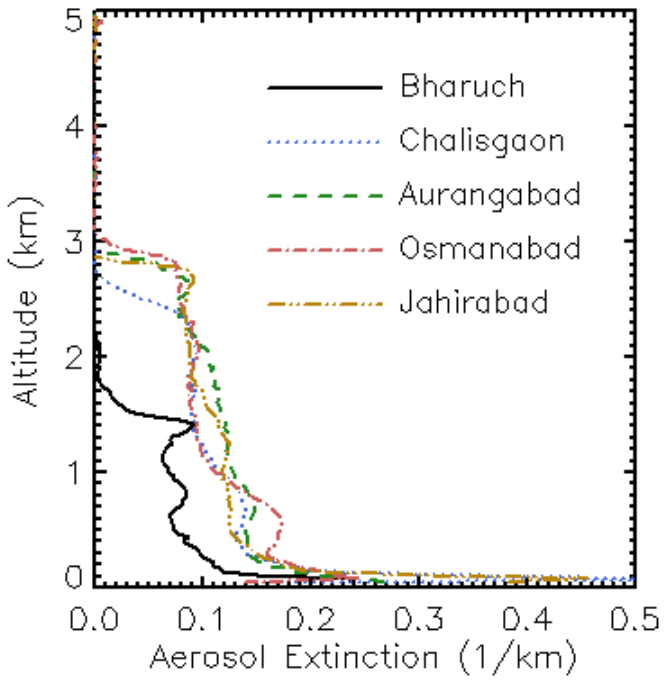

Figure 4.16. Aerosol extinction profiles observed at selected locations are shown for (a) daytime (b) nighttime.

There is a large difference seen in the boundary layer height (altitude where a sharp decrease in aerosol extinction is observed) between the Kheda and other stations. Similarly the nighttime profiles obtained over Bharuch, the second station after Ahmedabad, show the lowest boundary layer height in comparison to other stations. Kheda, Bharuch and Surat have boundary layer height around 1.75 km whereas over other stations it ranges from 2.5 to 3.0 km except Sakri where boundary layer height is around 2.0 km. There are two possibilities for the observed difference in boundary layer height between these stations. One possibility is the temporal variation in boundary layer height as winter to summer transition takes place during February over India. Indeed it is found that boundary layer height is higher during the return journey than in onward journey if compared over same location. Over Surat during return journey meteorological condition, mass concentration, size distribution, scattering and absorption coefficients, etc. were completely different. Boundary layer height over Surat during return journey is higher than onward journey but in comparison to its nearest location on Deccan plateau i.e. Sakri during return journey it is about 1000 m lower. Unfortunately, lidar failed on the 29 February night and measurements could not be taken from Surat onwards i.e. over Bharuch and Kheda. Another possibility is due to difference in the geography of the places. Lower boundary layer height is observed at four stations including Ahmedabad in first week of February. These four stations are close to coastline in comparison to all other stations. Land surface gets more heated than ocean surface for equal amount of solar insolation. Such a differential heating is responsible for large scale wind pattern such as Walker Circulation. Monthly mean vertical wind speed (omega) averaged over latitude band 15^0N to 22.5^0N (typical of LC-1 latitude range) in the unit of Pascal/s is shown in Figure 4.17 for February 2004. Data (known as NCEP reanalysis data) are obtained from Climate Diagnostic Center (CDC), NOAA, USA. Negative sign means upward motion of air parcel. Surface level value of omega over first four stations is between 0 to -0.01 Pascal/s whereas over interior stations it is between -0.02 to -0.03 Pascal/s. Also change in the sign of

omega takes place at around 900 mbar over longitudes between 72.5^{0}E and 73^{0}E whereas over interior locations sign change takes place at 700 mbar which closely correspondence to boundary layer height observed using lidar.

Increase in boundary layer height is also observed by *Wandinger et al.* (2004) as distance from Atlantic Ocean increases into Europe. *Wandinger et al.* (2004) have found that boundary layer height is around 1.5 km over Aberystwyth, which is located at west coast of Wales in North West Europe, whereas boundary layer height is about 2.8 km over Minsk, an interior continental station in Belarus.

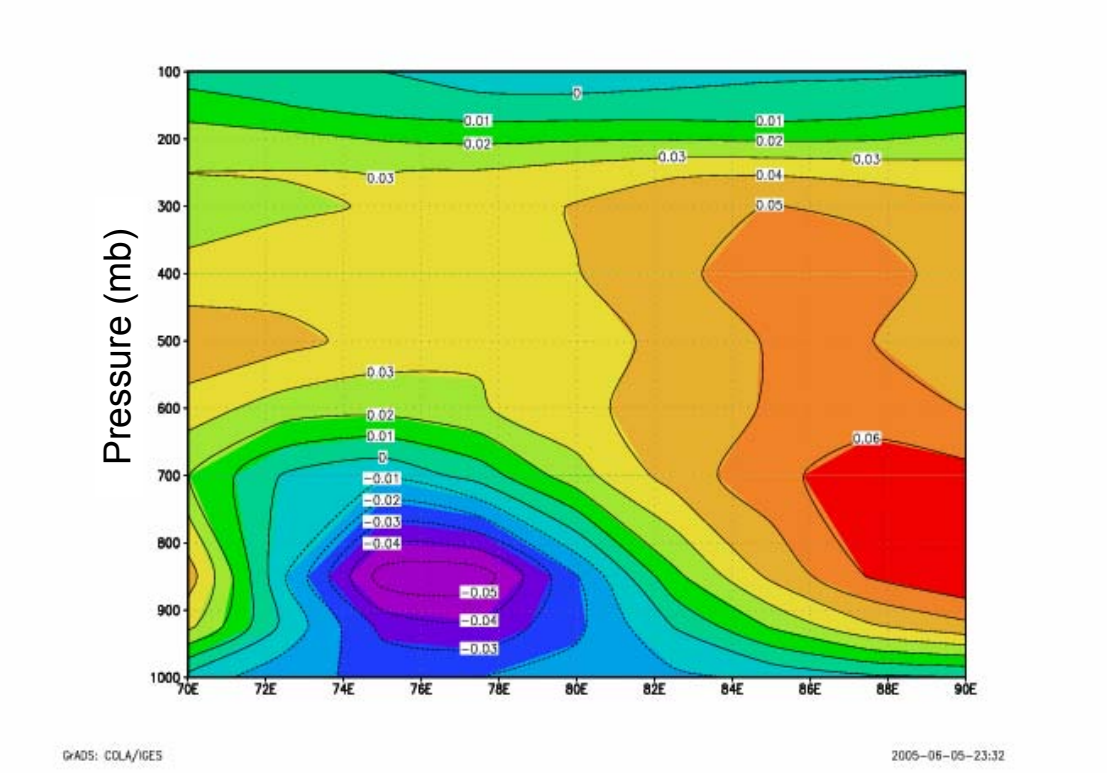

Figure 4.17. Monthly mean vertical wind speed (Pascal/s) during February 2004 averaged over latitude 15^0 N to 22.5^0 N.

Another interesting observation came from LC-1 is difference between day and night time aerosol profiles. A layer between 300 to 900 meter is seen in all day time profiles, while it is absent in night time profiles. Similar difference in day and night time profiles is also observed during Gujarat Road Campaign (see section

4.2). Aerosol extinction profiles are integrated and AOD for day and nighttime are calculated. Figure 4.18 shows the observed AOD during this land campaign for daytime and nighttime separately. Nighttime AOD is consistently lower than daytime AOD. Nighttime AOD is found 12 to 80% lower than the nearest neighbour day time AOD.

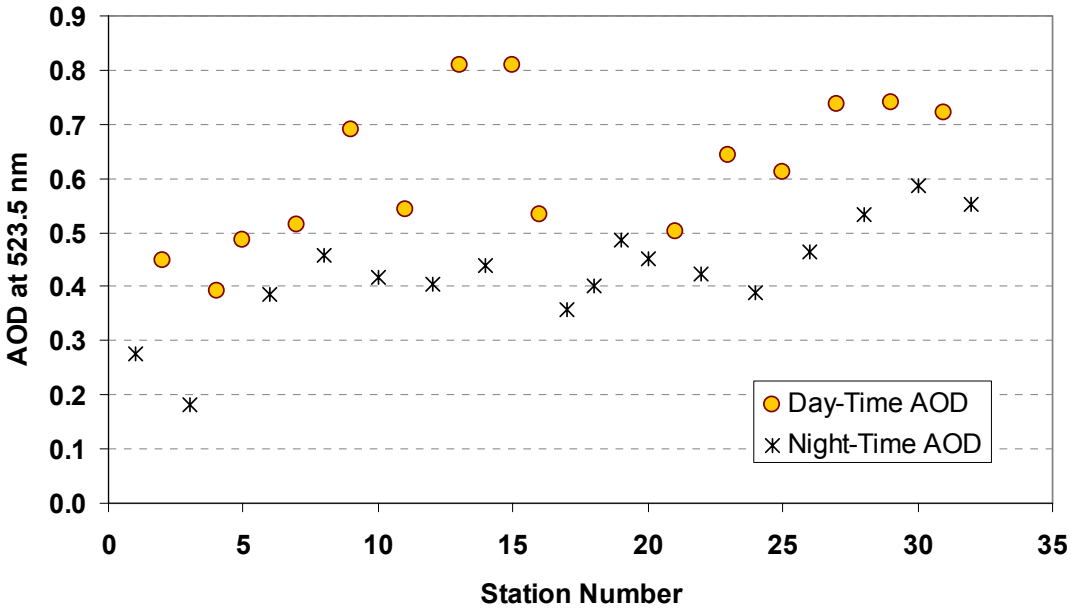

Figure 4.18. AOD values obtained by integrating the lidar measured aerosol extinction profiles. Circles show the daytime AOD and stars show the nighttime AOD values.

4.4 Air-borne MPL Measurements over Hyderabad

During the ISRO-GBP land campaign (LC-1) aircraft based lidar measurements were carried out for the first time over India. These measurements were explorative in nature and conducted to assess the possible scientific advantages for future space-borne lidar measurements.

4.4.1 Instrumentation

The same Micro Pulse Lidar (MPL) system, used for ground based observation and described in Chapter 2 was used for the air-borne study. A special mounting

and mechanical adapter were fabricated at PRL workshop to install the lidar inside the aircraft looking down through a glass window in the base of aeroplane kept for aerial photography. Aircraft (Raytheon Aircraft, Beech Super King Air 200 series) was provided by the National Remote Sensing Agency. Unlike the ground based measurements aircraft can tilt when measurements are in progress, which is recorded by a digital roll and pitch inclinometer developed at PRL. Also required software to get inclinometer data online was developed in house. MPL was kept tilted around 6^0 with respect to plumb line to avoid the light reflected from the glass window entering into MPL.

Aircraft was flown at a height of about 8 km. As the lidar system is mono-static and coaxial there will be no error in range estimation and related calculations due inclination of lidar with respect to vertical direction. However, height assigned to various layers from ground level will be overestimated by a factor equal to inverse of cosine of inclination. Data obtained at high inclination particularly during the turning of aircraft were avoided in analysis. For rest of the data inclination was within 10 degree with respect to nadir. Error in estimate of height for aircraft could be around 100 m for 10 degree inclination and error in the estimate of boundary layer top could be only 30 m, hence no specific correction for inclination was applied to data.

There were two sorties made each of about 2 hrs duration, one on 17 February 2004 evening and another on 18 February 2004 morning. Aircraft travelled repeatedly the stretch of around 150 km in south north direction with an average speed of 320 km/hour. This route was preferred so as to travel perpendicular to wind direction as climatological mean wind direction is easterly over Hyderabad during winter.

4.4.2 Data Reduction Algorithm

Aircraft and satellite based lidar measurements are relatively new and very little literature exists for data reduction. Algorithms available for ground based

measurements can not be used readily because computation of extinctions in forward direction is unstable for small errors in boundary conditions (*Klett*, 1981). Extinction calculations are to be carried out in reverse direction by specifying boundary condition at far end. In case of ground based lidar measurements far end is lower stratosphere or free troposphere. One may use climatological mean or model value and there will be very little error in extinction at lower altitude (see Chapter 2). In case of aircraft based measurements far end is near the Earth's surface where aerosol concentration is not only high but also variable in space and time.

Three algorithms were studied to find its suitability for the analysis of aircraft lidar data. *Klett* (1985) method in forward direction is used during the INDOEX aircraft based measurements near Kaashidoo Iceland of Maldives by *Pelon et al.* (2002). Integrated ratio method is proposed by *Palm et al.* (2002) for use in Geoscience Laser Altimeter System (GLAS). In this technique first the transmission of aerosol layer is calculated by taking the ratio of integrated measured photon counts to that computed for aerosol free atmosphere. In this algorithm first backscattering coefficient is calculated and then extinction coefficient is obtained by multiplying it with lidar ratio in order to get the extinction profile. In case of present aircraft lidar data, the algorithm is found to underestimate aerosol extinction coefficients.

In the present study extinction coefficient is calculated by adapting algorithm proposed by *Stephens et al.* (2001). The most obvious advantage of this algorithm is that it allows the incorporation of AOD in the algorithm in very straight forward manner. Also, by incorporating AOD in this algorithm, it is possible to estimate the lidar ratio. However, it was found that calculations of lidar ratio are quite sensitive to calibration of lidar signal, therefore results of lidar ratio are not discussed here. However, when AOD measurements are available, there is very small error produced in extinction profile due error in calibration of lidar. This algorithm is based on optimal estimation method (*Rodgers*, 2000). Following paragraphs describe this algorithm briefly.

$$\hat{\mathbf{x}}^{n+1} = \mathbf{S}_x^n(\mathbf{S}_a^{-1}\mathbf{x}_a + \mathbf{K}^{nT}\mathbf{S}_y^{-1}[\mathbf{y} - \mathbf{f} + \mathbf{K}^n\hat{\mathbf{x}}^n]) \quad 2.25$$

In the above equation **x** is the quantity to be retrieved and is known as result vector. In present case it is the extinction values at different altitudes. **y** is the quantity measured, known as measurement vector, and in present case it is the range corrected signal or aerosol optical depth as described in the equation 2.27. The '**f**' is known as forward function, and relates measurements to retrievable quantity as shown in equation 2.28. $\mathbf{S}_x^n$ is the error co-variance matrix for *n*th iteration. $\mathbf{S}_a$ and $\mathbf{S}_y$ are error co-variance matrix for a priori knowledge of aerosol extinction and measurement error. Superscript T denotes the transpose of matrix.

$$\begin{aligned} x_j &= \{\sigma_{A,j};\ j = 1,...,N\} \\ x_{N+1} &= k \end{aligned} \quad 2.26$$

$$\begin{aligned} y &= \{\ln(C\,P(r_j)\,r_j^2);\ j = 1,...,N\} \\ y(N+1) &= AOD \end{aligned} \quad 2.27$$

$$\begin{aligned} \mathrm{f}_j &= \ln(\beta_{M,j} + \beta_{A,j}) - 2\sum_{l=1}^{j}[\sigma_{M,l} + \sigma_{A,l}]\Delta R \\ \mathrm{f}_{N+1} &= \sum_{l=2}^{N}\sigma_l\,\Delta R \end{aligned} \quad 2.28$$

For i and j varying from 1 to N

$$\begin{aligned} K_{ij} &= 0 \quad i < j, \\ K_{ij} &= -2\,\Delta R \quad i > j, \\ K_{ij} &= \frac{k}{\beta_{M,i} + k\,\sigma_{A,i}} - 2\,\Delta R \\ K_{i,N+1} &= \frac{\sigma_{A,i}}{\beta_{M,i} + k\,\sigma_{A,i}} \\ K_{N+1,j} &= \Delta R \end{aligned} \quad 2.29$$

In equation 2.26, 2.28 and 2.29 subscript M and A denote air molecules and aerosol respectively. ΔR is the range resolution of lidar system. The constant *k* in equation 2.26 and 2.29 is defined as $4\pi\beta_A/\sigma_A$, inverse of it is known as the lidar ratio. Equivalent quantity for Rayleigh scattering can be calculated theoretically and it is 8 π/3. Equation 2.27 requires the knowledge of calibration constant '*C*' of lidar, which can be calculated through regression analysis from that part of the signal where lidar return is entirely from Rayleigh scattering. Equation 2.25 requires a priori knowledge of aerosol extinction. Normally in optimal estimation method a priori knowledge is specified through climatological data however for the aerosol extinction no such data exists. To specify a priori aerosol extinction and to start the iteration an approximate aerosol extinction profile is computed using following equation:

$$\sigma_{A,i} = \{\exp(y_i + 2\sum_{l=1}^{i-1}[\sigma_{M,l} + \sigma_{A,l}]\Delta R) - \beta_{M,i}\}/k \qquad 2.30$$

In equation 2.25, error co-variance matrices are taken diagonal and can be calculated as follows,

$$\begin{aligned} S_{a,ii} &= \sigma_a^2 \\ S_{y,ii} &= \varepsilon_y^2 + \sigma_{b1}^2 + \sigma_{b2}^2 \\ \mathbf{S}_x^n &= \left(\mathbf{S}_a^{-1} + \mathbf{K}^{nT}\mathbf{S}_y^{-1}\mathbf{K}^n\right)^{-1} \end{aligned} \qquad 2.31$$

Here ε_y is the error in measurement, likewise σ_{b1} and σ_{b2} are the error factors arising out of error in Rayleigh back-scattering and lidar ratio. They can be calculated as follows,

$$\begin{aligned} \sigma_{b1} &= \frac{0.02\beta_{M,i}}{\beta_{M,i} + k\,x_i}; \text{ when 2\% error in Rayleigh backscattering} \\ \sigma_{\mathrm{b2}} &= \frac{\Delta k_i x_i}{\beta_{M,i} + k\,x_i} \end{aligned} \qquad 2.32$$

4.4.3 Results and Discussion

(a)

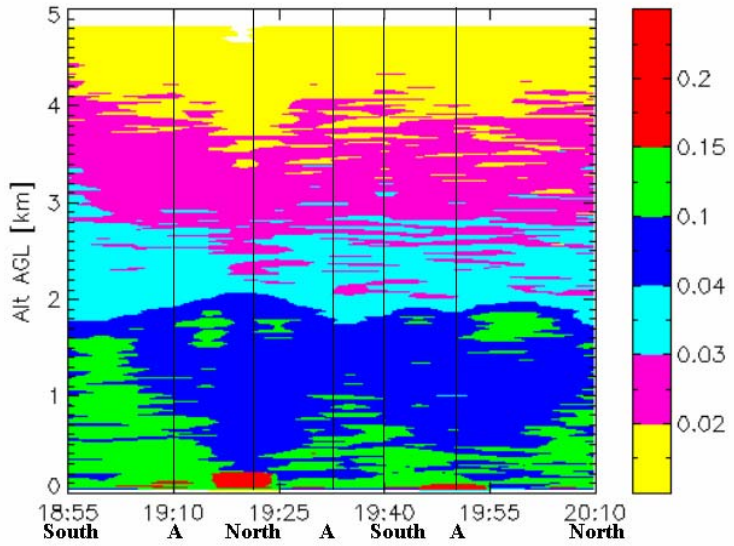

(b)

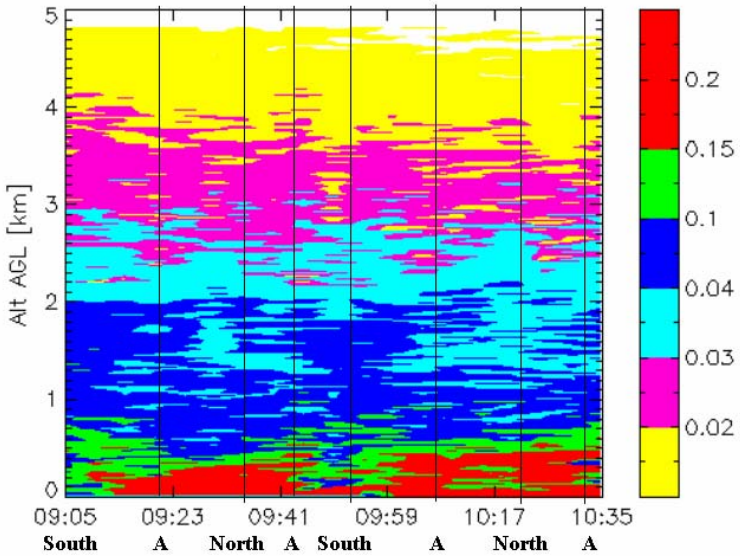

Figure 4.19. Aerosol extinction observed over Hyderabad from aircraft based measurements on (a) 17 Feb 2004 Late Evening and (b) 18 Feb 2004 Morning hours.

Figure 4.19(a-b) shows the aerosol extinction observed on 17 February 2004 late evening and 18 February 2004 morning. Height of the boundary layer is found to

be constant at around 2 km on both days and over the full stretch of 150 km. However state of mixing is quite different between two days. On 17 February 2004 aerosols are well mixed in boundary layer up to 2 km, particularly in the region south of the airport. On the 18 February 2004 aerosol distribution is uniform in south and north part and stratified within a layer of about 300 meter. The difference in state of mixing between two days may be because of diurnal variability. During nighttime the earth's surface is radiatively cooled and air in contact with the Earth's surface has lower temperature than layer aloft. Hence inversion is formed, which traps the pollutants close to surface. Study over other places (*Murthy et al.*, 2004, *Pillai and Moorthy*, 2001, *Guasta*, 2002) indicates that inversion does not break until 10:30 hrs whereas our observations were carried between 9 to 10 hrs on 18 February 2004. In the free troposphere aerosol extinction is quite uniformly distributed over the region and almost same on both the days.

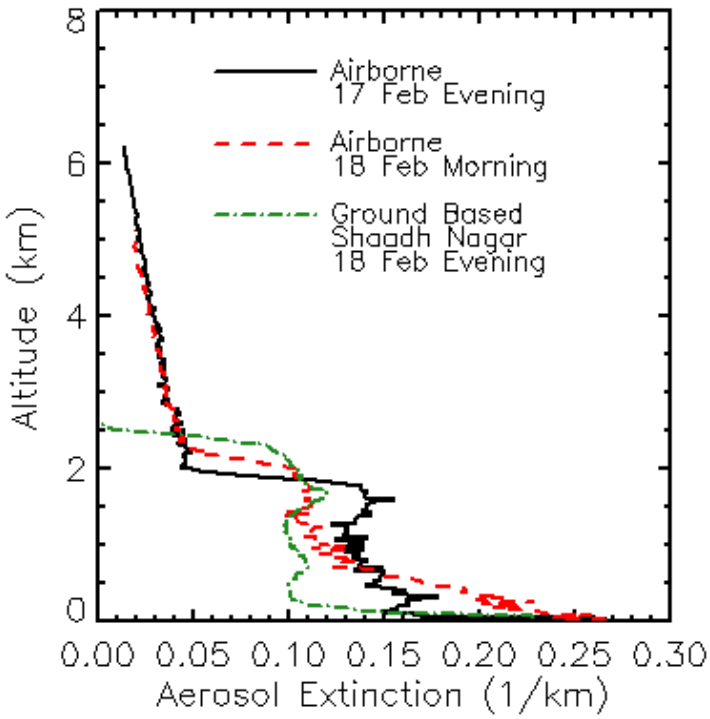

Figure 4.20. Comparison of average aerosol extinction profiles observed from Aircraft with the ground based measurements made at Shaadhnagar.

Figure 4.20 shows the comparison of average aerosol extinction profile observed on 17 and 18 February 2004 from aircraft with that obtained from ground based measurements made at Shaadhnagar on 18 February evening hours. Comparison reveals very obvious advantage of aircraft based study of aerosols in free troposphere. Free troposphere have low extinction values and weak signal from free troposphere is often masked out by high extinction values in lower altitude as it can be observed in the case of Shaadhnagar based lidar measurements. In case of aircraft based lidar measurements, signal to noise ratio is good through out the range from aircraft to ground. This is because laser pulse starts in region of low aerosol concentration and encounters high aerosol concentration at far end where intensity of scattered light is high.

MODELLING THE EFFECT OF OBSERVED AEROSOL PROPERTIES ON RADIATION BUDGET

Aerosols can affect the climate in various ways; important of them is their interaction with shortwave and long-wave radiation. Aerosols absorb and scatter back the solar radiation and hence reduce the net energy received at the surface of the Earth. Effect of aerosol on radiation budget is assessed by the parameter called "radiative forcing" which is defined as change in net radiative flux at given atmospheric level due to change in given parameter such as aerosol while holding all other parameters fixed.

5.1 Software Tools Used To Calculate Radiative Forcing

Radiative forcing is calculated in diagnostic manner i.e. first net downward radiative fluxes are calculated with and without aerosols then difference between them is taken as radiative forcing by aerosol. Radiative fluxes are calculated using software Santa Barbara DISORT Atmospheric Radiative Transfer (SBDART) code developed by *Ricchiazzi et al.* (1998). Acronym DISORT stands for Discrete Ordinate Radiative Transfer. Obvious from its name, software uses discrete ordinate method to integrate radiative fluxes from different directions. The software relies on low resolution band model (LOWTRAN) for the transmission calculations. SBDART is tested with actual observations and with well established codes, which calculate radiative transfer line by line, and the results are in excellent agreement.

5.2 Inputs (Other than Aerosol)

5.2.1 Atmospheric Profile

Atmospheric profiles of air density are calculated using FNL data (*Stunder*, 1997) for temperature and pressure at a given place and time. FNL data for temperature and height are available at 13 fixed pressure levels starting from surface to 20 mb

on 129x129 polar stereographic grid on northern and southern hemispheres separately. Apart from temperature and height (pressure), FNL data set also contains relative humidity, cloud cover, total precipitation etc. Values of relative humidity (RH) are available up to 300 mb. Water vapour profiles are calculated from relative humidity and temperature values using Goff-Gratch equation (*Goff and Gratch,* 1946). Profiles obtained from FNL data are merged with standard atmospheric profile for tropical atmosphere (*McClatchey et al.*, 1972) at higher altitude. Ozone profile is kept same as available in the standard tropical atmosphere, but scaled by the total column ozone concentration value measured using Microtops-II. Whenever Microtops-II measurements are not available, Ozone values from Total Ozone Mapping Spectrometer (TOMS) onboard Earth Probe satellite are used (http://toms.gsfc.nasa.gov/).

5.2.2 Surface Reflectance

Aerosol radiative forcing (ARF), particularly over land surfaces, highly depends on the surface reflectance values. Depending upon surface underneath ARF can vary from negative to positive for same aerosol amount and type. ARF calculations over oceans are relatively easy to do since spectral reflectance of ocean surfaces are better understood than other surfaces. In the present work, aerosol radiative forcing calculations over Bay of Bengal are done using surface reflectance from *Viollier* (1980). Snow surfaces also exhibit less variability in comparison to open land surfaces and hence model value for snow surfaces from *Wiscombe and Warren* (1980) is used for radiative forcing calculations over Maitri-Antarctica. Land surfaces are characterised by variety of surfaces e.g. sand, vegetation, wet surface, etc. To calculate the ARF over land, surface reflectance data from Moderate Resolution Imaging Spectroradiometer (MODIS) onboard Terra and Aqua satellites is used. Their seasonal characteristics over Ahmedabad are described in Chapter 3.

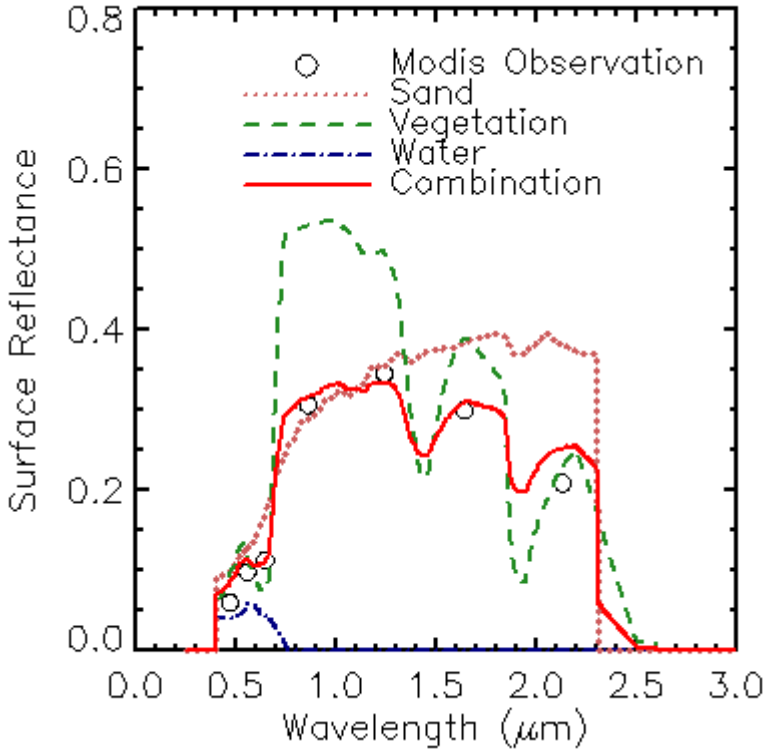

Figure 5.1. Reflectance from different types of surfaces and combination thereof along with reflectance observed by MODIS onboard Terra satellite. Combination is formed by 45 % sand, 35 % vegetation and 20 % water to model fit the MODIS measured surface reflectance over Ahmedabad.

As shown in Figure 5.1, spectral dependence of surface reflectance of sand and vegetation are not a smooth function of wavelength (*Staetter and Schroeder*, 1978, *Reeves et al.*, 1975), whereas surface reflectance from MODIS satellite data are available at only seven wavelength bands, spread between 469 and 2130 nm. Nevertheless, surface reflectance of many surfaces can be approximated by linear combination of surface reflectance such as sand, vegetation, water etc. e.g. wet soil can be well represented by combination of water and sand (*Ricchiazzi et al.,* 1998). To get the spectral reflectance at better spectral resolution than what MODIS provides, surface reflectance are created by combining sand, vegetation and water in certain proportion such that resultant spectrum of surface reflectance is close to observed values. Though this method is somewhat subjective there is very little

scope left for alternative combination which can explain the observed reflectance specially when due consideration is given to the geography of a place. One sample fitting is shown in Figure 5.1 for Ahmedabad. Combination is created by 45% sand, 35 % vegetation and 20% water reflectance. Similar approach is adopted for surface reflectance calculations over other places visited during LC-1.

5.3 Inputs (Aerosol parameters)

5.3.1 Aerosol Optical Depth

Aerosol Optical Depth (AOD) is the most important parameter for aerosol radiative forcing calculations. Measurements of AOD in the cases of Maitri-Antarctica, Bay of Bengal cruise and LC-1 (ISRO-GBP Land Campaign – 1) are done using sun-photometer. In the cases of Ahmedabad and Western Gujarat, AOD values are calculated by integrating extinction profiles obtained from micro pulse lidar. AOD values are available only at selected wavelengths, whereas aerosol radiative forcing calculations are required to be carried out over broad spectrum starting from 0.25 to 4.0 μm (shortwave radiative forcing) and in some cases further 4.0 to 40.0 μm (longwave radiative forcing). Since the AOD values are not available throughout the spectrum, different approaches are adopted depending upon the availability of data. In the case of Maitri-Antarctica, theoretical calculations of AOD are carried out using the newly suggested aerosol model (see Chapter 4, *Gadhavi and Jayaraman*, 2004) and software OPAC (*Hess et al.*, 1998). Similar approach was adopted for radiative forcing calculations for Ahmedabad, Bay of Bengal and Western Gujarat. In case of LC-1, instead of creating the composition as described above and then calculating optical properties, AOD spectrum outside the wavelength range of observations was obtained using Angstrom exponent. This extrapolation seems to be reasonable at least for shortwave range (0.25 to 4.0 μm) as evident from Figure 5.2. In Figure 5.2 AOD values calculated by Mie theory at each wavelength (AOD; Mie) is shown along with AOD spectrum calculated from the Angstrom parameter (AOD; Angstrom Parameter).

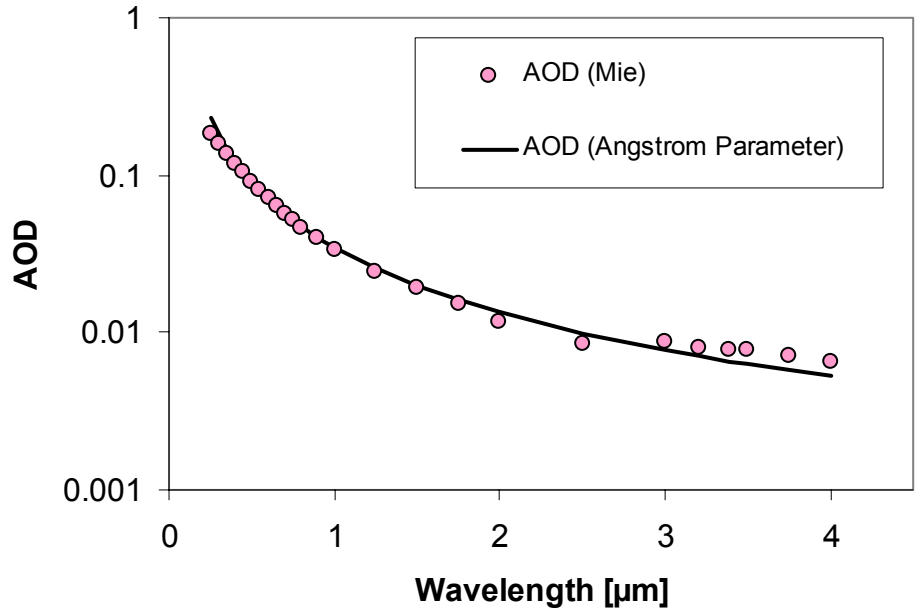

Figure 5.2. AOD spectrum for "continental average" type aerosol model. AOD (Mie) is aerosol optical depth calculated at each wavelength by Mie theory and AOD (Angstrom Parameter) is aerosol optical depth calculated from Angstrom parameter.

5.3.2 Single Scattering Albedo (SSA)

Other two important parameters for aerosol radiative forcing calculations are single scattering albedo (SSA) and asymmetry factor. During the field campaigns to Maitri-Antarctica, Bay of Bengal and Western Gujarat, no measurements were available for SSA and asymmetry factor as well as chemical composition, hence SSA and asymmetry parameter are calculated using software OPAC for suitable aerosol model. In order to do so first a reasonable aerosol model is created using a combination of different aerosol component out of 10 choices available in OPAC. Choices of aerosol components are constrained by the fact that calculated parameters such as size distribution, mass concentration, Angstrom exponent, etc should be close to observed values. Consideration is also given to those parameters for which measurements are not available, they should be physically realisable and consistent with climatology of the place. Though the uniqueness of

solution is not guaranteed, aerosol model created in this manner are fairly reasonable for the computation of radiative forcing. In the case of Ahmedabad, since data of single scattering albedo are available those are used to further constrain the aerosol composition for the calculations of optical properties. Single scattering albedo can change with season but in the case of Ahmedabad, there are not sufficient data of SSA that can be used as representative of season and hence though seasonally varying AOD is used, SSA is taken constant for all season.

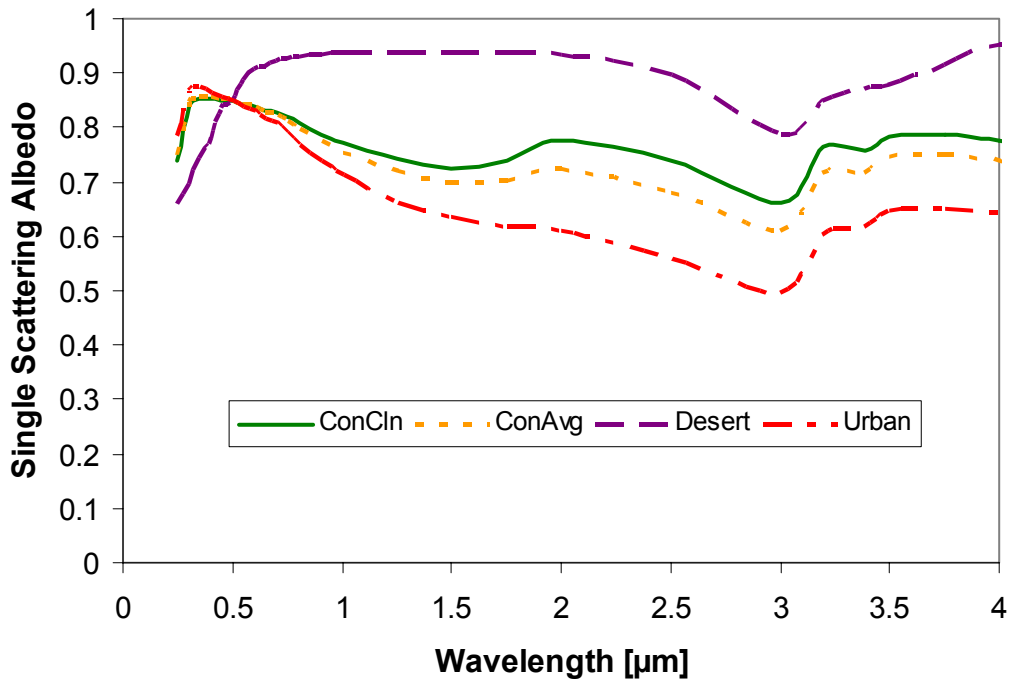

Figure 5.3. Spectral variation of single scattering albedo (SSA) for different aerosol models, where 0.5 µm SSA is scaled to "continental average" aerosol model.

In the case of LC-1 a different approach is taken. Though SSA observations are available during LC-1, they are at only one wavelength. In order to get spectral SSA, two aerosol models out of 10 default models available in OPAC software are identified based on SSA and Angstrom exponent. Spectral SSA obtained from these two aerosol models are scaled in such a manner that the calculated SSA is equal to the observed SSA. Figure 5.3 shows the spectrum of SSA for different

aerosol model scaled to "continental average" model at 500 nm wavelength. SSA for different aerosol models scaled at one wavelength can be quite different at other wavelengths. But still this approach seems to work well at least for shortwave radiative forcing since a very small difference in radiative forcing values is found when two different aerosol models, scaled at observed values, are used.

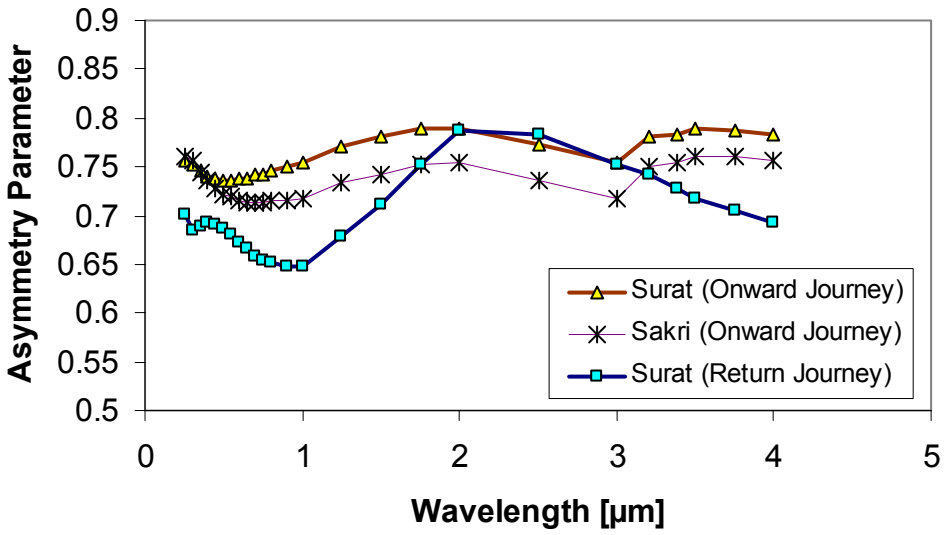

Figure 5.4. Asymmetry parameter calculated from aerosol size distribution measured during the ISRO-GBP land campaign for selected locations.

5.3.3 Asymmetry Parameter

Asymmetry parameter in case of LC-1 is obtained by detailed calculation using Mie scattering theory (*Bohren and Huffman*, 1983) and observed size distribution. Mie scattering theory assumes spherical shape for particles. Though it is an oversimplification, but in situations where no other data are available, this approach seems to be the most appropriate. Figure 5.4 shows spectral asymmetry parameter for few selected locations and Figure 5.5 shows the single scattering albedo and asymmetry parameter at one wavelength used to calculate radiative forcing.

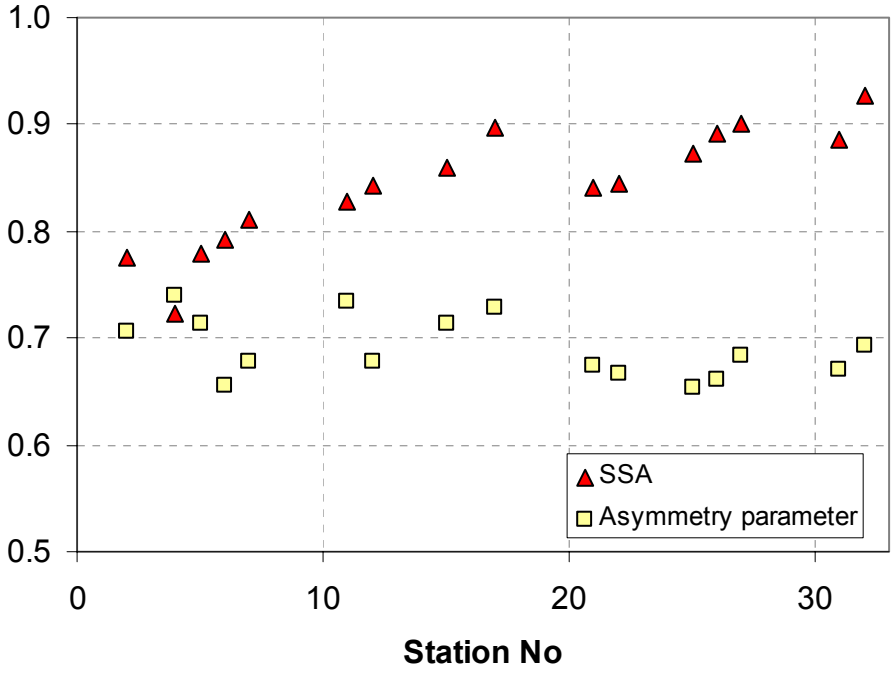

Figure 5.5. Single scattering albedo at 525 nm and asymmetry parameter at 500 nm during LC-1. Station number correspondence to numbers in Table 4.3.

5.3.4 Vertical Distribution of Aerosol

During the field campaigns to Antarctica and Bay of Bengal, observations of vertical distribution of aerosol were not available. In these cases, standard vertical profile of aerosol is used (*McClatchey et al.,*1972). For rest of the places micro pulse lidar measurements are used for vertical distribution of aerosol. In case of Ahmedabad vertical distribution of aerosol at higher altitude i.e. above 15 km is substantiated with data from Stratospheric Aerosol and Gas Experiment-II (SAGE-II) onboard Earth Radiation Budget Satellite (http://www-sage2.larc.nasa.gov/). In addition, two separate aerosol models are specified for boundary layer and free troposphere in the case of Ahmedabad. Above three kilometre of altitude, "continental clean" aerosol model is used for getting the aerosol optical properties.

5.4 Radiative Forcing Results

5.4.1 Aerosol Radiative Forcing over Ahmedabad

Aerosol radiative forcing (ARF) calculations over Ahmedabad are carried out for shortwave range (SW; 0.25 to 4.0 μm) using monthly mean extinction profiles. Diurnal variation of solar zenith angle on 15th of each month is used to calculate the variation in solar insolation. Single scattering albedo is kept constant for all the seasons and is equal to the mean of all measurements (see Chapter 3). Spectral dependence of SSA and asymmetry factor shown in Figure 5.6 is calculated as explained in previous sections.

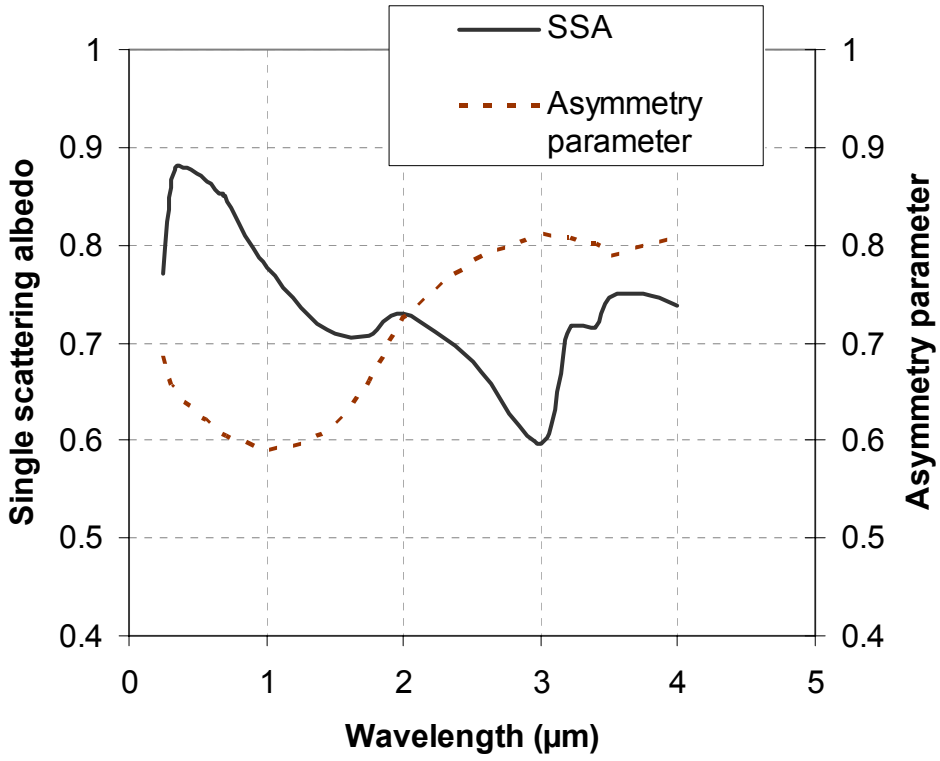

Figure 5.6. Spectral SSA and asymmetry parameter used for boundary layer aerosol to calculate radiative forcing over Ahmedabad.

Figure 5.7 (a-b) shows the seasonal variation in aerosol radiative forcing at top of the atmosphere (TOA) and ground level over Ahmedabad. TOA radiative forcing is in the range of -1.25 to -4.5 W/m^2. Low values in terms of magnitude occur

during the months of April, May and June whereas high values are found during the months of October and November. Surface level radiative forcing also shows seasonal variation ranging from -20 to -70 W/m^2.

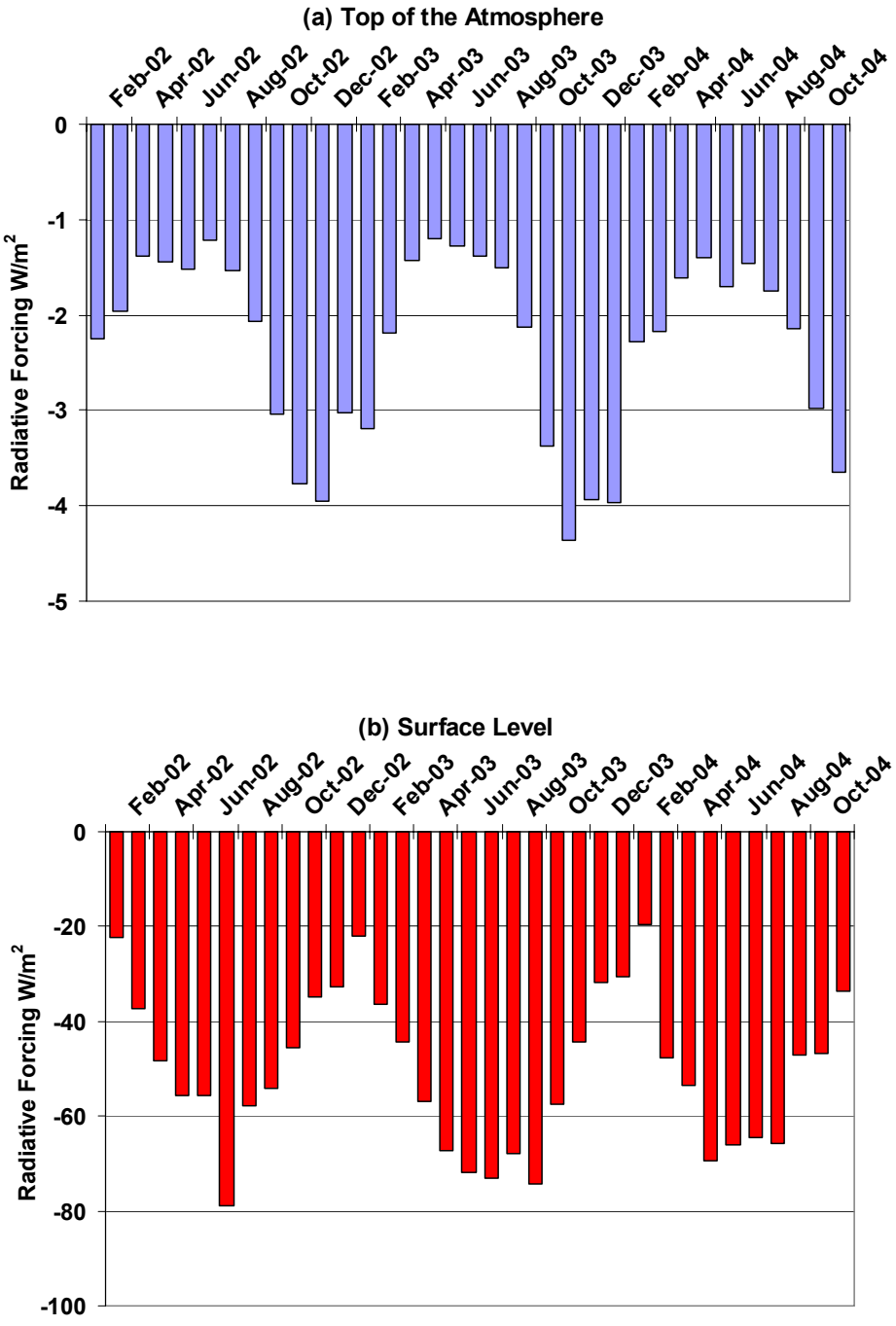

Figure 5.7. Seasonal variation in aerosol radiative forcing obtained over Ahmedabad (a) at top of the atmosphere and (b) at surface level.

Interesting feature of seasonal variation of aerosol radiative forcing (ARF) over Ahmedabad is that the variation at TOA and surface level is almost six months out of phase. Surface level forcing in terms of magnitude peaks during May-June and it is lower during December-January. This could be because of the fact that the aerosol type and variation are different for boundary layer and for free troposphere. Though SSA in boundary layer and free troposphere is kept constant with season in the forcing calculations, due to change in AOD with season particularly in boundary layer, relative aerosol absorption in the boundary layer also changes. This results in modulation of SSA in a manner that an increase in AOD decreases the column averaged SSA and vice versa

In Figure 5.8 SW aerosol radiative forcing (ARF) efficiency i.e. variation in radiative forcing per unit change of AOD is plotted as a function of single scattering albedo (SSA). Calculations are carried out for spectral SSA of "continental average" aerosol model scaled to value shown in figure at 500 nm and for standard atmosphere and surface reflectance observed over Ahmedabad. Figure 5.8 shows that SSA value less than 0.8 will give positive radiative forcing at TOA and increase in SSA beyond 0.8 will result in increase in forcing efficiency (in terms of magnitude). In the case of surface level radiative forcing increase in SSA results in decrease in radiative forcing efficiency. This results in more ARF at surface level than would have been expected from AOD change. At top of the atmosphere, decrease in SSA not only compensates the increase of ARF due to AOD but it results in net decrease of ARF.

Difference between TOA and ground level radiative forcing is absorption within the atmosphere. Since ground level ARF is quite high as compared to TOA ARF, absorption within the atmosphere have seasonal variation and magnitude similar to surface level forcing but positive in sign. This results in differential heating i.e. cooling of the surface and heating of the atmosphere. Vertical distribution of ARF for two months i.e. February and May 2002 is shown in Figure 5.9. Since

majority of aerosols are found in the boundary layer, there is very small difference in radiative forcing above 6.0 km between two months. However, at surface level, ARF in May is factor of ~2.5 higher than February values. Converting this into heating rate, May-2002 heating rate is almost 1^0 K/day higher than Feb-2002 values. Similar difference between summer and winter months is also there for years 2003 and 2004. With such a high heating rate, aerosols contribute toward stabilization of atmosphere during monsoon months, that can suppress convection and hence rainfall (*Chung and Ramanathan*, 2004). The major influence of aerosol on climate will come through the way they redistribute energy vertically rather than their contribution in energy budget at TOA. Later on in this thesis, it is shown that TOA ARF is of the same magnitude over Ahmedabad and Southern Indian Ocean though there is an order of magnitude difference in AOD between them.

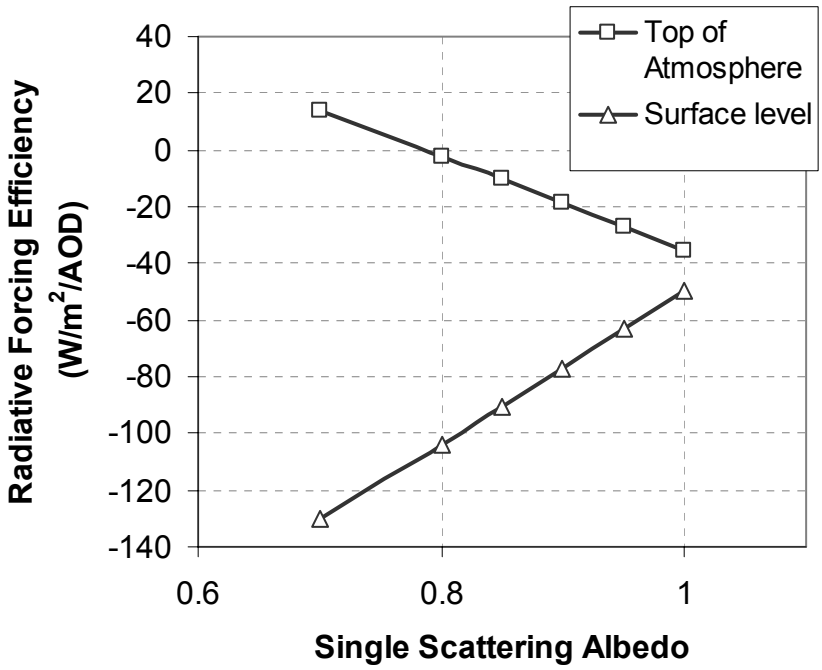

Figure 5.8. Shortwave aerosol radiative forcing efficiency as a function of single scattering albedo at top of the atmosphere and surface level.

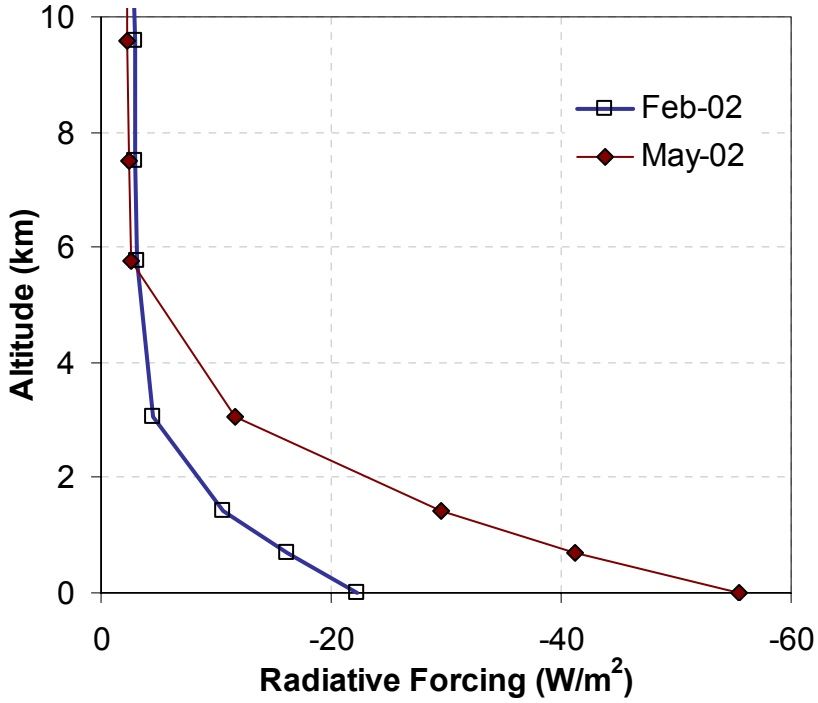

Figure 5.9. Vertical distribution of radiative forcing obtained over Ahmedabad for February (square) and May 2002 (filled diamond).

5.4.2 ARF over Maitri-Antarctica

In case of Maitri-Antarctica, aerosol radiative forcing (ARF) calculations are carried out for short wave (SW; 0.25 to 2.5 μm) and long wave (LW; 2.5 to 40 μm) separately. Note that for SW radiative forcing computation the wavelength range used is 0.25 to 2.5 μm while for all other computation it is 0.25 to 4.0 μm. However, this difference in wavelength range for Maitri-Antarctica will not make any significant difference in SW ARF for comparison purpose as evident from low value of ARF in this region of spectrum over Antarctica. The computed diurnally averaged ARF at surface and TOA for SW and LW are shown in Figure 5.10. The forcing is positive at TOA for both SW and LW, but at the surface, it is negative for SW and positive for LW. The net forcing is 0.95 W/m^2 at TOA and –0.83 W/m^2 at the surface, with absorption of 1.78 W/m^2 within the atmosphere. Positive radiative forcing at TOA over Maitri is due to high surface albedo, typical of the polar region.

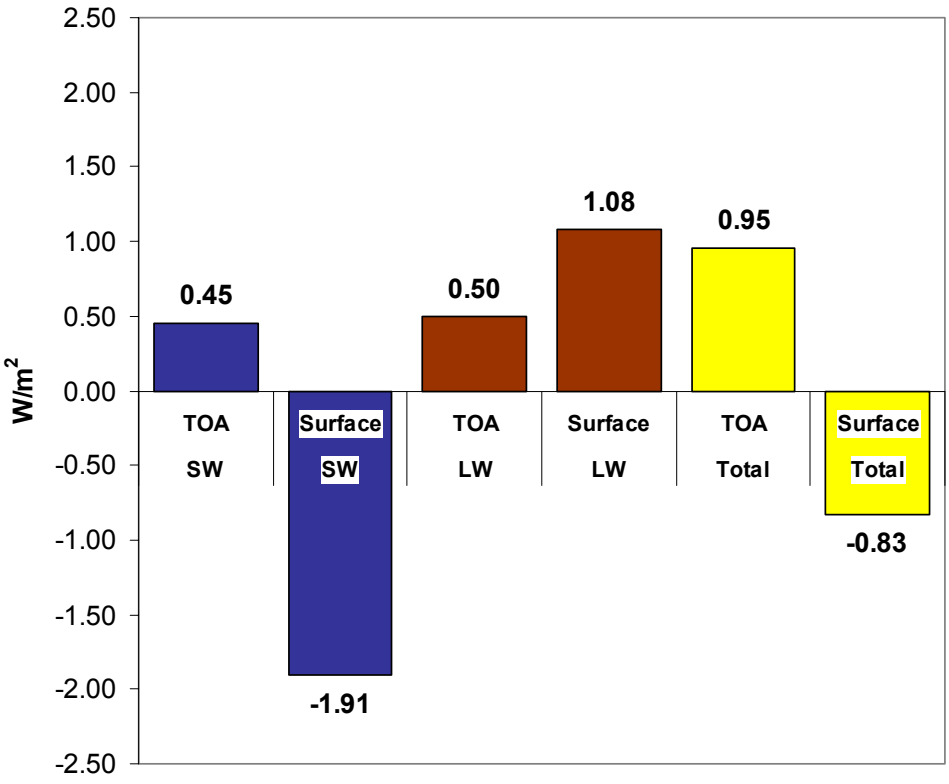

Figure 5.10. Diurnally averaged mean aerosol direct radiative forcing obtained over Maitri, Antarctica for the Jan-Feb 2001 period.

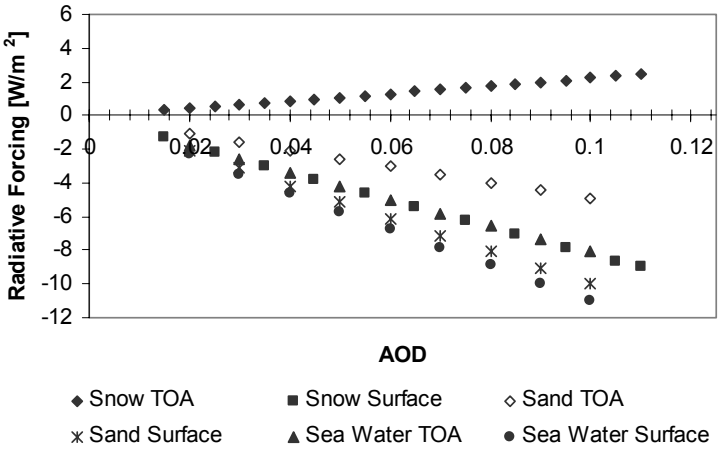

Figure 5.11. Variation in computed aerosol radiative forcing for the same aerosol composition and amount but for different surface types with varying surface albedo.

In order to study the effect of surface albedo on TOA radiative forcing, the model computations are repeated for sand and sea-water surfaces, keeping the aerosol characteristics and amount same as that found over Maitri (Figure 5.11). For unit AOD change, the TOA SW forcing will change by 22.5 W/m^2, –43.9 W/m^2 and –72.9 W/m^2 for snow, sand and sea-water types of surfaces respectively. The observed large change in the radiative forcing efficiencies, from a high-reflective snow surface to low-reflective water surface can be understood, as explained by *Harshvardhan* (1993) that the presence of aerosols over bright surfaces has an overall effect of reducing the planetary albedo, while over dark surfaces it has an overall effect of enhancing the albedo.

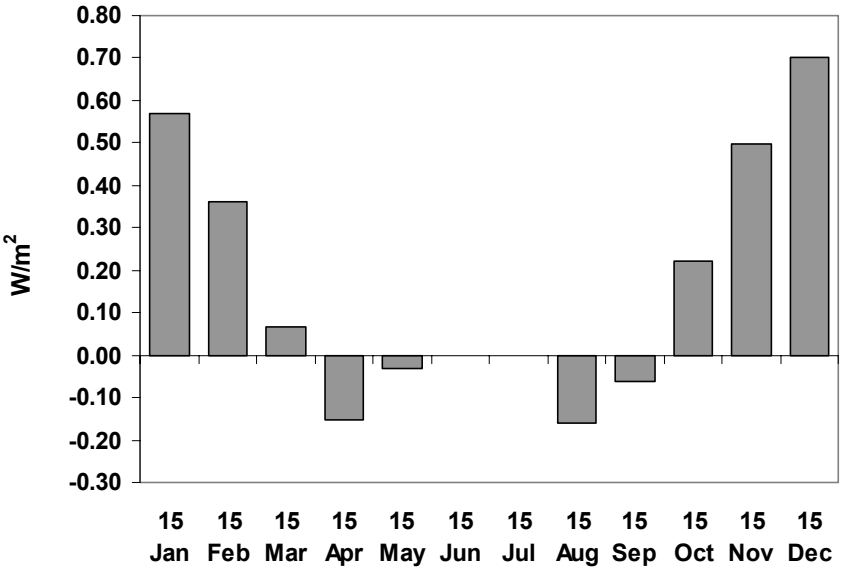

Figure 5.12. Annual variation in computed SW aerosol radiative forcing due to varying sun–earth geometry over Maitri, Antarctica while the aerosol properties are unchanged.

Another interesting difference in ARF over high-latitude regions such as Antarctica arises due to the sun–earth geometry. Over Antarctica, sunshine duration varies significantly from season to season and hence the SW aerosol radiative forcing. The computed variation in ARF that arises due to varying sun–earth geometry is shown in Figure 5.12 for the 15th of each month, while the

AOD is kept constant. SW radiative forcing by aerosol varies from a positive value of 0.7 W/m^2 in December to -0.15 W/m^2 in April and August, and it becomes zero for no sunshine days during June and July.

5.4.3 ARF over Bay of Bengal

Aerosol radiative forcing (ARF) calculations over Bay of Bengal (BoB) are carried out using the aerosol properties measured during a ship cruise conducted in February 2003 (*Ganguly et al.*, 2005). Radiative transfer calculations are made in SW (Short Wave, 0.25–4.0 μm) and LW (Long Wave, 4.0–40.0 μm) regions under clear sky conditions. In order to study the sensitivity of ARF for changes in the aerosol composition, radiative forcing are estimated each day corresponding to two different sets of aerosol mixture with single scattering albedo (ω) for the combination lying close to 0.85 and 0.90 at 500 nm wavelength. We found that SW forcing is negative at the surface as well as at TOA while LW forcing is always positive for both these cases. Moreover, the magnitude of LW forcing is much less (~10%) compared to its SW counterpart, meaning, only about 10% of the SW forcing is compensated by the LW forcing both at surface and TOA. The difference of the forcing values at the surface and TOA represents the energy trapped within the atmosphere by aerosols and results in heating of the atmosphere. It is found that for the same optical depth values and for the same aerosol mass loading over BoB, a decrease in the single scattering albedo for the mixture of aerosols from 0.90 to 0.85 can increase the radiation flux trapped within the atmosphere from 16.1 to 22.2 W/m^2. With the increase in the amount of absorbing aerosols, magnitude of SW forcing increases at the surface level and decreases at the TOA (Figure 5.13). It is also observed that the column water vapour amount as well as its vertical distribution obtained from FNL data showed large variations during the cruise period. A sensitivity test of LW aerosol radiative forcing is performed for different values of water vapour concentration and it is found that the magnitude of LW aerosol forcing at the surface level decreases with an increase in column water vapour while the TOA aerosol forcing is not much sensitive to the variation in water vapour (Figure 5.14). A similar test

conducted for the SW region shows no significant correlation between the SW aerosol radiative forcing and water vapour concentration in the atmosphere.

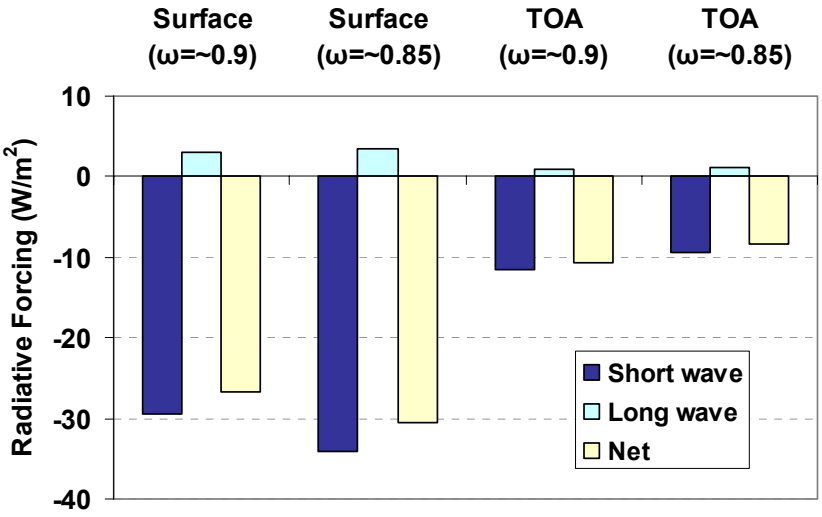

Figure 5.13. Spatially and diurnally averaged aerosol direct radiative forcing estimated over the Bay of Bengal using the aerosol properties measured during a cruise experiment conducted in February 2003.

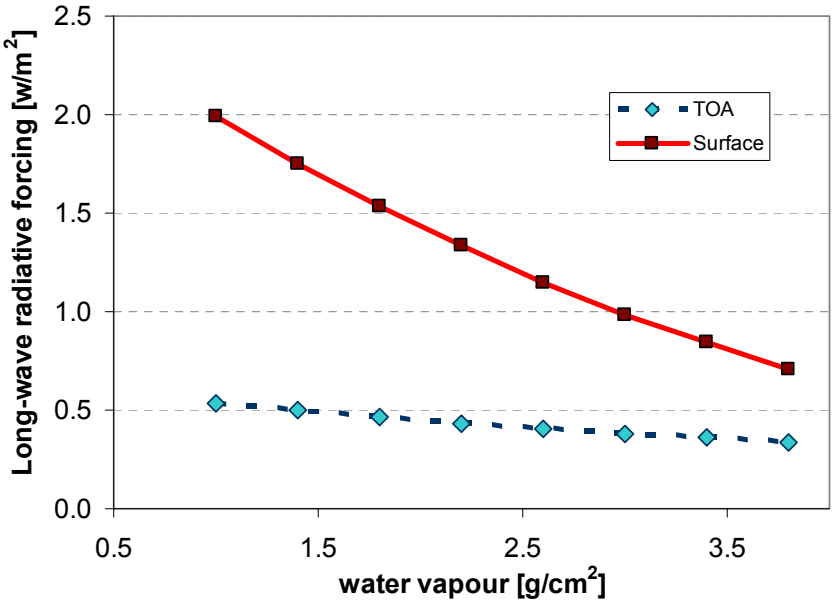

Figure 5.14. Sensitivity of long wave (4 to 40 μm) radiative forcing to variation in columnar water vapour.

5.4.4 ARF over Western/Central India

During ISRO-GBP land campaign-I (LC-1) comprehensive measurements of aerosol optical and microphysical properties were carried out. Average aerosol properties for each station are used to calculate clear sky short wave (0.25 to 4.0 μm) ARF. Figure 5.15 (a-b) shows the aerosol radiative forcing for clear sky condition at top of the atmosphere (TOA) and surface level. Stations in Figure 5.15 are mentioned in the same order in which observations were made. Ahmedabad, Chalisgaon, Osmanabad, Sangareddi, Hyderabad and Shaadhnagar are abbreviated as A'bad, C'gaon, O'bad, S'reddi, H'bad, S'nagar. Latitudes and longitudes for all stations are given in Table 4.3. An overall increase in radiative forcing is found during the campaign period that has resulted due to an overall increase found in AOD and single scattering albedo (SSA). TOA ARF is in the range of 0 to -10 W/m^2. It is low (almost zero) for Ahmedabad and Kheda due to low AOD and low SSA whereas the highest value is found over Surat. It is interesting to note that the highest as well as the lowest SSA was observed over same station Surat during LC-1. During onward journey (8 February 2004) the lowest SSA of 0.72 was observed when winds over Surat were predominantly from continent side. Whereas during return journey (29 February 2004) the highest SSA of 0.93 was observed, when winds were from marine region. In addition, large decrease in Angstrom exponent and increase in coarse mode particles is observed over Surat on 29 February 2004. TOA ARF over Surat is comparable to that observed over Bay of Bengal. Surface level ARF is in the range of -15 to -38 W/m^2 with low value over Ahmedabad. Instead of Surat, the largest value of ARF is found over Hyderabad. AOD over Hyderabad and Surat during return journey are comparable but SSA is low over Hyderabad.

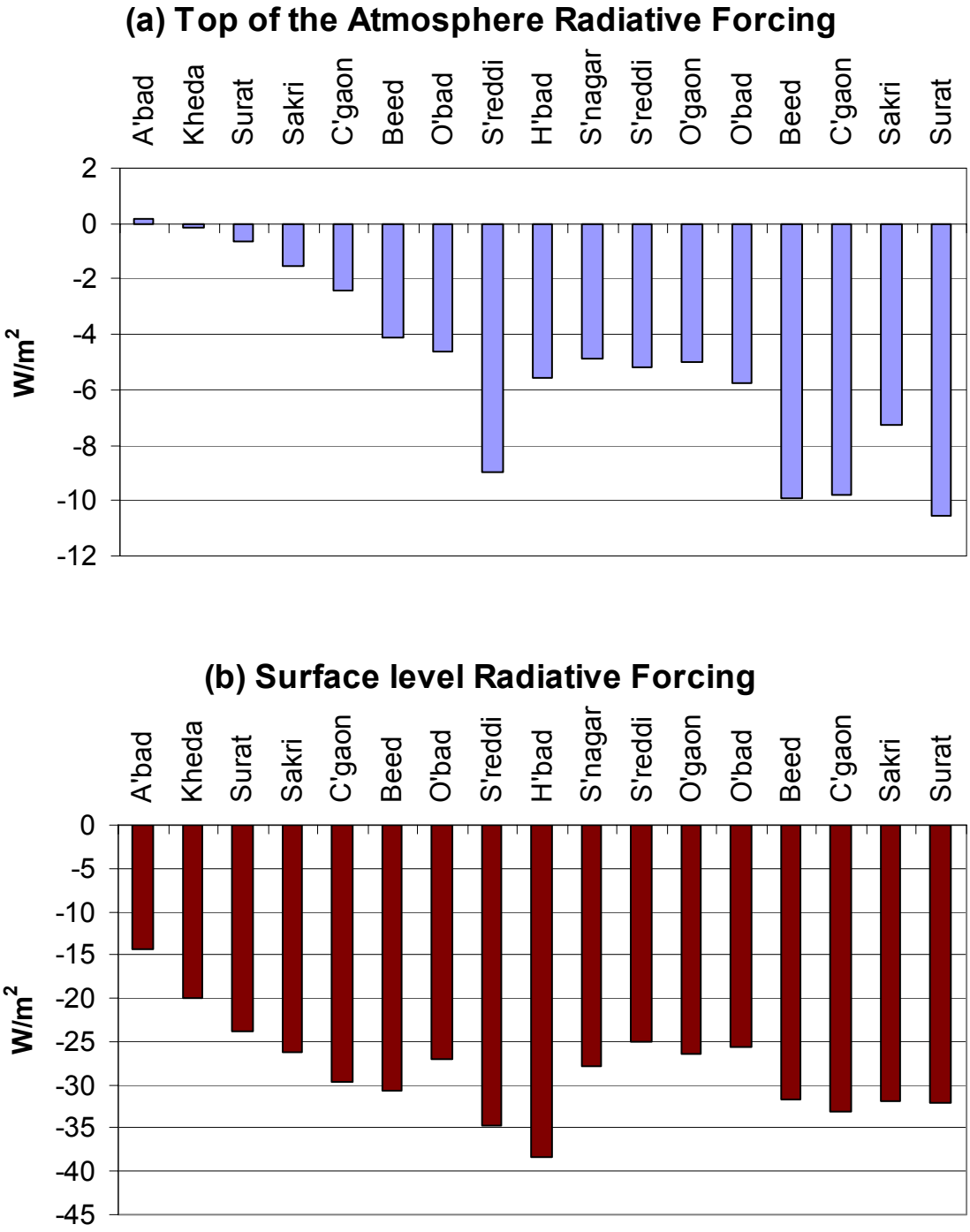

Figure 5.15. Shortwave (0.25 to 4.0 μm) clear sky aerosol radiative forcing at (a) top of the atmosphere and (b) surface level during ISRO-GBP land campaign conducted during February 2004. See text for the explanation of name of the stations.

Figure 5.16 shows the comparison of aerosol radiative forcing at (a) top of the atmosphere and (b) surface level between geographically different locations during February to March. When TOA ARF is compared, one finds very little difference between Hyderabad, Ahmedabad and Narayan Sarovar. ARF at these locations is around -3 to -4 W/m^2. These three locations are over land having more or less similar surface reflectance. TOA ARF over Maitri is very low and positive because of low AOD and higher surface albedo from snow surface underneath. TOA ARF is maximum (-9.5 W/m^2) over Bay of Bengal though AOD is comparable to that over Ahmedabad and Hyderabad. This is because for short wavelength range ocean surfaces are dark (see Figure 5.1). Except Maitri, Surface level aerosol radiative forcing values are comparable between all other stations. In case of surface level radiative forcing AOD is the critical parameter whereas for TOA aerosol radiative forcing both AOD and SSA become very critical.

In comparison to regions of high anthropogenic activity, aerosol radiative forcing over Antarctica is low. *Jayaraman* (2001) has reported TOA SW aerosol forcing of about –6.9 W/m^2 over coastal India, –4.7 W/m^2 over the Arabian Sea and –1.45 W/m^2 over the tropical Indian Ocean. Over Bay of Bengal (*Ganguly et al.,* 2005) TOA ARF is found to be -10.5 W/m^2. *Higgnet et al.* (1999) have found –9 W/m^2 over the Atlantic Ocean. However, in comparison to Ahmedabad, Indian Ocean ARF values are not very different though there is an order of magnitude difference in AOD. TOA SW radiative forcing is -2 to -3 W/m^2 over Ahmedabad during February and March. Similar is the case for other land stations for example *Pandithurai et al.* (2004) have reported TOA SW radiative forcing between -7 to +9 with average close to zero from December to April over Pune (18.5^{0}N, 73.9^{0}E). *Ramana et al.* (2004) have also found TOA ARF close to zero over Kathmandu (27.67^{0}N, 85.31^{0}E) in Himalayan region. Overall conclusion for aerosol radiative forcing is that surface reflectance is very important for determining radiative environment and TOA radiative forcing and aerosols play very important role in redistributing the radiative energy between the Earth's surface and the atmosphere.

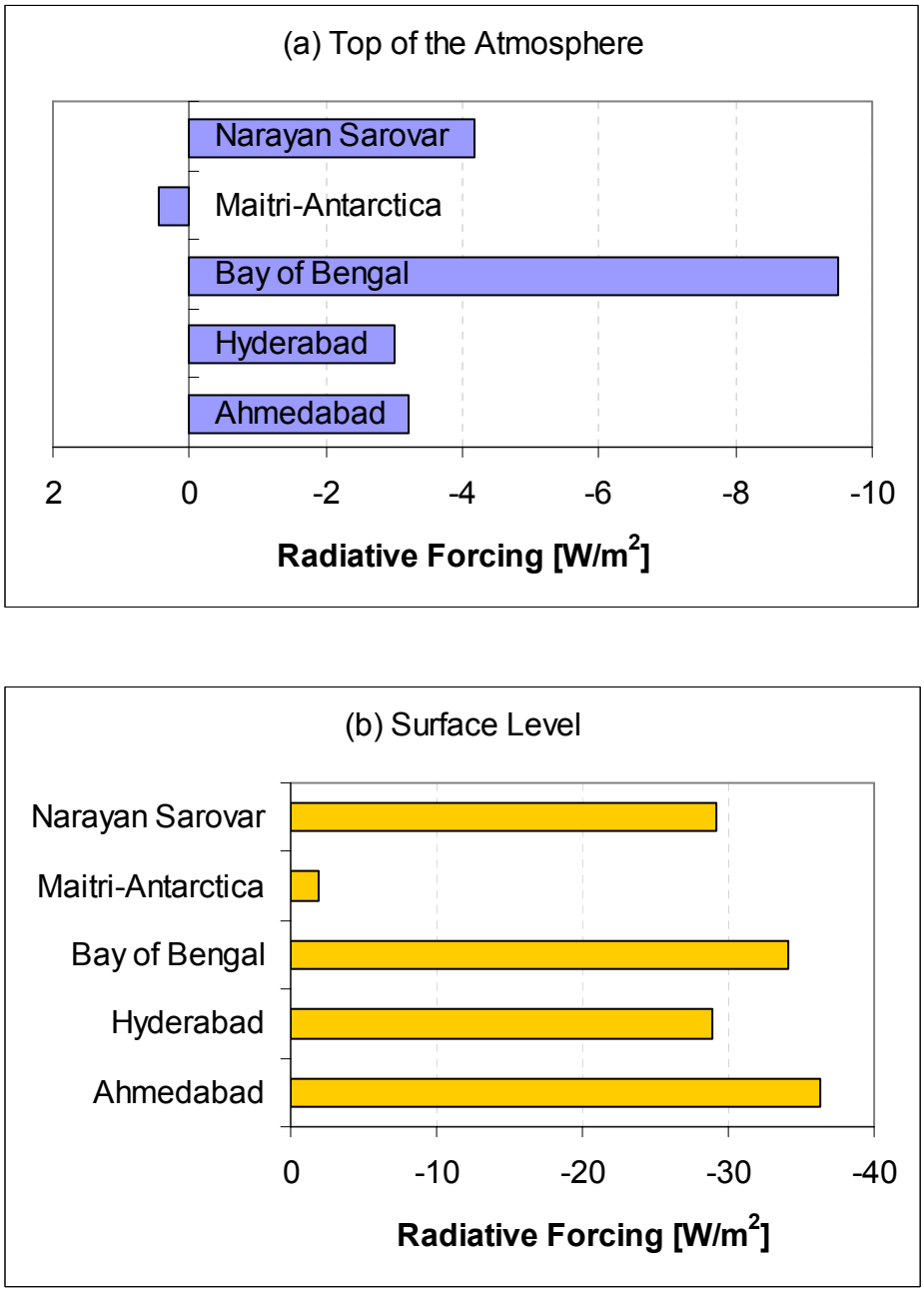

Figure 5.16. Comparison of clear sky short wave aerosol radiative forcing for the Feb-Mar period over selected locations.

Chapter 6

SUMMARY AND SCOPE FOR FUTURE WORK

6.1 Summary

A detailed study of aerosol vertical profile and other aerosol properties is carried out over Ahmedabad from February 2002 to November 2004. This study provided important information on seasonal variation of aerosol properties at different altitude levels. Quite different seasonal response is found between the surface layer and the layer above it. Reasons for this are probed in the light of meteorological data and other ancillary information. Short-term field experiments during the period of study are also carried out. Such field campaigns have provided the opportunity to study the influence of meteorological phenomena ranging from synoptic scale to mesoscale in influencing the vertical distribution of aerosols.

Influence of the observed aerosol properties on the Earth's radiation budget is studied by modelling the radiative fluxes with and without aerosol. Surface reflectance is found to be a critical parameter for aerosol radiative forcing. Present study covers the geographic regimes from pristine Antarctica to populated Ahmedabad where apart from anthropogenic influence, surface types also varies from snow, ocean to arid and semi arid land.

Airborne lidar measurements are carried out for the first time in India. The experience gained is useful for future space borne lidar measurements in India.

Listed below are the major outcome of the present study:

- Large day to day variability is observed in aerosol extinction profiles, resulting in large standard deviation from 17 % to 67 % in monthly mean values. The seasonal and interannual variations are however significantly

higher than this large standard deviation. Among the three years data, the extinction values for 2003 are the highest, much higher than 2002 and marginally higher than the 2004 values.

- Seasonal variation is different for surface layer (0 to 300 m) and for the layer above it, (henceforth referred as the first layer and the second layer). Extinction value in the first layer is high during winter and low during summer, while the reverse is the trend for the second layer.

- Aerosol optical depth (AOD) over Ahmedabad is low (~0.2) during winter and high (~0.8) during summer. AOD is highly correlated with relative humidity. Altitude break up of AOD shows that the value above 1 km is mainly responsible for the seasonal variation in the column integrated AOD. Scale height of aerosol profile obtained by fitting an exponential curve to observed extinction profile is also found to have annual cycle similar to AOD and the values are low (~0.5 km)during winter and high (~3.5 km) during summer.

- Comparison of extinction profile measured over Ahmedabad with that over Arabian sea and coastal locations during the western Gujarat campaign shows increased aerosol amount in the lowest layer which is attributed to larger aerosol production by anthropogenic activities typical of polluted urban location.

- Absorption coefficient over Ahmedabad is high during winter ($3.68 \pm 1.32 \times 10^{-5}$ m^{-1}) and low during summer ($0.92 \pm 0.39 \times 10^{-5}$ m^{-1}). Average value of scattering coefficient is $1.63 \pm 0.96 \times 10^{-4}$ m^{-1}. Average aerosol single scattering albedo (SSA) calculated from scattering and absorption coefficient is 0.87 ± 0.09 which is very close to SSA of "continental average" aerosol model.

- Surface reflectance over Ahmedabad does not show much seasonal variation except during September when reflectance is reduced due to summer monsoon rain in preceding months and increased vegetation.

- Observation of aerosol optical depth and size distribution are made during Jan-Feb 2001 over Maitri-Antarctica. AOD over Maitri is found very low and spectral dependence is flat, which is typical of a pristine region. Average AOD at 400 nm for the entire campaign period is 0.036 ± 0.018. The average mass concentration of the PM_{10} particles at Maitri for the campaign period is 9.1±6.0 μg/m^3, of which 63 % of mass is contributed by coarse mode particles. After correcting for relative humidity mass of PM_{10} particle can be calculated to 6.97 μg/m^3 at 0 % and 7.87 μg/m^3 at 50% RH. Based on these observations and using knowledge gained from previous researchers a new aerosol model to compute optical properties is suggested and further used to compute aerosol radiative forcing over Antarctica (*Gadhavi and Jayaraman*, 2004).

- From 26 Dec 2002 to 13 Jan 2003 a field campaign was carried out over western part of Gujarat using a mobile micro pulse lidar (MPL) and sun-photometer. Interestingly, the highest AOD observed during this campaign is neither an urban nor an industrial location but a coastal location on western coast of the gulf of Khambhat.

- Under the Indian Space Research Organization's Geosphere Biosphere Program a road campaign (LC-1) was undertaken from Ahmedabad to Hyderabad and back during February 2004. A large difference of about 1 km in boundary layer height is found between locations in Gujarat and Central Southern India. It is found that convection is stronger and deep over Central India than Gujarat, which is responsible for affecting the vertical distribution of aerosol. Interesting difference between day and night time aerosol profile is observed. A layer between 300 to 900 m is

seen in all daytime profiles while it is absent in night time profile resulting in significant decrease in night time AOD. Nighttime AOD is found to be 12 to 80 % lower than the nearest neighbour daytime AOD. Overall increasing trend is observed in AOD and SSA from start of the campaign to the end of campaign due to season transition from winter to summer.

- First time in India, airborne lidar measurements are carried out during LC-1 to assess the possible scientific advantage for future space-borne lidar measurements. Necessary instrumentation, software and data reduction algorithms are developed/adapted for these measurements.

- Comparison between the airborne and ground based lidar measurements revealed the advantage of airborne measurements for studying free tropospheric aerosol content apart from gaining a better spatial coverage. In the free troposphere because of low aerosol amount signal is weak which is further attenuated by higher extinction values in lower altitude for ground based measurements, but is not the problem for lidar measurements made from airborne platform.

- Observed aerosol properties are modelled to study their influence on radiation budget of the Earth. Aerosol Radiative Forcing (ARF) calculations are carried out in shortwave (SW; 0.25 to 4 μm) and long-wave (LW; 4 to 40 μm) separately. Top of the atmosphere (TOA) ARF over Ahmedabad is in the range of -1.5 to -4.5 W/m^2 with minimum during April, May and June and maximum during October, November and December. Surface level radiative forcing also shows large seasonal variation ranging from -20 W/m^2 to -80 W/m^2. Seasonal variations of ARF at TOA and Surface level are out of phase by almost 6 months. This is because of the fact that boundary layer aerosol and aerosol in free troposphere have different seasonal variation and optical properties.

- Study on vertical profile of ARF reveals important role of aerosol for thermally stabilizing the atmosphere. In the boundary layer, ARF during May is factor of 2.5 higher than February values and produces a heating rate of ~1 K/day.

- TOA ARF over Maitri-Antarctica is found to be positive 0.45 W/m^2 mainly because of highly reflective snow surface underneath. In the sensitivity analysis, it is shown that for the aerosol model used over Antarctica TOA shortwave ARF will change as 22.5 W/m^2, -43.9 W/m^2 and -72.9 W/m^2 for snow, sand and sea-water types of surfaces respectively for unit AOD change. An interesting feature in ARF over Antarctica is found due to the varying sun-earth geometry. For same amount of aerosol, ARF over Maitri varies from +0.7 W/m^2 in December to -0.15 W/m^2 in April and August, and it becomes zero for no sunshine days during June and July.

- Aerosol radiative forcing calculation over Bay of Bengal (BoB) is carried out using the aerosol properties measured during a ship cruise conducted in February 2003. TOA short wave radiative forcing over BoB is found to be -10 W/m^2 and surface level forcing is around -30 W/m^2. Long wave (LW) ARF is positive at surface as well as at TOA but the magnitude is much less about 10% of the SW forcing. In a sensitivity analysis, it is found that for the same optical depth values a decrease in the single scattering albedo from 0.90 to 0.85 can increase the radiation flux trapped within the atmosphere from 16.1 to 22.2 W/m^2. Sensitivity test is also performed for different values of water vapour concentration and found that the magnitude of longwave ARF at surface level decreases with the increase in column water vapour.

- Aerosol radiative forcing calculations over western/central India are carried out based on measurements made during LC-1. The highest TOA radiative

forcing observed is over Surat around -10 W/m^2 during return journey, interestingly minimum and maximum single scattering albedo (SSA) found during LC-1 is also over Surat during onward and return journey respectively. Spatial variation in surface level radiative forcing is found to be from -15 W/m^2 to -37 W/m^2 during LC-1.

- Comparison of the forcing values obtained for different geographical regions reveals the importance of surface reflectance in determining the TOA ARF. However surface level radiative forcing is not that sensitive to surface reflectance.

6.2 Scope for future work

Many European countries have experienced a decreasing trend in aerosol amount during the last decade (*Shahgedanova and Lamakin*, 2005, *Bodhaine and Dutton*., 1993) whereas an increasing trend is observed over India (*Ramachandran and Jayaraman*, 2002, *Moorthy et al.*, 2002, *Niranjan et al.*, 2000, *Parameshwaran et al.*, 1998). With increase in population and increased usage of fossil fuel further increase in aerosol amount is anticipated over India. Awareness for environment protection in the society is also increasing leading to stricter emission norms. Large-scale efforts in terms of technology inputs are underway in many major cities of India. It is not only of academic interest but also for society in general to know future evolution of trends for pollutants such as aerosol. Hence measurements started during this study needs to be continued on a long-term basis that will be useful for deducing the anthropogenic influence on aerosol amount and its impact on climate etc.

Study on seasonal variation of AOD has revealed new facts. High correlation between aerosol optical depth (AOD) and relative humidity (RH) is found. However observed increase in RH is not able to fully explain the observed increase in AOD during summer. There may be other factors such as change in boundary layer height, emission levels, wind direction, increased production of sulphate in wet environment etc. responsible for it along with RH. In addition, it is

found that seasonal variation is not same for surface layer and layer above the surface layer. Two possibilities have been proposed in the present study. One is surface-atmosphere interaction i.e. moist surface injects less amount of aerosol into atmosphere than drier surface. Second possibility is chemical separation of aerosol species with altitude i.e. aerosol above surface layer are more hygroscopic than aerosol in the surface layer. While difference in stratosphere and tropospheric aerosol chemistry is well documented, study of altitude resolved aerosol chemistry within troposphere is emphasised in the light of these findings.

Orography plays very important role in dispersion of aerosol particles. Study of biomass burning produced haze layer over the Amazon basin using space-borne lidar (Lidar in Space Technology Experiment; LITE) has shown the influence of Andes in controlling the dispersion of haze layer (*Heintzenbern et al.*, 2003). Thar desert (the great Indian desert) about 300 North of Ahmedabad is big source of mineral dust (*Prospero et al.*, 2002). Quantification of role of Aravalli mountain range located between Ahmedabad and Thar desert in controlling the dispersion of aerosols is very important for studying transport of aerosols over North West India. Similarly AOD measurements made from satellite based platform has revealed high AOD values over Gangetic basin (*Di Girolamo et al.*, 2004) where influence of Himalaya in controlling the aerosol dispersion over North East India can be studied in same context.

During the western Gujarat road campaign and from satellite based measurements it is found that aerosol amount instead of showing gradient from urban to remote region, high value of AOD is often found away from source regions such as that observed over Gulf of Khambhat region. It is very important to investigate factors responsible for accumulation of AOD over this region in full detail as such studies can be useful to identify the regions, which are more vulnerable for the accumulation of aerosol and other pollutants.

Having studied in detail the aerosol radiative forcing over different regions and during different seasons, it is now possible to do a detailed numerical experiment

using Global Circulation Models to assess the impact of aerosol forcing on regional and global scale climate. Estimation of the impact of different aerosol types on regional climate change will help policy makers in taking decision to control aerosol emission.

REFERENCES

Anderson T. L., S. J. Masonis, D. S. Covert, R. J. Charlson and M. J. Rood (2000), In situ measurement of the aerosol extinction-to-backscatter ratio at a polluted continental site, *J. Geophys. Res., 105,* 26907-26915.

Balin Y. S., S. I. Kavkyanov, G. M. Krekov, and I. A. Razenkov (1987), Noise-proof inversion of Lidar equation, *Opt. Lett., 12(1),* 13-15.

Bates, T. S., B. J. Huebert, J. Gras, F. Griffiths, and P. A. Durkee (1998), International Global Atmospheric Chemistry (IGAC) Project's First Aerosol Characterization Experiment (ACE 1): Overview, *J. Geophys. Res., 103*, 16297–16318.

Bissonnette L. R. and D. L. Hutt (1995), Multiply scattered aerosol lidar returns: inversion method and comparison with in situ measurements, *Appl. Opt., 34(30)*, 6959-6975.

Bodhaine, B. A. and E. G. Dutton (1993), A long-term decrease in Arctic haze at Barrow, Alaska, *Geophys. Res. Lett., 20(10)*, 947-950, doi:10.1029/93GL01146.

Bohren, C. F. and D. R. Huffman (1983), Absorption and Scattering of Light by Small Particles, *A Wiley-Interscience Publication, New York*, USA p. 530.

Campbell J. R., D. L. Hlavka, E. J. Welton, C. J. Flynn, D. D. Turner, J. D. Spinhirne, V. S. Scott III and I. H. Hwang (2002), Full-Time, Eye-safe Cloud and Aerosol Lidar Observation at Atmospheric Radiation Measurement Program Sites: Instruments and Data Processing, *J. Atmos. Oceanic Technol., 19*, 431-442.

Campbell, J. R., E. J. Welton, J. D. Spinhirne, Q. Ji, S.-C. Tsay, S. J. Piketh, M. Barenbrug, and B. N. Holben (2003), Micropulse Lidar observations of tropospheric aerosols over northeastern South Africa during the ARREX and SAFARI 2000 dry season experiments, *J. Geophys. Res., 108(D13)*, 8497, doi:10.1029/2002JD002563.

Chand, D., and S. Lal (2004), High ozone at rural site in India, *Atmos. Chem. Phys. Discuss.*, 4, 3359-3380.

Charlson R. J., S. E. Schwartz, J. M. Hales, R D. Cess, J. A. Coakley, Jr. J. E. Hansen and D. J. Hofmann, (1992), Climate Forcing by Anthropogenic Aerosols, *Science, 255,* 423-430.

Chung, C. E. and V. Ramanathan (2004), Aerosol loading over the Indian Ocean and its possible impact on regional climate, *Indian J. Marine Sci., 33(1)*, 40-55.

Coakley, J. A., Jr., W. R. Tahnk, A. Jayaraman, P. K. Quinn, C. Devaux, and D. Tanré (2002), Aerosol optical depths and direct radiative forcing for INDOEX derived from AVHRR: Theory, *J. Geophys. Res., 107(D19)*, 8009, doi:10.1029/2000JD000182

d'Almeida, G. A., P. Koepke and E. P. Shettle (1991), Atmospheric Aerosols: Global Climatology and Radiative Characteristics, *A. Deepak Publishing*, p. 561.

Devara, P. C. S., P. E. Raj, and G. Pandithurai (1995), Aerosol-profile measurements in the lower troposphere with four-wavelength bistatic argon-ion lidar, *Appl. Opt., 34(21)*, 4416-4425.

Devara, P. C. S. (2000) In: long-term changes and trends in the atmosphere, Ed. G. Beig, *New Age International (P) Ltd, New Delhi, India*, 172-202.

Dho S. W., Y. J. Park and H. J. Kong (1997), Experimental determination of a geometric form factor in a lidar equation for an inhomogeneous atmosphere, *Appl. Opt., 36(24)*, 6009-6010.

Di Girolamo, L., T. C. Bond, D. Bramer, D. J. Diner, F. Fettinger, R. A. Kahn, J. V. Martonchik, M. V. Ramana, V. Ramanathan, and P. J. Rasch (2004), Analysis of Multi-angle Imaging SpectroRadiometer (MISR) aerosol optical depths over greater India during winter 2001–2004, *Geophys. Res. Lett., 31*, L23115, doi:10.1029/2004GL021273.

Draxler, R. R. and G. D. Rolph (2003), HYSPLIT (HYbrid Single-Particle Lagrangian Integrated Trajectory) model access via NOAA ARL READY website: http://www.arl.noaa.gov/ready/hysplit4.html, *NOAA Air Resources Laboratory*, Silver Spring, MD.

Eck, T. F., B. N. Holben, O. Dubovik, A. Smirnov, I. Slutsker, J. M. Lobert and V. Ramanathan (2001), Column-integrated aerosol optical properties over the Maldives during the northeast monsoon for 1998-2000, *J. Geophys. Res., 106(22)*, 28555-28566.

Ferguson J. A. and D. H. Stephens (1983), Algorithm for inverting Lidar returns, *Appl. Opt., 22(23)*, 3673-3675.

Fernald F. G. (1984), Analysis of atmospheric Lidar observations: some comments, *Appl. Opt., 23(5)*, 652-653.

Gadhavi H. and A. Jayaraman (2004), Aerosol characteristics and aerosol radiative forcing over Maitri - Antarctica, *Curr. Sci., 86(2)*, 296-304.

Ganguly, D., A. Jayaraman, and H. Gadhavi (2005), In situ ship cruise measurements of mass concentration and size distribution of aerosols over Bay of Bengal and their radiative impacts, *J. Geophys. Res., 110*, D06205, doi:10.1029/2004JD005325.

Goff, J. A. and S. Gratch (1946), Low-pressure properties of water from -160 to 212 F, *Transactions of the American society of heating and ventilating engineers*, pp 95-122, New York, USA.

Gonzalez R. (1988), Recursive technique for inverting the lidar equation, *Appl. Opt., 27(13),* 2741-2745.

Guasta, M. D. (2002), Daily cycles in urban aerosols observed in Florence (Italy) by means of an automatic 532–1064nm LIDAR, *Atmos. Environ, 36*, 2853-2865.

Gupta P., H. Gadhavi and A. Jayaraman (2003), Aerosol optical depth variation observed using sun-photometer over Indore, *Indian J. Radio and Space Phys., 32*, 229-237.

Hall, J. S. and E. W. Wolff (1998), Causes of seasonal and daily variations in aerosol sea-salt concentrations at a coastal Antarctic Station, *Atmos. Environ., 32*, 3669–3677.

Hansen J. E. and A. A. Lacis (1990), Sun and dust versus greenhouse gases: an assessment of their relative roles in global climate change*, Nature, 346*, 713-719.

Harshvardhan (1993), Aerosol-climate interactions, In: Aerosol–Cloud–Climate Interactions (ed. Hobbs, P. V.), *Academic Press*, p.233.

Haywood, J. and V. Ramaswamy (1998), Global sensitivity studies of the direct radiative forcing due to anthropogenic sulfate and black carbon aerosols, *J. Geophys. Res., 103(D6)*, 6043–6058.

Haywood, J., V. Ramaswamy, and B. J. Soden (1999), Tropospheric aerosol climate forcing in clear-sky satellite observations over the oceans, *Science, 283*, 1299-1303.

Haywood, J., and O. Boucher (2000), Estimate of the direct and indirect radiative forcing due to tropospheric aerosols: A review, *Rev. Geophys., 38(4)*, 513-543.

Heintzenberg, J., et al. (2003) Tropospheric Aerosols, In: Brasseur G., R. Prinn, A. Pszenny (ed), Atmospheric Chemistry in a Changing World, *Springer*, Germany, 125-156.

Herber, A., L. W. Thomason, V. F. Radionov, and U. Leiterer (1993), Comparison of trends in the tropospheric and stratospheric aerosol optical depths in the Antarctic, *J. Geophys. Res.,98*, 18441–18447.

Herber, A., L. W. Thomason, K. Dethloff, P. Viterbo, V. F. Radionov, and U. Leiterer (1996), Volcanic perturbation of the atmosphere in both polar regions: 1991–1994, *J. Geophys. Res., 101*, 3921–3928.

Herman, J. R., P. K. Bhartia, O. Torres, C. Hsu, C. Seftor, and E. Celarier (1997), Global distributions of UV-absorbing aerosols from Nimbus 7/TOMS data, *J. Geophys. Res., 102 (D14)*, 16911-16922, doi:10.1029/96JD03680

Hess, M., P. Koepke and I. Schult (1998), Optical properties of aerosols and clouds: The software package OPAC, *Bull. Am. Meteorol. Soc., 79*, 831–844.

Higgnet, P., J. P. Taylor, P. N. Francis and M. D. Glew (1999), Comparison of observed and modeled direct aerosol forcing during TARFOX, *J. Geophys. Res., 104*, 2279–2287.

Holben, B. N., et al. (1998), Aeronet – A federal instrument network and data archive for aerosol characterization, *Remote Sens. Environ., 66*, 1-16.

Huebert, B. J., T. Bates, P. B. Russell, G. Shi, Y. J. Kim, K. Kawamura, G. Carmichael, and T. Nakajima, An overview of ACE-Asia: Strategies for quantifying the relationships between Asian aerosols and their climatic impacts, *J. Geophys. Res., 108(D23)*,8633, doi:10.1029/2003JD003550, 2003.

Hughes H. G., J. A. Ferguson and D. H. Stephens, (1985), Sensitivity of a lidar inversion algorithm to parameters relating atmospheric backscatter and extinction, *Appl. Opt., 24*, 1609-1613.

IPCC, (2001), In: Houghton, J.T., et al. (Eds.), Climate Change, 2001: The Scientific Basis – Summary for policy makers (Working group report 1). *Cambridge University Press, Cambridge*, UK, p. 944.

Jain, S. L., S. D. Ghude, and B. C. Arya (2004), Signature of early ozone hole recovery during 2002, *Curr. Sci., 86(7)*, 963-965.

Jayaraman, A., Y. B. Acharya, B. H. Subbaraya, and H. Chandra (1995a), Nd:YAG backscatter lidar at Ahmedabad (23^0N, 72.5^0E) for tropical middle atmospheric studies, *Appl. Opt., 34(30)*, 6937-6940.

Jayaraman, A., S. Ramachandran, Y. B. Acharya, and B. H. Subbaraya (1995b), Pinatubo volcanic aerosol layer decay observed at Ahmedabad (23^0N), India, using neodymium:yttrium/aluminium/garnet backscatter lidar, *J. Geophys. Res., 100(D11)*, 23209-23214.

Jayaraman, A., Y. B. Acharya, H. Chandra, B. H. Subbaraya, S. Ramachandran, and S. Ramaswamy (1996), Laser radar study of the middle atmosphere over Ahmedabad, *Indian J. Radio and Space Phys., 25*, 318-327.

Jayaraman, A., et al. (1998), Direct observations of aerosol radiative forcing over the tropical Indian Ocean during January-February 1996 pre-INDOEX cruise, *J. Geophys. Res., 103(D12)*, 13827-13836.

Jayaraman, A., S. K. Satheesh, A. P. Mitra, and V. Ramanathan (2001), Latitude gradient in aerosol properties across the inter tropical convergence zone: Results from the joint Indo–US study onboard Sagar Kanya. *Curr. Sci., 80*, 128–137.

Jayaraman, A. (2001), Aerosol radiative forcing over the tropical Indian Ocean, *Proc. Indian Natl. Sci. Acad., 67*, 385–394.

Jayaraman, A., H. Gadhavi, D. Ganguly, A. Misra, S. Ramachandran and T. Rajesh (2005), Spatial variation in aerosol characteristics over central India observed during the February 2004 road campaign experiment, *(submitted to Atmos. Environ.)*.

Kaestner M., (1986), Lidar inversion with variable backscatter/extinction ratios: comment, *Appl. Opt., 25*, 833-835.

Kerminen, V., K. Teinila and R. Hillamo (2000), Chemistry of sea-salt particles in the summer Antarctic atmosphere, *Atmos. Environ., 34*, 2817–2825.

Klett J. D., (1981), Stable analytical inversion solution for processing lidar returns, *Appl. Opt., 20*, 211-220.

Klett J. D., (1985), Lidar inversion with variable backscatter/extinction ratios, *Appl. Opt., 24*, 1638-1643.

Kovalev V. A. (1993), Lidar Measurement of the vertical aerosol extinction profiles with range-dependent backscatter-to-extinction ratios*, Appl. Opt., 32(30)*, 6053-6065.

Kovalev V. A. (1995), Sensitivity of the lidar solution to errors of the aerosol backscatter-to-extinction ratio: influence of a monotonic change in the aerosol extinction coefficient, *Appl. Opt., 34*, 3457-3462.

Kovalev V. A. (2003), Stable near-end solution of the lidar equation for clear atmospheres, *Appl. Opt., 42(3)*, 585-591.

Kunz G. J. and G. Leeuw (1993), Inversion of lidar signals with the slope method*, Appl. Opt., 32(18)*, 3249-3256.

Kunz G. J. (1996), Transmission as an input boundary value for an analytical solution of a single-scatter lidar equation, *Appl. Opt., 35(18)*, 3255-3260.

Liou K. (2002), An Introduction to Atmospheric Radiation, 2nd Edition, *Academic Press,* USA, pp 583.

Liu Z., N. Sugimoto and T. Murayama (2002), Extinction-to-backscatter ratio of Asian dust observed with high-spectral-resolution lidar and Raman lidar, *Appl. Opt., 41*, 2760-2767.

Marenco F., V. Santacesaria, A. F. Bais, D. Balis, A. Sarra, A. Papayannis and C. Zerefos, (1997), Optical properties of tropospheric aerosols determined by lidar and spectrophotometric measurements (Photochemical Activity and Solar Ultraviolet Radiation campaign), *Appl. Opt., 36*, 6875-6886.

Mazzera, D. M., D. H. Lowenthal, J. C. Chow, J. G. Watson and V. Grubisic (2001), PM_{10} measurements at McMurdo Station, Antarctica, *Atmos. Environ, 35*, 1891–1902.

McClatchey, R. A., R. W. Fenn, J. E. A. Selby, F. E. Volz, and J. S. Garing (1972), Optical properties of the atmosphere, 3rd ed., *Environ. Res. Pap. 411*, 108 pp., Air Force Cambridge Res. Lab., Cambridge, Mass.

Meeus J. (1991), Astronomical algorithms, *Willmenn-Bell Inc*, USA

Moorthy, K. K., A. Saha, B. S. N. Prasad, K. Niranjan, D. Jhurry and P. S. Pillai (2001), Aerosol optical depth over Peninsular India and adjoining oceans during the INDOEX campaigns: Spatial, temporal and spectral characteristics, *J. Geophys. Res., 106(22)*, 28539-28554.

Moorthy, K. K., K. Niranjan, and B. Parasad (2002), 15 years of aerosol measurements over peninsular India – Climatology and trends, *34th COSPAR Scientific Assembly*, The second world space congress, 10-14 October, Houston, TX, USA.

Mulders, J. M. (1984), Algorithm for inverting lidar returns: comment, *Appl. Opt., 23(17)*, 2855-2856.

Murthy, B. S., S. S. Parasnis, and M. Ek (2004), Interaction of land surface with the atmospheric boundary layer: case studies from LASPEX, *Curr. Sci., 86(8)*, 1128-1134.

Nanavati, S., and P. K. Panigrahi (2004), Wavelet transform- A new mathematical microscope, *Resonance*, 50-64.

Nicolet, M. (1984), On the molecular scattering in the terrestrial atmosphere: An empirical formula for its calculation in the homosphere, *Planet. Space Sci., 32(11)*, 1467-1468.

Niranjan, K., Y. Ramesh Babu, G. V. Satyanarayana and S. Thulasiraman (1997), Aerosol optical depths and typical size distributions at a coastal urban location in India, *Tellus, 49B*, 439-446.

Niranjan, K., S. Thulasiraman, G. V. Satyanarayana, and Y. Ramesh Babu (2000), Temporal characteristics of aerosol optical depths and size distribution at Visakhapatnam, India, *Aerosol Sci. Tech., 32*, 284-292.

Pal., S. R., W. Steinbrecht and A. I. Carswell (1992), Automated method for lidar determination of cloud-base height and vertical extent, *Appl. Opt., 31(10)*, 1488-1494.

Palm, S., et al (2002), Geoscience Laser Altimeter System (GLAS), Algorithm Theoretical Basis Document Version 4.2, *Goddard Space Flight Center, Greenbelt*, USA, pp 136.

Pandithurai, G., R. T. Pinker, T. Takamura, and P. C. S. Devara (2004), Aerosol radiative forcing over a tropical urban site in India, *Geophys. Res. Lett., 31*, L12107, doi:10.1029/2004GL019702.

Parameswaran, K., R. Rajan, G. Vijayakumar, K. Rajeev, K. K. Moorthy, P. R. Nair, and S. K. Satheesh (1998), Seasonal and long term variations of aerosol content in the atmospheric mixing region at a tropical station on the Arabian sea-coast, *J. Atmos. Solar-Terrestrial Phys., 60(1)*, 17-25.

Parameswaran, K., S. V. Sunilkumar, K. Rajeev, P. R. Nair, and K. K. Moorthy (2004), Boundary layer aerosols at Trivandrum tropical coast, *Adv. Space Res., 34(4)*, 838-844, doi:10.1016/Jasr.2003.08.059.

Pelon, J., C. Flamant, P. Chazette, J.-F. Leon, D. Tanre, M. Sicard, and S. K. Satheesh (2002), Characterization of aerosol spatial distribution and optical properties over the Indian Ocean from airborne LIDAR and radiometry during INDOEX'99, *J. Geophys. Res.*, 107(D19), 8029, doi:10.1029/2001JD000402.

Petit, J. R., et al. (1999), Climate and atmospheric history of the past 420000 years from the Vostok ice core, Antarctica, *Nature, 399*, 429-436.

Pillai, P. S., and K. K. Moorthy (2001), Aerosol mass-size distributions at a tropical coastal environment: response to mesoscale and synoptic processes, *Atmos. Environ., 35*, 4099-4112.

Press, W. H., S. A. Teukolsky, W. T. Vellerling and B. P. Flannery (1998), Chapter 15 Modelling of Data, In: Numerical Recipes in Fortran: The Art of Scientific Computing, 2nd Ed., *Cambridge University Press*, UK.

Prospero J. M., P. Ginoux, O. Torres, S. E. Nicholson, and T. E. Gill (2002), Environmental Characterization of global sources of atmospheric soil dust identified with the nimbus 7 total ozone mapping spectrometer (TOMS) absorbing aerosol product, *Rev. Geophys., 40(1)*, 1002, doi:10.1029/2000RG000095.

Rajeev, K., and V. Ramanathan (2001), Direct observations of clear-sky aerosol radiative forcing from space during Indian Ocean Experiment, *J. Geophys. Res., 106*, 17221-17235.

Ramachandran, S., A. Jayaraman, Y. B. Acharya and B. H. Subbaraya (1994), Features of Aerosol Optical Depths over Ahmedabad as Observed with a Sun-Tracking Photometer, *Beitr. Phys. Atmosph., 67(1)*, 57-70.

Ramachandran, S. (1995), Aerosols in the tropical middle atmosphere, *Ph.D. Thesis*, Gujarat University, Ahmedabad, India, p. 173.

Ramachandran, S., and A. Jayaraman (2002), Premonsoon aerosol mass loadings and size distributions over the Arabian Sea and the tropical Indian Ocean, *J. Geophys. Res., 107(D24)*, 4738, doi:10.1029/2002JD002386.

Ramachandran, S., and A. Jayaraman (2003), Balloon-borne study of the upper tropospheric and stratospheric aerosols over a tropical station in India, *Tellus, B 55(3)*, 820-836.

Ramana, M. V., V. Ramanathan, I. A. Podgorny, B. B. Pradhan, and B. Shrestha (2004), The direct observations of large aerosol radiative forcing in the Himalayan region, *Geophys. Res. Lett., 31*, L05111, doi:10.1029/2003GL018824.

Ramanathan, V., C. Chung, D. Kim, T. Bettge, L. Buja, J. T. Kiehl, W. M. Washington, Q. Fu, D. R. Sikka, and M. Wild (2005), Atmospheric brown clouds: Impacts on South Asian climate and hydrological cycle, *Proc. Natl. Sci. Acad., USA*, doi:10.1073/pnas.0500656102.

Ramanathan, V., P. J. Crutzen, A. P. Mitra and D. Sikka (2002), The Indian ocean experiment and the Asian brown cloud, *Curr. Sci., 83(8)*, 947-953.

Ramanathan, V., et al. (2001), Indian Ocean Experiment: An integrated analysis of climate forcing and effects of the great Indo-Asian haze, *J. Geophys. Res., 106(D22)*, 28371-28399.

Ramaswamy, V., et al. (2001), In: Houghton et al (Eds), Climate Change 2001: Scientific basis, *Cambridge University Press*, USA, 349-416.

Rastogi, N., and M. M. Sarin (2005), Chemical characteristics of individual rain events from a semi-arid region in India: Three-year study, *Atmos. Environ.*, 39, 3313-3323, doi:10.1016/j.atmosenv.2005.01.053.

Reddy, M. S. and C. Venkataraman (2000), Atmospheric optical and radiative effects of anthropogenic aerosol constituents from India, *Atmos. Environ., 34*, 4511-4523.

Reeves, R. G., A. Anson, D. Landen, Ed.(1975), Manual of Remote Sensing, *American Society of Photogrammetry*, 1st ed. Falls Church, Va., p. 2144.

Ricchiazzi, P., S. Yang, C. Gautier and D. Sowle (1998), SBDART: A research and teaching software tool for plane-parallel radiative transfer in the Earth's atmosphere, *Bull. Am. Meteorol. Soc.*, 79(10), 2101-2114.

Richardson, C. (1976), Phase relationships in sea ice as a function of temperature, *J. Glaciol., 1976, 17*, 507–519.

Rocadenbosch, F., C. Soriano, A. Comerón, and J. Baldasano (1999), Lidar inversion of atmospheric backscatter and extinction-to-backscatter ratios by use of a Kalman filter, *Appl. Opt., 38(15)*, 3175-3189.

Rodgers, C. D. (2000), Inverse methods for atmospheric sounding: Theory and Practice, *World Scientific*, Singapore, pp. 238.

Rolph, G. D. (2003), Real-time Environmental Applications and Display sYstem (READY) website: http://www.arl.noaa.gov/ready/hysplit4.html, *NOAA Air Resources Laboratory*, Silver Spring, MD.

Roy G., G. Vallée, and M. Jean (1993), Lidar-inversion technique based on total integrated backscatter calibrated curves, *Appl. Opt., 32(33)*, 6754-6763.

Russell, P., P. V. Hobbs, and L. Stowe (1999), Aerosol properties and radiative effects in the United States east coast haze plume: An overview of the Tropospheric Aerosol Radiative Forcing Observational Experiment (TARFOX), *J. Geophys. Res., 104*, 2213-2222.

Sagar, R., B. Kumar, U. C. Dumka, K. K. Moorthy, and P. Pant (2004), Characteristics of aerosol spectral optical depths over Manora Peak: A high-altitude station in the central Himalayas, *J. Geophys. Res., 109*, D06207, doi:10.1029/2003JD003954.

Sakai T., T. Nagai, M. Nakazato, Y. Mano and T. Matsumura, (2003), Ice clouds and Asian dust studied with lidar measurements of particle extinction-to-backscatter ratio, particle depolarization, and water-vapor mixing ratio over Tsukuba, *Appl. Opt., 42*, 7103-7116.

Sassen, K., and Z. Wang (1999), The need for universal cloud property algorithm for active remote sensors, *Ninth ARM Science Team Meeting Proceedings, March 22-26*, San Antonio, Texas.

Satheesh, S. K., and V. Ramanathan (2000), Large differences in tropical aerosol forcing at the top of the atmosphere and Earth's surface, *Nature, 405*, 60-63.

Satheesh, S. K. (2002), Radiative forcing by aerosols over Bay of Bengal region, *Geophys. Res. Lett., 29(22)*, 2083, doi:10.1029/2002GL015334.

Satheesh, S. K., V. Ramanathan, B. N. Holben, K. K. Moorthy, N. G. Loeb, H. Maring, J. M. Prospero, and D. Savoie (2002), Chemical, microphysical, and radiative effects of Indian Ocean aerosols, *J. Geophys. Res., 107(D23)*, 4725, doi:10.1029/2002JD002463.

Satheesh, S. K., and D. Lubin (2003), Short wave versus long wave radiative forcing by Indian Ocean aerosols: Role of sea-surface winds, *Geophys. Res. Lett., 30(13)*, 1695, doi:10.1029/2003GL017499.

Seinfeld, J. H. and S. N. Pandis (1998), Atmospheric chemistry and physics: From air pollution to climate change, *Wiley-Interscience publication*, USA, pp. 1326.

Shahgedanova, M., and M. Lamakin (2005), Trends in aerosol optical depth in the Russian Arctic and their links with synoptic climatology, *Sci. Total Environ.*, 341, 133-148, doi:10.1016/j.scitotenv.2004.09.018

Sharma, S. D. and M. C. Sharma (1999), Erythemal and aerosol studies at Maitri, Antarctica during austral spring of 1995, *Indian J. Phys.,73B*, 463–472.

Shaw, G. (1982), Atmospheric turbidity in the polar regions, *J. Appl. Meteorol., 21*, 1080–1088.

Shaw, G. (1983), Sun Photometry, *Bull. Am. Meteorol. Soc., 64(1)*, 4-10.

Sicard M., P. Chazette, J. Pelon, J. G. Won and S. Yoon (2002), Variational method for the retrieval of the optical thickness and the backscattering coefficient from multiangle lidar profiles, *Appl. Opt., 41(3)*, 493-502.

Singh, R. P., S. Dey, S. N. Tripathi, V. Tare, and B. Holben (2004), Variability of aerosol parameters over Kanpur, northern India, *J. Geophys. Res., 109*, D23206, doi:10.1029/2004JD004966.

Staetter, R., and M. Schroeder (1978), Spectral characteristics of natural surfaces, *Proceeding of the tenth Int. Conf. on Earth Obs. from Space*, 6-11 March 1978, (ESA-SP, 134)

Stephens G. L., R. J. Engelen, M. Vaughan, and T. L. Anderson (2001), Toward retrieving properties of the tenuous atmosphere using space-based lidar measurements, *J. Geophys. Res., 106(D22)*, 28143-28157.

Stunder, Barbara J. B. (1997), NCEP Model Output – FNL Archive Data, *National Climate Data Center*, NOAA- Air Resources Laboratory, USA.

Subbaraya, B. H., A. Jayaraman, K. Krishnamoorthy, and M. Mohan (2000), Atmospheric aerosol studies under ISRO's geosphere biosphere programme, *J. Ind. Geophys. Union, 4(1)*, 77-90.

Torres, O., P. K. Bhartia, J. R. Herman, Z. Ahmad, and J. Gleason (1998), Derivation of aerosol properties from a satellite measurements of backscattered ultraviolet radiation: Theoretical basis, *J. Geophys. Res., 103(D14)*, 17099-17110, doi:10.1029/98JD00900

Venema, V., H. Russchenberg, A. Apituley, A. van Lammeren, and L. Ligthart (2000), Cloud boundary height measurements using lidar and radar, *Phys. Chem. Earth.*, 24(2), 129-134.

Venkataraman, C., G. Habib, A. Eiguren-Fernandez, A. H. Miguel, and S. K. Friedlander (2005), Residential biofuels in south Asia: Carbonaceous aerosol emissions and climate impacts, *Science, (307)*, 1454-1456.

Vermote, E.F. and A. Vermeulen (1999), Atmospheric correction algorithm: Special reflectances (MOD09), *ATBD version 4.0*

Vermote, E.F., N. Z. El Saleous, C. O. Justice, Y. J. Kaufman, J. Privette, L. C. Remer, and D. Tanre (1997), Atmospheric correction of visible to middle infrared EOS-MODIS data over land surface, background, operational algorithm and validation, *J. of Geophys. Res., 102(14)*, 17131-17142, doi: 10.1029/97JD00201

Viollier, M. (1980), Teledetection des concentrations de seston et pigments chlorophylliens contenus dans l'Ocean, *These de Doctorat d'Etat*, no 503.

Voss, K . J., E. J. Welton, P. K. Quinn, J. Johnson, A. M. Thompson and H. R. Gordon, (2001), Lidar Measurements during Aerosol99, *J. Geophys. Res.,106*, 20821-20831.

Wagenbach, D., F. Ducroz, R. Mulvaney, L. Keck, A. Minikin, M. Legrand, J. S. Hall and E. W. Wolff (1998), Sea-salt aerosol in coastal Antarctic regions, *J. Geophys. Res., 103(D9)*, 10961–10974.

Wandinger, U., et al. (2004), Air mass modification over Europe: EARLINET aerosol observations from Wales to Belarus, *J. Geophys. Res., 109*, D24205, doi:10.1029/2004JD005142.

Weisstein E. W. "Riccati Differential Equation." *From MathWorld--A Wolfram Web Resource.* http://mathworld.wolfram.com/RiccatiDifferentialEquation.html

Welton E. J., K. J. Voss, H. R. Gordon, H. Maring, A. Smirnov, B. Holben, B. Schmid, J. M. Livingston, P. B. Russell, P. A. Durkee, P. Formenti and M. O. Andreae, (2000), Ground-based lidar measurements of aerosols during ACE-2:

instruments description, results, and comparisons with other ground-based and airborne measurements, *Tellus, 52B*, 636-651.

Welton E. J., K. J. Voss, P. K. Quinn, P. J. Flatau, K Markowicz, J. R. Campbell, J. D. Spinhirne, H. R. Gordon and J. E. Johnson, (2002), Measurements of aerosol vertical profiles and optical properties during INDOEX 1999 using micro pulse lidars, *J. Geophys. Res., 107*, 8019, doi:10.1029/2000JD000038.

Wiscombe, W.J. and S.G. Warren (1980), A model for the spectral albedo of snow I: pure snow, *J. Atmos. Sci.*, 37, 2712-2733.

Wolter, K., and M. S. Timlin (1993), Monitoring ENSO in COADS with a seasonally adjusted principal component index, *Proc. of the 17th Climate Diagnostics Workshop,* Norman, OK, NOAA/N MC/CAC, NSSL, Oklahoma Clim. Survey, CIMMS and the School of Meteor., Univ. of Oklahoma, 52-57

Wolter, K., and M. S. Timlin (1998) Measuring the strength of ENSO - how does 1997/98 rank, *Weather, 53*, 315-324

Wood, D. C. (1979), Measurement of particulate aerosol mass concentration using a piezoelectric crystal microbalance, In: Aerosol Measurement ed: Lundgren et al, *University Presses of Florida*, Gainesville, USA, pp 716.

Wuebbles D. J., et al. (2003), Changes in the chemical composition of the atmosphere and potential impacts, In: Brasseur G., R. Prinn, A. Pszenny (ed), Atmospheric Chemistry in a Changing World, *Springer*, Germany, 1-17.

Young S. A., D. R. Cutten, M. J. Lynch and J. E. Davies (1993), Lidar-derived variations in the backscatter-to-extinction ratio in southern hemisphere coastal maritime aerosols, *Atmos. Environ., 27*, 1541-1551.

Young A. T. (1994), Air mass and refraction, *Appl. Opt., 33(6)*, 1108-1110.

LIST OF PUBLICATIONS

Publications in refereed journals

1) Ganguly D., A. Jayaraman, **H. Gadhavi**, and T. A. Rajesh (2005), Features in wavelength dependence of aerosol absorption observed over central India, *Geophys. Res. Lett., In Press*, doi:10.1029/2005GL023023.

2) Ganguly D., A. Jayaraman A. and **H. Gadhavi** (2005), In situ ship cruise measurements of mass concentration and size distribution of aerosols over Bay of Bengal and their radiative impacts, *J. Geophys. Res*., 110, D06205, doi:10.1029/2004JD005325.

3) **Gadhavi H.** and A. Jayaraman (2004), Aerosol characteristics and aerosol radiative forcing over Maitri, Antarctica, *Current Science, 86*, 296-304.

4) Gupta P., **H. Gadhavi** and A. Jayaraman, Aerosol optical depth variation observed using Sun-photometer over Indore, *Ind. J. Radio & Space Phys.*, 32, 229-237, 2003.

Papers presented at Symposium/Workshop/School

1) **Gadhavi H.** and Jayaraman A., Aerosol Characteristics over Antarctica during austral summer, *12th National Space Science Symposium*, Barkatullah University, Bhopal, Feb 25-28, 2002.

2) Jayaraman A., Acharya Y., Chandra H., **Gadhavi H**., Ramachandran S. and Sharma S., Lidar study of the long-term trends in the vertical profiles of aerosols, *12th National Space Science Symposium*, Barkatullah University, Bhopal, Feb 25-28, 2002.

3) **Gadhavi H**. and Jayaraman A., Direct aerosol radiative forcing experiment over Antarctica, *Indian Aerosol Science and Technology Association (IASTA) Conference*, SPL, VSSC, Thiruvananthapuram,Vol. 14(1), Sep 18-20, 2002.

4) Ganguly D., **Gadhavi H**. and Jayaraman A., Pre monsoon aerosol characteristics over Ahmedabad, *Indian Aerosol Science and Technology Association (IASTA) Conference*, SPL, VSSC, Thiruvananthapuram,Vol. 14(1), Sep 18-20, 2002.

5) Gupta P., **Gadhavi H**. and Jayaraman A., Aerosol Optical Depth variation observed using sun-photometer over Indore, *Indian Aerosol Science and Technology Association (IASTA) Conference*, SPL, VSSC, Thiruvananthapuram,Vol. 14(1), Sep 18-20, 2002.

6) **Gadhavi H**., Jayaraman A. and Rajesh T., Result from the mobile micro pulse lidar road campaign at Gujarat, *13th National Space Science Symposium*, Kottayam, 2004.

7) Jayaraman A., **Gadhavi H**., Ganguly D. and Misra A., Lidar, sun-photometer and QCM studies of summertime variation in aerosol characteristics over Ahmedabad, *13th National Space Science Symposium*, Kottayam, 2004.

8) Jayaraman A., **Gadhavi H**. and Ganguly D., Lidar observations of inter and intra annual variations in aerosol profiles over an urban site in India, *8th International Global Atmospheric Chemistry Conference, Christchurch-New Zealand*, 2004.

9) Ganguly D., Jayaraman A. and **Gadhavi H**., Observational study on aerosol optical properties over the Indian region and estimation of their radiative forcing, *European Research School on Atmospheres, Grenoble-France*, Jan-Feb 2005.

10) **Gadhavi H**. and Jayaraman A., Natural and anthropogenic induced variation in aerosol extinction profile observed over Ahmedabad in western India, *2nd AOGS Annual Meeting, Singapore*, 2005 (Accepted for Presentation).

11) Ganguly D., A. Jayaraman , T. A. Rajesh and **H. Gadhavi**, Modulation of aerosol physical properties during a fog episode in Delhi, *4th Asian Aerosol Conference, Mumbai*, 13-16 December, 2005.